JOURNAL OF THE
AERO/SPACE SCIENCES

VOLUME 26 APRIL, 1959 NUMBER 4

LIBRARY
APR 13
PURDUE UNIVERSITY

CONTENTS

Means and Examples of Aeronautical Research in France at ONERA (Twenty-Second Wright Brothers Lecture).....MAURICE ROY 193

Discussion of the Lecture....HUGH L. DRYDEN, A. H. FLAX, AND JOHN J. GREEN 207

Thermal Stresses and Deflections in Rectangular Sandwich Plates..P. P. BIJLAARD 210

The Tailored-Interface Hypersonic Shock Tunnel.....
.....CHARLES E. WITTLIFF, MERLE R. WILSON, AND ABRAHAM HERTZBERG 219

The Smallest Height of Roughness Capable of Affecting Boundary-Layer Transition
.....A. M. O. SMITH AND DARWIN W. CLUTTER 229

Readers' Forum..... 246

Published by
INSTITUTE OF THE AERONAUTICAL SCIENCES, INC.

MECHANICAL ENGINEERING
APR 17 1959
LIBRARY

JOURNAL OF THE AERO/SPACE SCIENCES

Editor: W. R. SEARS
Director, Graduate School of Aeronautical Engineering, Cornell University

Associate Editor: ROBERT R. DEXTER *Managing Editor:* RITA J. TURINO
Editorial Assistant: CAROLINE TAYLOR

Editorial Committee

Aerodynamics and Fluid Mechanics
H. Julian Allen
Holt Ashley
Dean R. Chapman
Francis H. Clauser
Hugh L. Dryden
John C. Evvard
Antonio Ferri
Alexander Flax
Wallace D. Hayes
R. T. Jones
Carl Kaplan
H. W. Liepmann
C. C. Lin
H. F. Ludloff
Harold Luskin
Clark B. Millikan
Henry T. Nagamatsu
H. J. E. Reid
George S. Schairer
G. B. Schubauer
John Stack
Theodore Theodorsen
Arthur N. Tifford
Th. von Kármán

Flight Testing
R. R. Gilruth
Melvin N. Gough
W. L. Howland
W. F. Milliken, Jr.

Rotating Wing Aircraft
F. B. Gustafson
K. H. Hohenemser
Bartram Kelley
R. B. Maloy
Ralph McClarren
R. H. Miller
R. H. Prewitt
Igor I. Sikorsky

Structures
John E. Duberg
R. R. Heldenfels
N. J. Hoff
Samuel Levy
J. F. McBrearty
W. Ramberg
E. E. Sechler
F. R. Shanley
C. R. Strang
S. Timoshenko

Meteorology
C. F. Brooks
D. M. Little
F. W. Reichelderfer
K. C. Spengler

Vibration and Flutter
Lee Arnold
M. A. Biot
R. L. Bisplinghoff
Harold A. Cheilek
I. E. Garrick
Martin Goland

Aircraft Design
W. E. Beall
E. H. Heinemann
Hall L. Hibbard
Richard Hutton
C. L. Johnson
A. A. Kartveli
F. K. Teichmann

Electronics
K. C. Black
M. V. Kiebert, Jr.
David S. Little
Paul Rosenberg
Giles J. Strickroth

Physiologic Problems
H. G. Armstrong
Louis H. Bauer
Robert J. Benford
W. Randolph Lovelace, II
Ross A. MacFarland

Flight Propulsion
William Bollay
George W. Brady
R. P. Kroon
Frank E. Marble
Abe Silverstein
E. S. Taylor

Instruments
Alan G. Binnie
Charles H. Colvin
Frank R. Cook
C. S. Draper
S. G. Eskin
C. F. Savage
R. C. Sylvander

SUBSCRIPTION RATES

JOURNAL OF THE AERO/SPACE SCIENCES (formerly Journal of the Aeronautical Sciences), Published Monthly. United States and Possessions: 1 Year, $15.00; Single Copies, $1.50. Foreign Countries Including Canada (American Currency Rates): 1 Year, $16.00; Single Copies, $1.50.

AERO/SPACE ENGINEERING, Published Monthly. United States and Possessions: 1 Year, $5.00; Single Copies, $0.50. Foreign Countries Including Canada (American Currency Rates): 1 Year, $6.00; Single Copies, $0.50.

Notices of change of address should be sent to the Institute at least 30 days prior to actual change of address.

Manuscripts for publication, proofs, and all correspondence should be addressed to the Editorial Office of the JOURNAL.

Publication Office, 20th and Northampton Sts., Easton, Pa. Correspondence regarding subscriptions may be addressed to the Editorial Office of the JOURNAL OF THE AERO/SPACE SCIENCES, 2 East 64th Street, New York 21, N.Y.

© *Copyright, 1959, by the Institute of the Aeronautical Sciences, Inc.*

Second-Class Mail Privileges Authorized at Easton, Penna. Acceptance for mailing at a special rate of postage provided for in Section 1103, Act of October 3, 1917, authorized April 29, 1937.

JOURNAL OF THE AERO/SPACE SCIENCES

VOLUME 26 APRIL, 1959 NUMBER 4

Means and Examples of Aeronautical Research in France at ONERA

The Twenty-Second Wright Brothers Lecture

MAURICE ROY*

Office National d'Etudes et de Recherches Aéronautiques

Opening Remarks

On this anniversary may I suggest that we turn our minds back fifty years to the end of 1908.

The exploit at Kitty Hawk was already 5 years old. An unfortunate accident has occurred on September 17, at Fort Myer, in which Orville Wright had been seriously injured.

Meanwhile, his brother Wilbur was in France, in the region of Le Mans. Since August 4, he had been making repeated flights of ever-increasing duration which had aroused immense enthusiasm and were to bring world-wide fame to the Wright brothers.

Fig. 1 shows the famous biplane flying in the twilight above the military camp at Auvours before landing after nightfall. In France on that day, October 3, 1908, Wilbur Wright made the first night flight in the history of aeronautics.

Fig. 2 dates back to October 15, 1908. On that day, flying with his passenger at an average height of 33 ft. above a racetrack and its surrounding meadows, Wright remained airborne for 1 hr. 9 min. 45 sec. Officially, he had covered a distance of 34 miles, but, in fact, the figure lay between 45 and 50. In so doing, Wright simultaneously smashed the world distance and duration records for flights made with or without a passenger, and this feat was to secure for him a contract worth $100,000.

For me today, this particular picture, which recalls that triumphant exploit, has a very special significance, for Wright's passenger on that flight was none other than Paul Painlevé, who was both a Member of the French Academy of Sciences and Professor of Mechanics at our "Ecole Polytechnique"—two titles which, it so happens, are also held by the Frenchman whom the Institute of the Aeronautical Sciences has called upon this year to deliver the Wright Brothers Lecture.

Perhaps then, when I tell you here how grateful I am for this great honor conferred upon me, which I deeply appreciate, you will bear with me if I let my thoughts go back fifty years to Wilbur Wright's flights in my country and to the man who was with him when he established that record—the man whose pupil I was at the Ecole Polytechnique 30 years before I returned there to occupy the same Chair.

Before starting my lecture I would like to give well-merited tribute and thanks to all of my collaborators at ONERA who helped me in preparing this paper.

Presented before the Institute of the Aeronautical Sciences in the Natural History Building Auditorium, Smithsonian Institution, Washington, D.C., December 17, 1958.

* Director. Also, Member of the Academy of Science.

Introduction

Cosmonautics is currently very much to the forefront in the news. It embraces and extends aero-

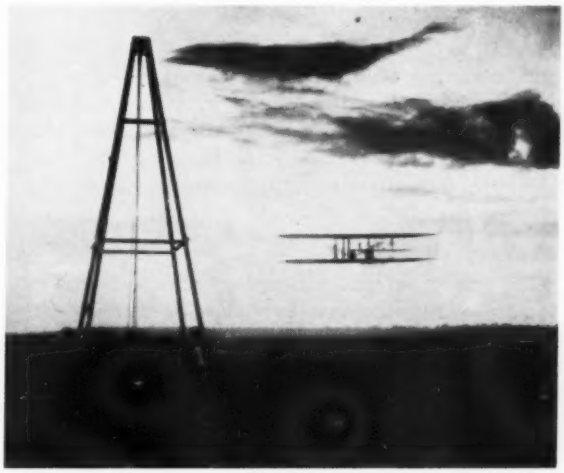

Fig. 1.

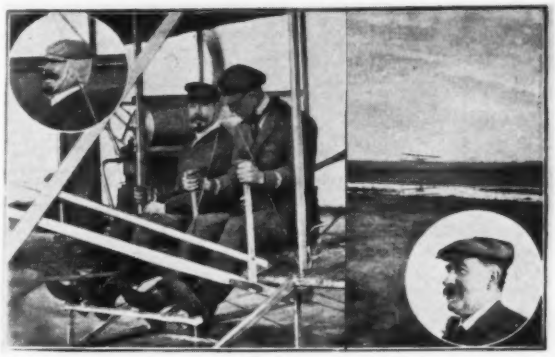

Fig. 2.

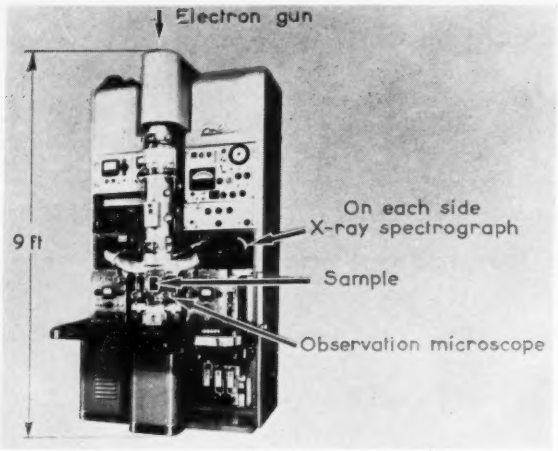

FIG. 3.

nautics, and I would like to propose including both, at least on certain occasions, under a general denomination of "aerocosmonautics."

In your country, the sciences and technology of space are subjects which have been backed by initial advances and abundantly treated.

Since France has not yet launched any artificial satellite or built any circumlunar space vehicle, I propose to confine myself here to the field of aeronautics, where there is still so much progress of manifest utility to accomplish.

I shall accordingly content myself with presenting some examples of aeronautical research and experiments undertaken in my country by ONERA, a body whose mission is akin to that of the illustrious NACA, now NASA, but bearing in mind the considerable difference between the scales of the respective resources.

MATERIALS

The progress in materials always influences construction and sometimes even determines design. The history of aeronautics, as will that of "cosmonautics" in the future, bears striking testimony to this.

First, the characteristics of metallic materials have evolved to a great extent; their behavior has assumed ever-increasing importance under conditions of high temperature—initially in piston engines, then in jet engines and rocket motors, and, finally, in every form of structure subjected to aerodynamic heating due to very high speeds.

Second, materials of a very different nature, rather improperly called plastics, have made their appearance. Obtained by a solidifying and hardening polymerization process, these materials were at first usable only at low temperatures, but in the future they too will be subjected to more and more stringent requirements under heat conditions.

In the wide field of metal and plastic research, the work undertaken by ONERA has been directed mainly at acquiring a deeper knowledge of the relationship which exists between the structure of such materials and their behavior when subjected to mechanical and thermal stresses. In all this work, emphasis has been laid on the time-history of the phenomena, that is to say, on the influence of the time factor and, hence, of velocities and accelerations.

This objective, in itself highly scientific, is a very difficult one to attain. It falls sufficiently outside the usual targets sought by industry to preclude any overlapping in research work, though at the same time fostering intelligent and understanding cooperation between research and industry.

I propose, first of all, to cite two means of investigation developed on these lines.

The first example relates to the ONERA electronic probe (see references 2, 3, 4, 5, and 6 and Fig. 3) which, by spectrography of the X-rays emitted and diffracted by a test sample when struck by a beam of electrons, enables the local composition of the metal to be analyzed quantitatively and its mode and state of crystallization to be known.

The quantitative analysis provides a very satisfactory degree of accuracy (threshold of detection: 0, 02%) but takes into account only those elements of which the atomic numbers are greater than that of sodium. Like the crystallographic analysis, for any selected point on the surface of the sample, the quantitative analysis affects only an extraordinarily minute area, which is of the order of two-thirds of a billionth of a square inch.

On the scale indicated for 20 microns, Fig. 4 shows the pin-point areas of a complex sulphide analyzed by the electronic probe.

The second example I wish to cite concerns machinery designed to investigate fatigue phenomena in materials subjected to very-high-frequency stress reversals; the frequency used initially for these tests was 6,000 cps, but we are currently working with 90,000 cps.

This particular machine (Fig. 5), which generates alternating tensile and compressive stresses, uses stationary longitudinal elastic waves formed in an assembly made up of successive bodies of revolution, these

FIG. 4.

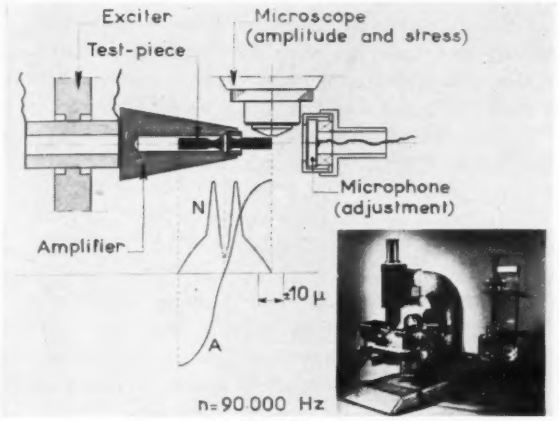

FIG. 5.

being, respectively, a piezoelectric exciter, a mechanical amplifier, and the test piece itself.

Amplitude, the peak value of which is about 10 μ, is observed by microscope and enables stress magnitude to be deduced in the elastic range. The frequency is measured by stroboscope.

As may be seen, this apparatus is attractive in its simplicity, yet allows fatigue tests of an entirely new order to be made, it being possible to complete a three-billion-stress-reversal test program in only nine hours, which is three thousand times faster than with conventional pulsators.

Among test data obtained in this way, I would like to mention only one fact observed, which is that alternating elastic strain, at any rate up to the maximum frequency used by us, does not alter the ageing process on an aluminium alloy of 4 per cent copper content, probably because fatigue failure occurred without any cold working. On the other hand, the effects of cold working can be observed if alternating strain exceeds the elastic limit.

A variety of equipment (see references 9 to 19) has been evolved to enable one to follow the evolution in the structure of materials while under heat treatment during manufacture and when subjected to working conditions under thermal and mechanical loads. In this context, I would like to mention (a) the process of chemical attack known as "contrasting," whereby the surface tinting which takes place, before the precipitation themselves are actually observable, (b) the use of a reactive agent to condition a surface for the taking of alumina replicas which can then be observed under an electronic microscope and kept as testimony of successive stages in a given evolution process, and (c) radio-crystallography equipment to study, by the X-ray method, defects in homogeneity betrayed by satellite lines of diffraction patterns.

Another example of intensive study in the field of practical application, using fundamentally scientific means, is the surface heat chroming of metals belonging to the ferrous group and the plasticization of chromium. For such work, a halogenous reducing atmosphere is used.

Fig. 6 illustrates how penetration in depth of the chromium-vapor diffusion layer varies according to the duration of the treatment at 1,100°C. and the nature of the steel being processed.

Fig. 7 shows, with varying and highly significant degrees of magnification, the difference in purity between an example of trade-supplied chromium and the new metallic chromium obtained by sintering the plasticized powder product evolved by ONERA.

In the following moving pictures,* we shall see first the cobalt specimen being put into the furnace where controlled alternating heating is observed by a cine-microscope. Next small martensitic plates breaking surface will appear, then disappear. They show the almost reversible modification under study.

By means of a microphone and an amplifier, we shall hear the crackling of cobalt crystals, that is to say, the jerky noise which accompanies the allotropic modification of cobalt heated up to 500°C., a phenomenon which was revealed at ONERA and is still little known.

STRUCTURES AND VIBRATION

Almost the whole of the activity of ONERA's Structural Division is concentrated on investigating vibration phenomena in flight so as to constantly improve apparatus and methods used to detect these vibrations and to determine the critical speeds of aircraft

* At this point in the Lecture, a short film sequence was shown.

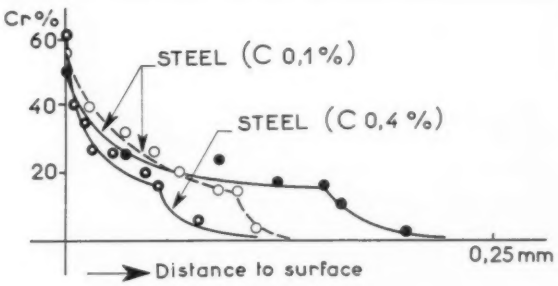

FIG. 6.

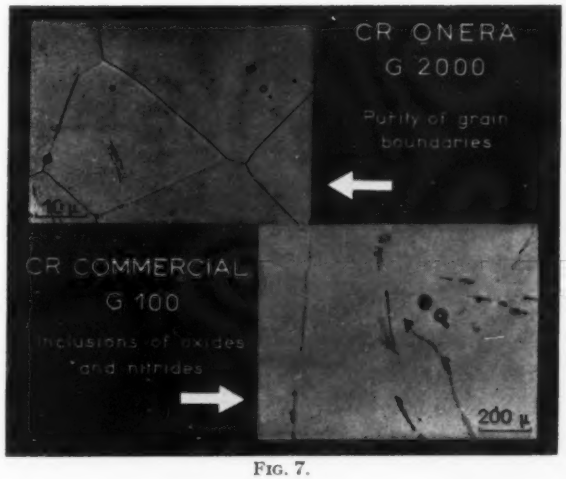

FIG. 7.

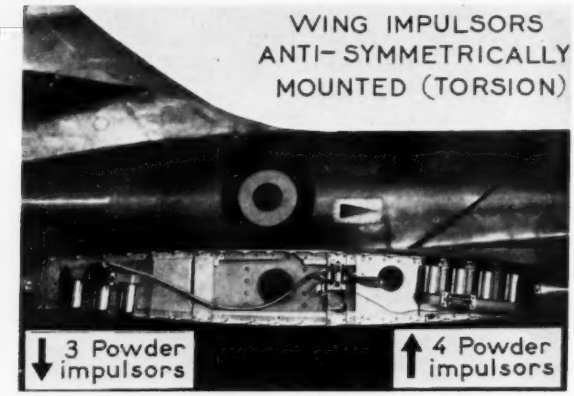

FIG. 8.

and the remedies to be applied for any shortcoming experienced.

During the six years that ONERA has made it its business to ascertain the critical speeds of all prototypes produced by French constructors before the first flight is made there has been no flying accident in France ascribable to structural flutter. In 1957, a dozen aircraft and missile prototypes were subjected to this investigation which includes ground testing of prototypes. For this purpose a road convoy, comprising all necessary equipment, visited each manufacturer concerned and even went to Italy. On one occasion, when tests had to be carried out at our Test Center at Modane, at a time when rail and road communications had been cut by severe floods, a smaller quantity of equipment was transported there by helicopter.

At present, about ten days are sufficient to put an aircraft through the full ground-test program, then some twenty days or so are needed for mechanical computation and interpretation.

I propose to draw attention to only three aspects of the recent evolution in investigation procedures for dealing with such problems, which are still so vitally linked with the safety of aircraft and missiles.

The first objective is to seek to obtain a precise knowledge and assessment of the structural damping occurring in an aircraft by in-flight experimentation and from tests carried out on the machine itself.

The first method used,[20,21] which is known as the impulse method and which has already been extensively developed, has notably enabled the maximum permissible speeds of certain recent aircraft to be raised by 30 knots and even by as much as 80 knots. In this method, powder-energized impulsors are used similar to those shown in Fig. 8 mounted on a wing which underwent in-flight torsional tests; the response signal of the structure to the disturbance produced when these impulsors are energized, is recorded by telemetry on the ground and then suitably filtered prior to being analyzed by a novel backwards-reading method. The impulsors are actually small rockets having a very short duration impulse and a thrust usually of between 40 and 1,000 lbs.

Fig. 9 gives an example of the signal recorded by telemetry and analyzed with respect to three different modes, and indicates the respective frequencies n and damping values α.

The second method, now being compared with the first,[22] uses in-flight harmonic excitation, as is usually done for ground vibration tests.

Vibrators, similar to those shown in Fig. 10 fitted to a Caravelle jet aircraft to investigate the feasibility of improving its present performance with a view to its future development, are fed by variable-frequency generators with power amplifiers and transistors. They put the structure into a state of harmonic vibration both the frequency and amplitude of which can be regulated at will, the amplitude being carefully monitored to obviate any risk of divergence.

Recent initial tests using the harmonic excitation method have given encouraging results; they have notably shown that the response signal can be picked not from noise by analysis, even when the amplitude of the random disturbances is several times greater than that of the signal.

Wind-tunnel tests have revealed also that models used to study vibration phenomena constitute excellent means for detecting parasitic excitation generated by the air stream in the wind tunnel. This form of excitation, which had generally escaped notice up to the present, manifested itself in our big transonic wind-tunnel

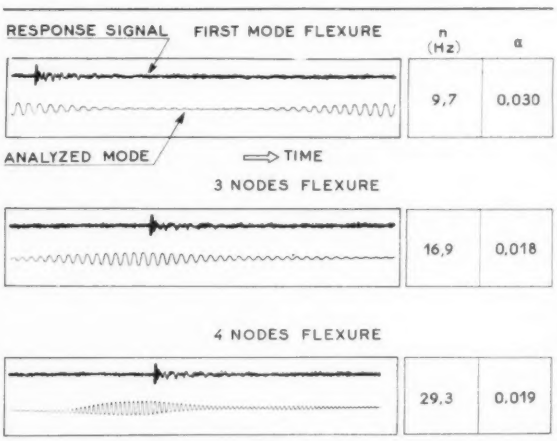

FIG. 9.

FIG. 10.

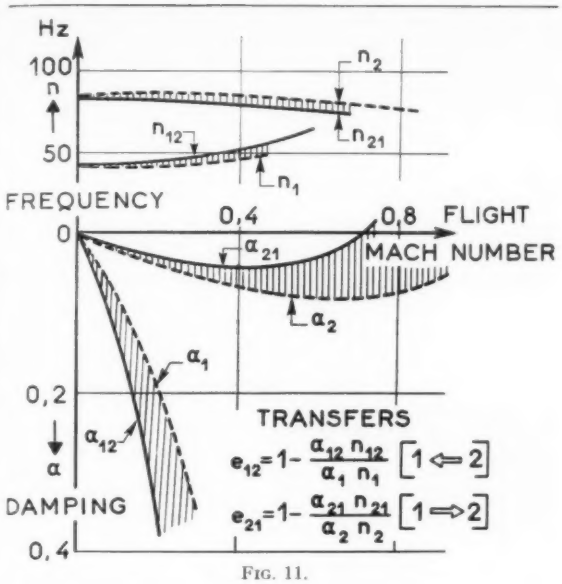

FIG. 11.

at Modane notwithstanding the fact that the test section is located more than 850 ft. from the fans. Such parasitic phenomena are worthy of attention by aerodynamicists.

A second example of research into vibration phenomena involves the introduction of an "energy method" for detecting combinations of fundamental vibration modes capable of giving rise to a grave risk of flutter.

This method of discrimination[23] is based on the somewhat simplified idea that, in an association of p modes, each of these modes receives—as an algebraic sum—a power for dissipation from the other modes which can be characterized by the sum of the differences between unity and the ratio of the power which the mode dissipates in binary association with each of the $(p - 1)$ other modes, to the power it dissipates alone.

Fig. 11 shows, plotted against air speed, the deviations in frequency and damping when an isolated mode is associated to another; it also shows the corresponding transfers.

In its present approximate form, this method provides for qualitative and rapid discrimination of dangerous associations, the latter being subsequently processed by much more precise, detailed computation.

It is possible—and this is a new and interesting approach—to release the energy method from the linearity limitations so generally accepted in the matter of structural vibration, yet which are so debatable when it comes to high—and even transonic—speeds, or again when such components as control surfaces are considered, owing to hinge clearance and friction.

Just as it has renovated theoretical and applied mechanics in many different fields, here also the energy concept can be beneficial.

The third example of ONERA research into dangerous aircraft and missile vibration concerns the way in which wind-tunnel or free-flight testing is being associated more and more closely to the testing carried out on the actual aircraft or missiles themselves, both on the ground and in the air, as already referred to above.

Every endeavor is made to obtain reasonable aeroelastic similarity in models, a thing which it is easier to achieve in missiles than in aircraft. An overall check of critical speeds is then carried out on these models, occasionally self-propelled, either dropped from an aircraft[24] or booster-launched from the ground.[25]

Fig. 12 shows, in position on its launcher and equipped with a booster, a missile model of this type featuring twin simulated ramjets connected to the central body by a straight stub wing.

Such tests, whether carried out by dropping or ground-launching, are also useful for checking and improving calculation methods.

Applied Physics

The importance of free-flight testing of models or missiles has instigated a great deal of research work in the field of applied physics in order first to design, develop, and improve the wide variety of apparatus needed to pick up and measure the interesting quantities, then to transmit, receive, process, and correct the experimental data.

Two typical setups of this kind designed at ONERA are: (1) the radio-trajectograph[26] which, while the test vehicle equipped with a radio transmitter describes its trajectory, records the variations of differences in phase detected by ground receiver stations, taken two at a time, and (2) the 5-channel (Fig. 13) ONERA telemetry unit,[27] or the 19 channel-type with 4 continuous

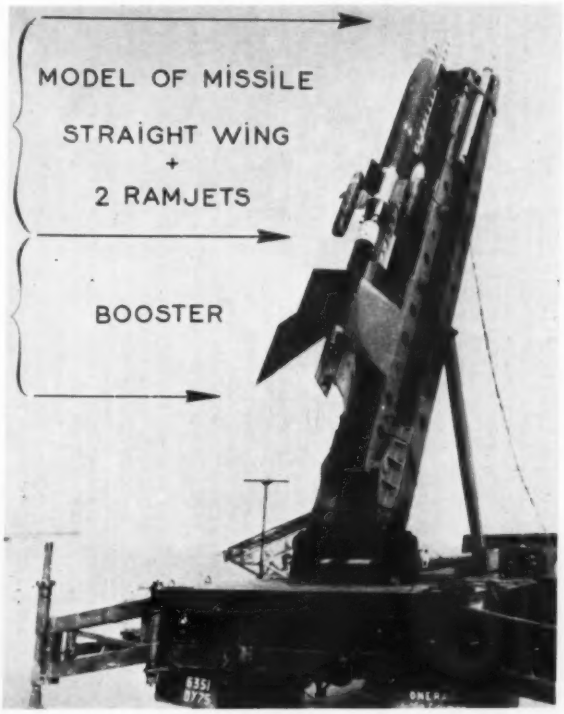

FIG. 12.

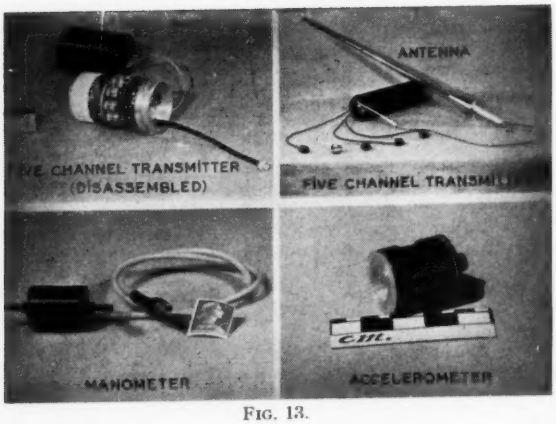

FIG. 13.

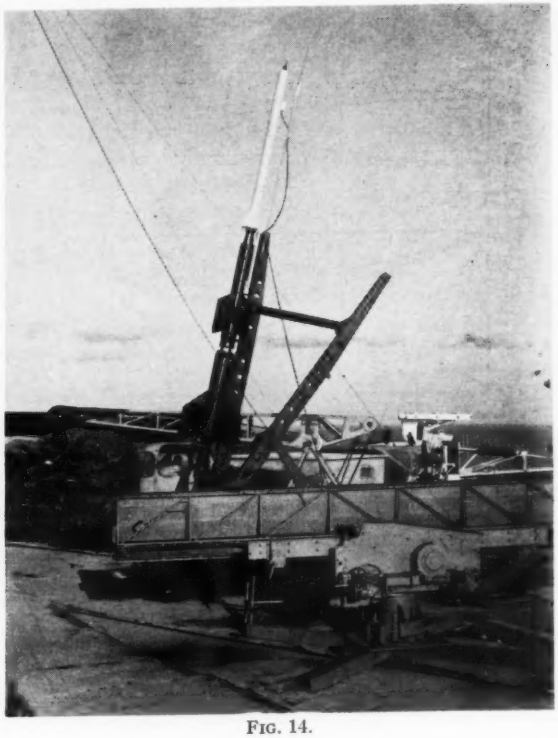

FIG. 14.

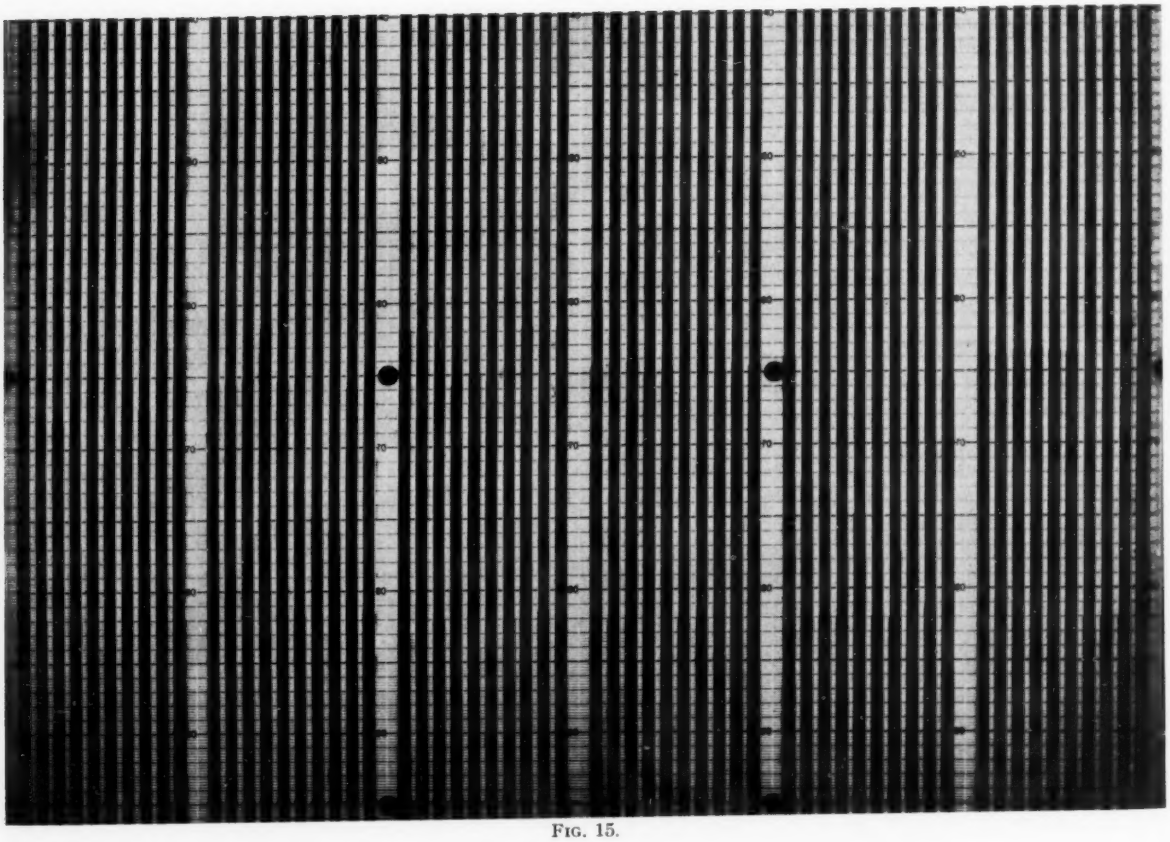

FIG. 15.

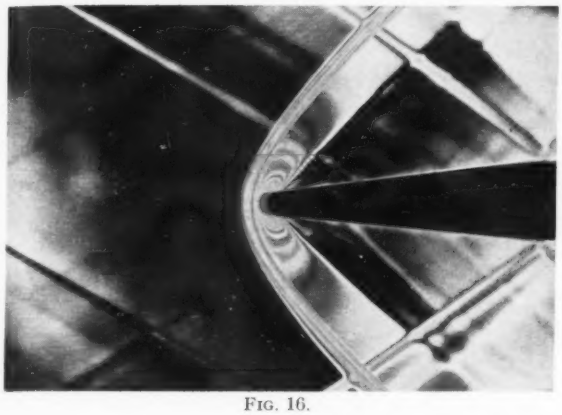

FIG. 16.

channels, which is associated with a very full range of frequency-modulated pickups; the complete equipment weighs very little and takes up little space, while the overall degree of accuracy is within 1 per cent.

If experiments involving model or missile launching and the exploitation of such flights are to be conducted both economically and efficiently, all primary tasks of preparation and execution must be closely coordinated and all operators must observe a rigorous discipline in work.

These requirements were fully met in a few years at ONERA with the formation of special "operational" teams, and it is indeed a pleasure for me to be afforded this opportunity of praising their competence, conscientiousness, and diligence.

Fig. 14 shows an ONERA experimental ram-jet designed for research into propulsion at altitudes of over 65,000 ft. and speeds in excess of 2,500 m.p.h. set up for launching by one of these teams.

Means used for the automatic handling and reduction of wind-tunnel and flight data have been considerably developed in France[29] as in the United States, but somewhat later.

In the case of our trajectograph, the seven receiver stations taken two-by-two yield 21 combinations and the plotting of about a thousand points of the trajectory is automatically accomplished in an hour and a half. An automatic tracking board traces this sequence of one thousand points with a positional accuracy better than 1 ft. in the three space coordinates.

Another piece of apparatus worthy of mention[30] concerns the automatic reading of photographs of wind-tunnel manometer banks (Fig. 15); these photographs are introduced into a machine in which a scanning photocell counts the number of lines not masked by the liquid. By means of electronic devices, these readings are recorded on teleprinter tape which then passes through the data-reducing machine.

In half an hour, 50 frames of a 50-tube manometer are read, processed, corrected, and recorded.

I would like to give two other examples of novel physical methods that find application in wind-tunnel research works.

(1) Interferential strioscopy (Fig. 16), which has been improved at ONERA, has very great sensitivity and can be used for fairly rapid quantitative evaluations.[31] By means of a film sequence, taken at 4,000 frames per sec., the little-known pulsations of a bow shock wave in the process of formation can be quantitatively analyzed at each point.

(2) Magnetic model-suspension,[32] which enables models to be held in a wind-tunnel test section without material means of support (Fig. 17), suppresses all disturbance and interaction. In this method, a group of coils creates magnetic fields, the intensities of which are controlled by the position assigned to the model, this position being defined in the three space coordinates by luminous beams directed at photoelectric receivers. A notable contribution of this system, which is particularly advantageous in research wind tunnels, has been to provide fundamental data about base and sting effects and about their interactions in the case of axisymmetrical bodies.

Concerning noise and vibrations, I should mention that recently some work has been undertaken on jet engine noise as well as on the vibrations and the mechanical and thermal effects induced by the hot exhaust gases on aircraft structures.[33]

Moreover, research on the sound-proofing of aircraft has been under way for a long time.

Fig. 18 illustrates the progress made in France in this latter respect over the period extending from 1947 to 1957, thanks to the pioneering work of ONERA which

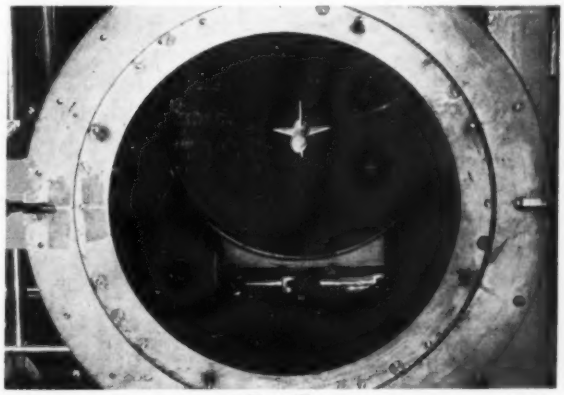

FIG. 17.

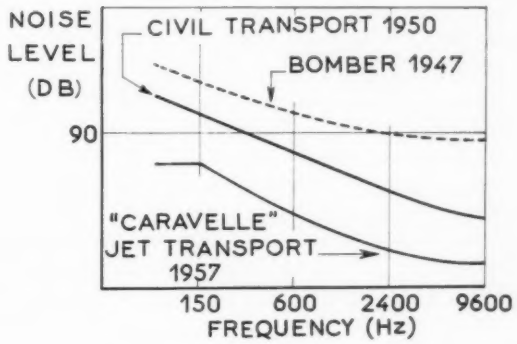

FIG. 18.

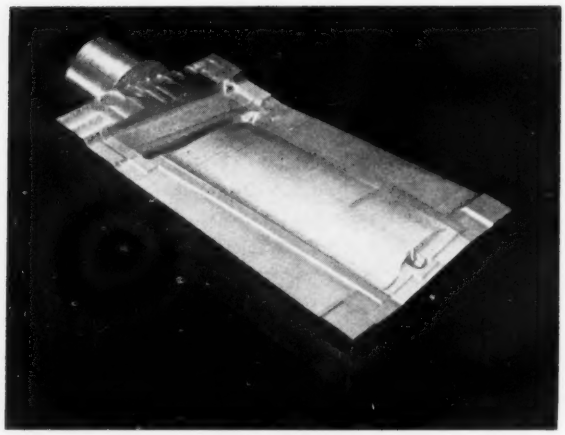

FIG. 19.

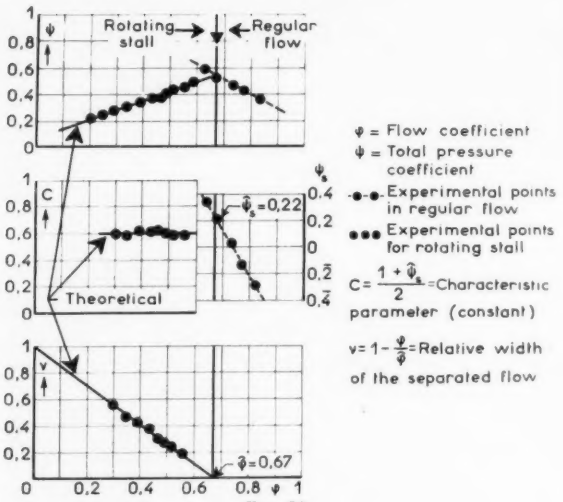

FIG. 20.

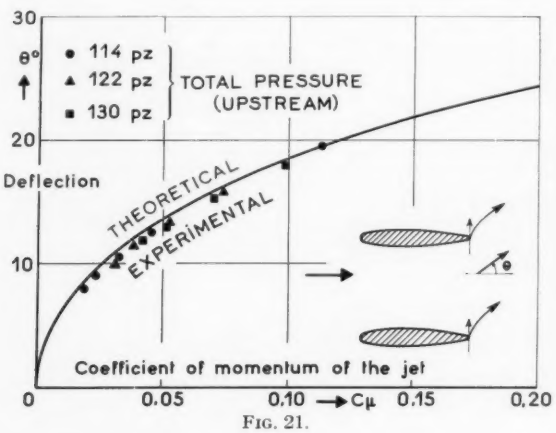

FIG. 21.

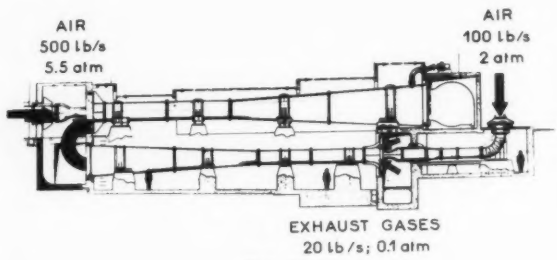

FIG. 22.

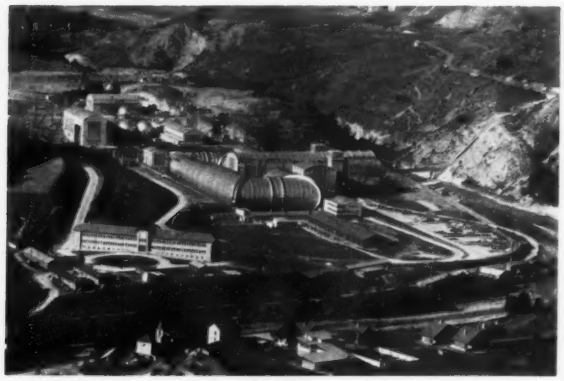

FIG. 23.

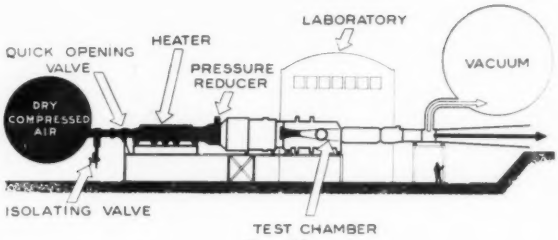

FIG. 24.

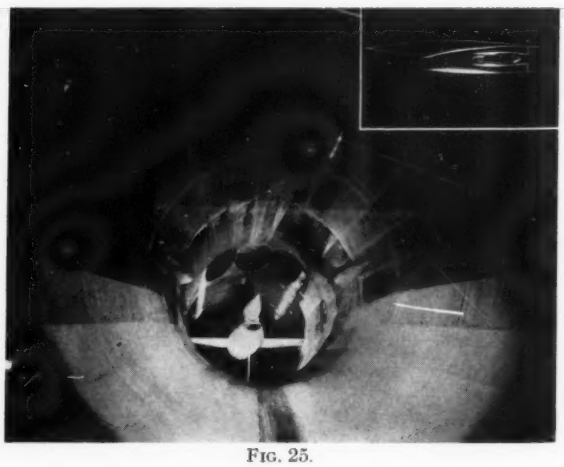

FIG. 25.

has resulted in the very remarkable acoustic comfort offered by the French medium-range jet liner Caravelle.

A last example of scientific research work in general physics applied to a very practical case of engineering, particularly in the aeronautical industry, concerns the ONERA three-dimensional milling machine, all operations of which are controlled, according to a concept of my own, solely by mathematical equations defining the shape of the object to be reproduced.[35]

This can be applied with advantage to the reproduction of wings or blades, the contours of which are reasonably easy to define with a few terms from a Fourier series, easily handled by simple electronic computers.

By ways of example, Fig. 19 shows one half of a stamping die machined by this process and used, in this instance, for mass-producing axial compressor blades.

Energy and Propulsion

ONERA research work on energy and propulsion problems has been mainly directed—and deliberately so—towards fundamental subjects, and this has been done in close liaison with industry, which naturally tends to concentrate more on progress in technological fields.

Numerous special and rather interesting measuring instruments have been developed, and I would like to mention some of these as examples: (a) a gas analyzer, based on infrared absorption, which can be used in flight[36] to monitor jet-engine operation and rating; (b) a very sensitive and accurate flowmeter,[37] for use in connection with propellants tested in our microrockets[38–40] (as a matter of fact, this flowmeter has been adopted to measure blood flow in the "artificial heart" now in service in a Paris hospital); (c) a continuous-type electro-optical thermometer[41] with a response time of 10^{-5} sec., to measure flame temperatures between 1,400 and 3,300°K.; and (d) a spectrograph to study the distribution of chemical reactions in a combustion zone.[42]

Thanks in particular to the use of such equipment, fruitful research techniques have been recently developed for the study of combustion in ramjets and the chemical kinetics of liquid propellants.

For example, film sequences have been made to study combustion instability in an ONERA microrocket equipped with transparent tanks which are photographed at the rate of a thousand frames per second to provide accurate flow measurements, while pressures are recorded to within a tenth of a millisecond.

In studying aerodynamic heating at high and very high speeds—and this has a bearing on propulsion as well—rocket jets can be used to provide high-temperature supersonic flows, as can be shown in film sequences in which an AGARD B ogive is placed in a Mach 2.5 rocket exhaust jet at an absolute temperature of 2,600°K. These films* show that the nose of the ogive melts almost instantaneously, but that the shouldering thus formed causes separation of the outer flow and delays downstream heating.

This example of a simplified experiment is linked with the fundamental problem[43] of heat exchange phenomena occurring in the boundary layer, upstream and downstream of separation—a problem which is now being studied and which may give new solutions for the shape and structure of re-entry noses on hypersonic aircraft and missiles.

Insofar as gas turbines are concerned, I would like to mention the research work devoted to the phenomenon of rotating stall which is so detrimental to high-efficiency axial compressors and whose underlying theory has been established and confirmed,[44,45] as Fig. 20 shows in summarized form.

As one of the possible ways of delaying or opposing this highly undesirable phenomenon, I suggested air blowing at the trailing edges of guide vanes, the theory of which has since been established and verified, as shown in Fig. 21.

This method, which transposes jet-flap research on isolated wings (research which I will consider in a moment) to airfoil cascades, can find useful application in various types of gas turbines, for, as can be seen, moderate blowing is capable of markedly deflecting the relative air flow and can therefore replace a cascade of adjustable stationary blades.

I will also mention a third example of mixed theoretical and experimental research which likewise resulted in what I will term an "elegant" theory, in the sense that such theories are not only all-encompassing but also highly accurate in their application. This concerns the theory of ejectors in which the driving flow is supersonic.[47,48] In distinguishing between supersonic, saturated, and mixed regimes, this theory has linked up a very wide and complex variety of experiments. It has been utilized to establish the design of the ejectors used at ONERA's aerothermodynamic laboratory at Palaiseau to simulate very high altitudes.

A similar application (Fig. 22) of the theory, though on a larger scale, is projected for an intermittent wind-tunnel for ramjets and rockets at Modane. A flow at 20 lb./sec. of burnt exhaust gases at a pressure of 0.1 atm would be extracted by a two-stage air ejector and then discharged into the open air.

Large-Size Wind Tunnels

While on the subject, I would like to point out that ONERA has built an Aerothermodynamic Test Center[49] at Modane, at the foot of the Alps (Fig. 23), which makes direct use of a waterfall with a height of 3,000 ft.

By direct action on water turbines, this waterfall drives the 50 ft.-diameter fans of an 85 megawatt transonic wind-tunnel, called S1MA, which, until the Arnold Engineering Development Center tunnels at Tullahoma came into operation, was the most powerful in the world. The waterfall also drives the 65 megawatts compressor of the closed circuit S2MA supersonic wind tunnel now being completed and to which are associated two intermittent tunnels, one of which is the hyper-

* At this point in the Lecture, a short film sequence of this kind was shown.

sonic S3MA while the other, the S5MA, is especially intended for high supersonic tests on ram-jets and rockets. The large 26-ft.-diameter transonic wind tunnel has been in operation for 5 years and has been used for numerous tests already.

Though direct hydraulic drive is not used in the United States, our plant at Modane is well up to U. S. dimensional standards, as many of our American friends have been able to see for themselves.

Fig. 24 shows the layout of S3MA which is now ready for the first testing.

Fig. 25 gives an example of one of recent tests. The Nord-Aviation "Griffon" has undergone very full high-subsonic testing with its turbo-ram-jet engine running, and under the control of the same pilot who later put the aircraft through its flight testing.

Fig. 26 shows yet another example: here a Dassault "Mystère" aircraft is set up in the test section in readiness for cockpit jettisoning inside the tunnel at speeds of up to 500/550 m.p.h.; these tests, in fact, proved particularly instructive.

Another type of full-scale test, carried out in the big open-circuit wind tunnel operating at Chalais-Meudon since 1930, is shown in Fig. 27. The Deltaviex model, seen here with its pilot aboard, is fully airborne, but a funicular suspension—improved at ONERA—reduces the number of degrees of freedom. This system now allows low-speed stability and maneuverability studies to be undertaken—studies in which there is a renewed interest because of STOL and VTOL problems.

Aerodynamics

The science of aerodynamics, with its attendant complications of compressibility, viscosity, and turbulence has been, and continues to be, the object of much activity, both theoretical and practical, at ONERA, and has given rise to unceasing development of wind tunnels of all types as well as of their equipment, which has become more and more automatic.

Thus, for example, eight years ago, and at about the same time as the NACA, though each was ignorant of the secret work the other was doing, ONERA was completing a transonic device which was immediately used to throw light on numerous problems connected with French aircraft, then just beginning to cross the notorious sound barrier.

Of the great number of aerodynamic studies and of the aerodynamic facilities developed at ONERA over the last ten years or so, I can obviously quote only a few, though this is inevitably unfair to the rest of the work done.

I shall therefore mention only three of these, each of different character.

The first example relates to the fundamental problem of flow separation on a three-dimensional body. By making certain judicious assumptions in conjunction with a principle known as "prevalency"—a generalization of an idea put forward by L. Prandtl—ONERA engineers[50,51] have established a separation theory for the laminar boundary layer, whereby the line of separation is defined as the ultimate position of a streamline passing through a characteristic point of separation on the body.

The transition problem was analyzed concurrently and, by combining two criteria of longitudinal and transverse stability,[52] it became possible to make a number of forecasts later borne out by experience.

To check the theory of three-dimensional separation in a laminar boundary layer, calculations were made, particularly in respect to a 10 per cent thickness-ratio, symmetrical-airfoil delta wing of elliptic cross section.

Fig. 28 shows that the calculated line of separation is consistent with the actual flow conditions observed in a hydrodynamic tunnel which I designed in 1950 and which is very widely utilized when complex phenomena must be detected and understood.

As a second example of fundamental research work, to enable the valuable nature of these detections to be appreciated, a film sequence will show us the flow around a thin delta wing the angle of attack of which is progressively increased, then decreased and reduced to zero. The first frames concern the flow outside the boundary layer of the upper surface seen from above. They show the formation of vortex sheets rolling up into scrolls from the apex on both leading edges, in accordance with my theory on rotational subsonic flow for wings of this type.[54]

Then there is a progressive decrease in delivery of the colored liquid used to show up the streamlines. We shall see the flow pattern changing and turning into the boundary-layer streamlines close to the wing surface.*

The next sequence shows a further example of these visualizations, this time relating to the flow along an ellipsoid set at zero incidence; with a change from outer flow to flow along the body, the theoretical "separation line" already mentioned is seen to settle down fairly well.

My third example deals with recent theoretical investigations on very new effects of hypersonic aerodynamics.

A good intrinsic and physical definition of these effects might well be to state that they take up where nonlinear phenomena—in particular, the entropy variation linked with local dissipation of energy—cease to play a secondary role, a condition usually corresponding to Mach Numbers greater than 5.

In such flows, if they are stationary, waves of entropy variation are propagated—in the Hugoniot sense of the word—along the streamlines, while expansion and compression waves are propagated along the Mach lines in the same way (Fig. 29).

The approach theory which I made known twelve years ago[55] consists in neglecting on the body, when this is permissible, the effect of compression waves reflected by the front shock wave. In this way very simple calculations become feasible, and in a recent study one of my collaborators was able to specify the second-order approximation.

---

* At this point in the Lecture, two short film sequences were shown.

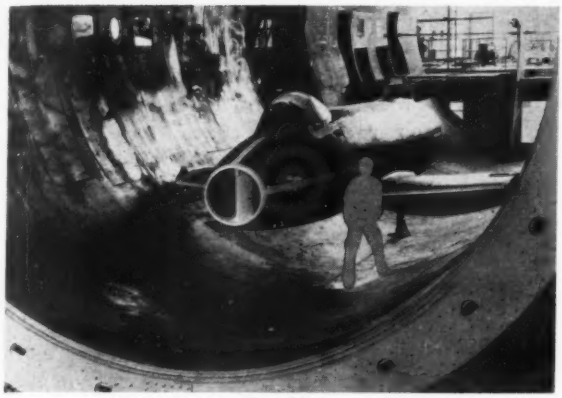

FIG. 26.

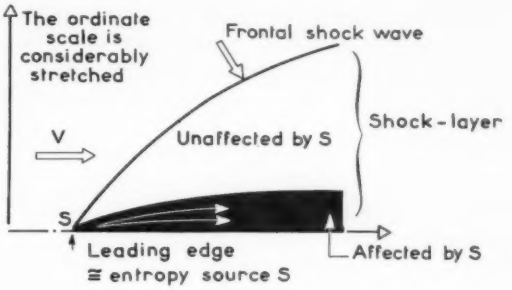

FIG. 30.

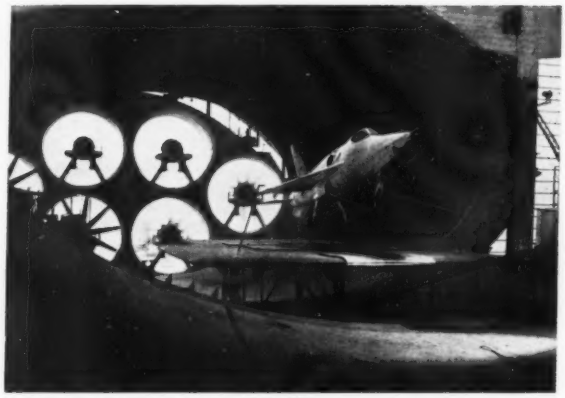

FIG. 27.

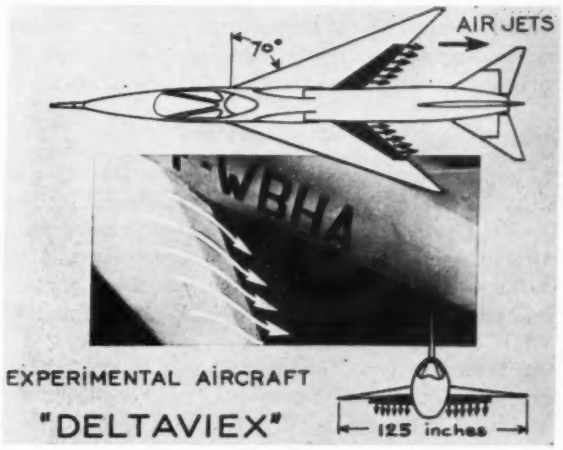

FIG. 31.

FIG. 28.

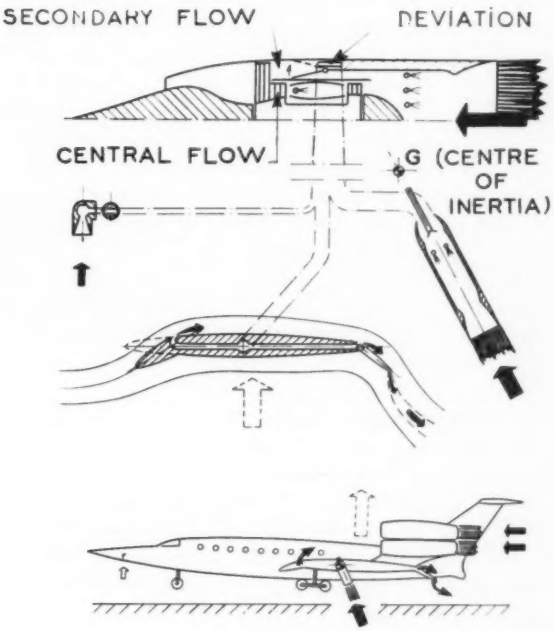

FIG. 32.

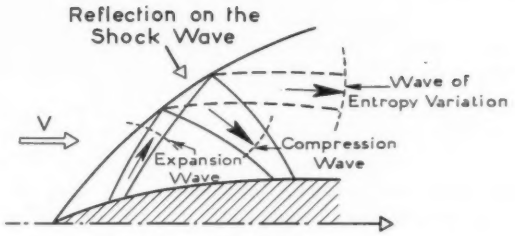

FIG. 29.

Parallel to this, he made a deep investigation of the structure of the "shock layer" and rigorously demonstrated that in this layer the streamline pattern is virtually superposable on the geodetic pattern of the surface of the body.[56]

This theoretical study has led to a most instructive analysis of the "shock layer" in the case of a flat plate parallel to the airstream, having a leading edge of finite thickness.[57]

In the conventional representation given in Fig. 30, this leading edge behaves as a "source of entropy" which influences a partial and limiting layer of low density and considerable thickness.

It is around this layer that the fluid flows away unaffected by the leading-edge effect, and the flow is so to speak "aware" of the obstacle only by virtue of this "shock layer," which is generated by an extremely narrow strip of upstream flow of given breadth and astonishing expansion and rarefaction characteristics.

STOL AND VTOL

Despite the great progress made since the flight at Kitty Hawk, birdlike zero-length take-off and landing have not yet been achieved by conventional aircraft. Although the helicopter has been quite successful in certain uses, there is no doubt that part of aeronautical research must still be devoted to STOL and, ultimately, VTOL designs.

Several different solutions of this problem are being experimented with in your country: either the aircraft is vertical to the ground, then tilts over to the horizontal and returns to a vertical attitude while in flight, or else the engines—with or without the wings—swivel through 90° after take-off and again prior to landing. That these methods are claiming equal attention indicates that none is superior to the others.

In connection with STOL, ONERA has carried out and published extensive work on the controlled and forced circulation by boundary-layer suction and blowing at wing leading or trailing edges. The most recent of these works have mainly been devoted to trailing-edge blowing, associated or not with the action of a flap, which is itself blown at its hinge.

A theory has been elaborated[58–60] which suitably links up experimental results and which is quite literally "lit up" by flow visualization.[61]

Applications leading to a quite notable reduction in take-off and landing runs can be deduced from this theory, provided that blowing air is supplied in reasonable abundance, which may well lead to the use of special turbo-blowers on aircraft.

I shall only mention an interesting application on our Deltaviex experimental flying model. The take-off weight of this tiny machine (Fig. 31) is 2,080 lbs. and its lifting area is 36 sq.ft. only; the wing span does not exceed 124 in., sweepback at the leading edge being 70°, while maximum static thrust of its turbojet is 940 lb. It is probably the jet plane with both the sharpest sweepback and narrowest wing span in the world.

Piloting this machine proved very difficult, as its very low roll inertia gave it a response time shorter in many instances than that of its excellent pilot. However, by using a blowing system at the wing-flap trailing edges involving no more than a 2 per cent bleed from the engine air flow and by subordinating the action of these air jets on each wing to the angle and rate of roll, ONERA succeeded in achieving a forced stabilization which restored normal piloting characteristics to the aircraft, as you will be able to see now by watching this uncommon aircraft take off (short film sequence).

To return to the problem of STOL and VTOL, I would like to mention the result of a study carried out in accordance with a personal concept of mine aiming at utilizing in various ways, for lift and thrust, a dual flow turbojet, which one might term a turbojet with "polyvalent secondary flow." The flow is given moderate mechanical compression, the magnitude of which is adjusted to flying speed. Compression, at a maximum on take-off, gradually diminishes until it is zero at maximum flying speed—envisaged at Mach 2 to 2.5 at least. This variable compression is achieved by using pivoted guide-vanes for the two-stage compressor and for the single-stage turbine of the free low-pressure rotor, the latter being left to windmill after low-pressure compression has been cut off.

The secondary flow, the output of which is of the order of 1.5 times that of the central flow, can also be used (Fig. 32) for blowing on wings and tail units during certain stages of take-off and landing.

When such blowing is resorted to, the secondary flow is almost wholly diverted to nozzle combustors used for lift, so located and set as to cause their thrust to be almost exclusively transformed into lift and to contribute to trimming of the aircraft, their jets being discharged at an adequate distance not only from the engine air intakes to preclude the possibility of exhaust gas being inadvertently recycled, but also from any sensitive part of the aircraft.

I shall not dwell here on the advantages nor on certain technological difficulties inherent in this solution, which dispenses with the need for any tilting of the propelling jets or of their exhaust gases but which will remain a speculative solution until some jet constructor takes up the experiment, which is of course more likely to occur in this country than in Europe for obvious reasons.

Two designs may be conceived, according to the basic diagrams in Fig. 33, with associated or separated flows. In these diagrams, the main sections of the two flows are shown in their true relative magnitudes, the only varying sections apart from the intake, which is not shown, being the throat and outlet of the propulsion nozzles, which must differ somewhat.

As in the United States, direct lift by jets has already been achieved in Great Britain, France and the USSR—in an experimental form only: it is true, but which nonetheless shows the way for the future. This type of performance requires the vertical thrust to exceed the all-up weight by at least 15 per cent.

One immediately realizes that an equivalent conventional jet engine would use such thrusts for ultra-accelerated—and hence very short—take-offs. Thus, from a comparison with the concept of the jet engine with my polyvalent secondary flow, one can estimate that conventional propulsive jet engines with the same frontal area would have a total thrust that would provide an initial acceleration of 1.5g and an extremely short take-off run—though not necessarily as short a landing run—and would subject passengers of a commercial aircraft to a degree of strain that would probably turn out to be prohibitive.

Fig. 34 compares this form of STO to a vertical riser conforming to my solution, for the case of a civil transport airplane capable in both cases of cruising at $M = 2.5$ over stage lengths of the order of 3,000 kilometers, carrying a payload attaining 10 per cent. Of an all-up weight of 90,000 lbs. such an aircraft would be powered by six jet engines with polyvalent secondary flow, and of 50 in. maximum diameter. Without laboring the point unduly, let it be said that transport by supersonic aircraft with zero-length take-off and landing characteristics is a solution offering numerous advantages for the future, and that its advent is perhaps certain.

Unavoidably, jet-achieved VTOL, with provision for conventional emergency landing, involves a considerable penalty in power, but when it is combined with the capacity for flying at supersonic speed—as much for military aircraft as for civil transports—does it not justify a search for appropriate powerplants?

In presenting this subject among others to you, I hope I have been able to show you that although Jules Verne's anticipations on the voyage from the earth to the moon are now giving rise to considerable and wonderful efforts in science and technique in the country of the Wright brothers, other scientists and technicians in Verne's own country, without overlooking space flight research, are continuing to work for the great and very useful progress that aviation can still accomplish by following the way so brilliantly opened up by the Wright brothers.

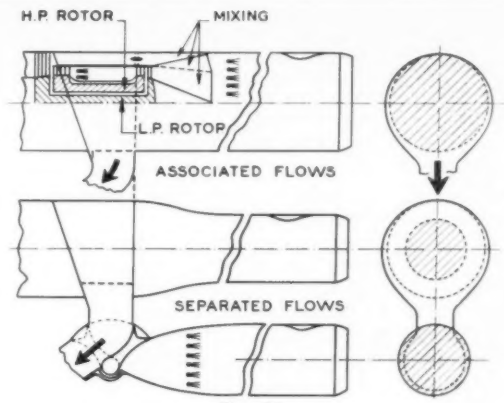

FIG. 33.

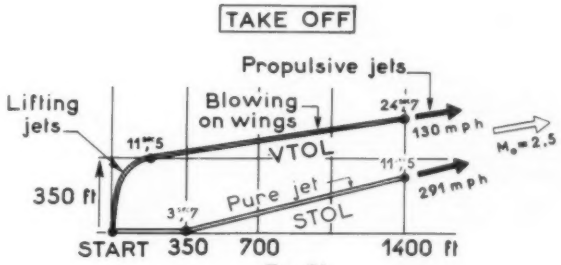

FIG. 34.

BIBLIOGRAPHY*

[1] Roy, Maurice, *The Contribution of Aeronautical Research to Progress in Aviation*, ONERA, Publ. No. 90, 1957.

[2] Castaing, R., *Application of Electronic Probes to a Method of Chemical and Crystallographic Pin-Point Analysis*, R.A. No. 23, p. 41, 1951.

[3] Castaing, R., *Microanalysis by Means of an Electron Probe*, Congress of the American Crystallographic Association, Chicago, October, 1951.

[4] Castaing, R., and Descamps, J., *On the Physical Bases of Pin-Point Analysis by X-Ray Spectrography*, Journal de Physique, 16, p. 304, 1955.

[5] Castaing, R., Philibert, J., and Crussard, C., *Electron Probe Microanalyzer and Its Applications to Ferrous Metallurgy*, Journal of Metals, p. 389–394, April, 1957.

[6] Descamps, J., and Philibert, J., *Improvements and Recent Applications of the Electron-Probe Microanalyzer*, Congress of the Association for the Advancement of Spectrographic Methods, Paris, June, 1957.

[7] Vidal, G., Girard, F., and Lanusse, P., *Machine for Studying Fatigue at 6,000 cps*, C.R. Ac. des Sciences, 242, pp. 986–988, 1956, and Journées d'Automne 1957 (Rev. Métall., Paris).

[8] Vidal, G., and Girard, F., *Machine for Studying Fatigue at 87,000 cps*, C.R. Ac. des Sciences, 243, pp. 1276–1278, 1956, and Journées d'Automne 1957 (Rev. Métall., Paris).

[9] Poulignier, J., and Jacquet, P. A., *High-Temperature Evolution of Micrographic Structures in 80/20 Ni-Cr Refractory Alloys*, Rev. Métall., Vol. 49, No. 8, p. 541, Paris, 1952.

[10] Buckle, Ch., Jacquet, P. A., and Poulignier, J., *Metallographic Determination of Operational Temperatures Sustained by Components of Thermal Machines*, C.R. Ac. des Sciences, 234, p. 718, 1952, and Rev. Métall., 50, No. 2, p. 105, Paris, 1953.

[11] Baillie, Y., and Gilles, P., *An Optical and Electric-Microscope Study of Precipitates in Ni-Cr-Ti-Al Alloys, Using a New Electro-Chemical Reagent*, Société Française de Métallurgie, October 24–29, 1955 (to be published in the Rev. Métall., Paris).

[12] Manenc, J., *On the Structural Evolution in a Modified 80/20 Ni-Cr Type Refractory Alloy*, C.R. Ac. des Sciences, pp. 2413–2415, June 20, 1955.

[13] Duriez, V., and Barboni, J., *Method of Chemical Analysis for Refractory Alloys*, ONERA NT No. 24, 1955.

[14] Malamand, F., and Vidal, G., *Effect of Heat-Treatment Oxidation on the Superficial Chemical Composition of a Ni-Cr, Ti-Al Alloy*, C.R. Ac. des Sciences, Vol. 240, pp. 186–188, January 10, 1955.

[15] Mathieu, M., *Micrographic Methods*, R.A. No. 51, May-June, 1956.

[16] Poulignier, J., *Research into Ni-Cr and Ni-Cr-Co Alloys Turbojet Moving Blades*, Revue du Nickel, 23, pp. 1–18, Paris, 1957.

[17] de Leiris, H., and Corfa, V., *Identifying Incipient Fatigue Cracks Having Paths Perturbed by the Anisotropy of the Metal*, Rev. Métall., Vol. 55, Paris, 1958.

* NOTE—The abbreviation R.A. is used to designate "Recherche Aéronautique," the bimonthly journal published by ONERA.

Titles have been translated into English for the convenience of the reader. Names of publications are given in the original language.

[18] Jacquet, P. A., *Improvements on, and New Applications of, the Nondestructive Metallographic Examination Techniques*, Rev. Métall., Vol. 55, Paris, 1958.

[19] Galmiche, Ph., *Bright-Annealing Refractory Alloys*, R.A., No. 59, Paris, 1957.

[20] Coupry, G., Valid, R., and Piazzoli, G., *A Study of In-Flight Vibration Damping by Percussion on the Lifting Surfaces*, R.A., No. 47, 1955.

[21] Coupry, G., *Sounding a Structure by Percussion*, Assoc. Techn. Marit. et Aéron., Paris, 1957.

[22] Nicolas, J., *A Comparison of Wind-Tunnel Test Results Obtained on an Airplane Wing With Application of the Harmonic and Impulse Methods of In-Flight Excitation*, R.A., No. 65, 1958.

[23] Beatrix, C., *An Energy Method of Detecting Vibration Modes Liable to Cause Flutter*, R.A., No. 58, 1957.

[24] Dat, R., Destuynder, R., Loiseau, H., and Trubert, M., *Flutter Tests in the Sonic Range on Free Falling Models*, R.A., No. 39, 1954.

[25] Loiseau, H., *Flutter Tests in the Trasonic Range on Self-Propelled Surface-to-Surface Models*, R.A., No. 66, 1958.

[26] Zakheim, J., *Applications of the ONERA Radio Beam and the ONERA Trajectograph*, R.A., No. 43, 1955.

[27] Le Boiteux, H., and Moussette, G., *The ONERA Telemetering System*, 1958 National Telemetering Conference, Baltimore, Maryland, June, 1958.

[28] Le Boiteux, H., Lygrisse, P., Zakheim, J., Dugay, R., Moussette, G., Benoist, R., Laurentjoye, R., Gouillou, R., and Palmieri, P., *Tests of Models in Free Flight Test Procedure and Applications*, R.A., No. 43, 1955.

[29] Le Boiteux, H., *Data Processing Procedure*, 1956, to be published by Groupement pour l'Avancement des Méthodes d'Analyse des Contraintes, Paris.

[30] Moreau, R., *Automatic Processing of Wind-Tunnel Pressure Data*, AGARD Report 167, March, 1958.

[31] Philbert, M., *Interferential Strioscopy as Applied to Aerodynamics*, R.A., No. 65, 1958.

[32] Tournier, M., and Laurenceau, P., *Magnetic Suspension of Models in Wind Tunnels*, R.A., No. 59, 1957.

[33] Le Boiteux, H., and Lienard, P., *Some Studies of the Effect of Jet Exhausts on Structures*, Proceedings of the First International Congress of the Aeronautical Sciences, Madrid, Spain, September, 1958, Pergamon Press, Ltd., London, England.

[34] Kobrynski, M., *Method of Soundproofing Civil Transports, With Particular Reference to the SE #210 Caravelle*, R.A., No 63, 1958.

[35] Fayard, G., *Design and Engineering of Two Automatic Machines, One for Outlining Airfoils, the Other for Machining Turbine-Engine Blades*, R.A., No. 58, 1957.

[36] Fructus, J., *Gas Analyzer of Combustion in Flight*, R.A., No. 67, 1958.

[37] Moutet, A., and Nadaud, L., *Flowmeter With Short Response Time*, R.A., No. 64, 1958.

[38] Barrere, M., Moutet, A., and Sarrat, P., *Combustion Instability in Rocket Motors—An Experimental Study*, ONERA, Publ. No. 82, 1956.

[39] Barrere, M., Moutet, A., and Sarrat, P., *Measuring Characteristic Time Factors in the Evolution of Combustion in a Rocket Chamber for Liquid Propellants*, R.A., No. 60, 1957.

[40] Moutet, H., Moutet, A., and Barrere, M., *Influence of Temperature and Pressure on the Ignition Lag of Hypergols*, ONERA, NT No. 45, 1958.

[41] Moutet, A., *Instantaneous Measurement of Flame Temperature*, ONERA, Publ. No. 88, 1957.

[42] Surugue, J., *Structure of the Stabilization Nucleus*, Brennstoff-Wärme-Kraft, No. 6, Düsseldorf, 1958.

[43] Bernard, J. J., and Siestrunck, R., *Heat Exchanges in Separated Flows*, Proceedings of the First International Congress of the Aeronautical Sciences, Madrid, Spain, 1958, Pergamon Press, Ltd., London, England.

[44] Siestrunck, R., Fabry, J., and Jarlan, L., *A Study of Nonstationary Critical Regimes in Slow-Speed Operation of Aviation Compressors*, Journées Int. de Sci. Aéron., ONERA, Paris, 1957.

[45] Fabri, J., and Siestrunck, R., *Rotating Stall in Axial Flow Compressors*, Journal of the Aeronautical Sciences, Vol. 24, No. 11, pp. 805–812, November, 1957.

[46] Paulon, J., *The Control of Cascade Deflection by Blowing on the Trailing Edge*, R.A., No. 67, 1958.

[47] Le Grives, E., Fabri, J., and Paulon, J., *Design Diagrams for Supersonic Air Ejectors*, ONERA NT No. 35, 1956.

[48] Fabri, J., and Siestrunck, R., *Advances in Appl. Mech.*, "Supersonic Air Ejectors," Vol. V, 1958.

[49] Roy, Maurice, *Characteristics and Possibilities of the ONERA Test Centre at Modane-Avrieux (France)*, ONERA Publ. No. 85, 1956.

[50] Legendre, R., *Separation in Three-Dimensional Laminar Flows*, R.A., No. 54, 1956.

[51] Eichelbrenner, E. A., *Three-Dimensional Laminar Separation on a Finite Body*, ONERA Publ. No. 89, 1957.

[52] Eichelbrenner, E. A., and Michel, R., *Comparison Between Theoretical and Experimental Determination of the Transition Line in Three-Dimensional Flow*, IUTAM Symposium, Freiburg, 1957.

[53] Werle, H., *The Water-Tunnel for Visualization and Its Applications in Aerodynamics*, Assoc. Techn. Marit. et Aéron., Paris, 1957.

[54] Roy, Maurice, *Some Comments on Rotational Flow Around Swept Wings*, ZAMP, Vol. IXb, fasc. 5/6, 1958.

[55] Roy, Maurice, *Nozzles, Ejectors, Rockets and Projectiles*, Publ. Scient. et Techn. du Ministere de l'Air, No. 23, Paris, 1947.

[56] Guiraud, J. P., *Streamlines in a Newtonian Flow*, C.R. Ac. des Sciences, Vol. 247, p. 736, 1958.

[57] Guiraud, J. P., *Hypersonic Flow of a Perfect Fluid Over a Flat Plate of Finite Leading-Edge Thickness*, C.R. Ac. des Sciences, Vol. 246, p. 2842, 1958.

[58] Roy, Maurice, *Study Principles of the Jet Wing*, R.A., No. 52, p. 3, 1956.

[59] Legendre, R., *The Principle of Jet-Flap Study*, R.A., No. 53, p. 20, 1956.

[60] Malavard, L., *A Linear Theory on Blowing at the Trailing Edge of Airfoils*, C.R. Ac. des Sciences, May 14, 1956.

[61] Werle, H., *New Experimental Possibilities Offered by the Water Tunnel*, ONERA NT No. 48, 1958.

✦ ✦ ✦

Discussion of the Lecture

Hugh L. Dryden, Deputy Administrator, NASA: The lecture just delivered by our illustrious French colleague, whose personal friendship I enjoy and value highly, is a fitting memorial to Wilbur and Orville Wright in its presentation of the current valuable contributions to aeronautical knowledge of an outstanding scientific leader and his collaborators. On your behalf and mine, I express appreciation to Professor Roy for his lecture and ask him to extend our compliments also to the ONERA group on their accomplishments under his guidance.

Professor Roy speaks briefly of the new field which he terms "Cosmonautics" and we in the U.S. call "Space Science and Technology" or, in some quarters, "Astronautics." Had we had the courage to adopt his terminology, the new National Aeronautics and Space Administration might have retained the old NACA initials. Though we like many others dream of travel to the stars and throughout the cosmos, we felt that for some time to come our travels would be confined to our solar system and so avoided the grander implications of "cosmonautics." We in NASA agree fully with the stress placed on the continuing importance of aeronautics research.

I have been greatly impressed by the broad attack of ONERA, its fundamental research in materials, dynamics of structures, and aerodynamics, its novel applications of physical principles and ingenious instrumentation, and its bold experimentation. Its work has supplemented and complemented the work of NASA and similar research organizations in other countries with unique contributions, demonstrating anew that creativity and originality are not confined to any one group or country.

Being originally an aerodynamicist, I was especially interested in the work on transition and flow separation, particularly in the study of flow separation on three-dimensional bodies. The work on flow visualization and hypersonic theory is noteworthy.

The extensive work of ONERA on controlled and forced circulation by boundary-layer suction and blowing has long been known and admired. We are intrigued by Professor Roy's description and film of the Deltaviex experimental flying model, an excellent illustration of the bold experimentation to which I referred previously.

Finally, I would call your attention to the many evidences throughout the paper of the personal contributions of Professor Roy himself, ranging from hypersonic flow theory to the analysis of propulsion systems for STOL-VTOL aircraft and his concept of the turbojet with "polyvalent secondary flow" as the most suitable type of power plant for these applications, particularly for supersonic transports capable of vertical take-off. This personal scientific productivity of the leader is a key element in the notable record of ONERA contributions.

A. H. Flax, Vice-President—Technical Operations, Cornell Aeronautical Laboratory, Inc.: No one can fail to have been impressed, not only by the technical breadth and depth of Professor Roy's lecture, but also by the genuine enthusiasm with which he delivered it. In this respect, he is a worthy successor to Professor Panlevé, his countryman, to whom he alluded in his historical introduction. If I may add a note to this introduction, it is recorded[1] that on taking his first flight Panlevé was in high spirits and was waving and gesturing gaily to the assembled crowds before the take-off. In the course of so doing, he inadvertently pulled a rope Wilbur Wright used to stop the engine, thus adding a light touch to the proceedings. As Professor Roy has told us, however, they ultimately got off and made a record-breaking flight.

It is difficult to select, from so overwhelming a display of scientific and technical accomplishment as we have had put before us here, some particular points for detailed comment—one can hardly do justice to even a small number of the subjects mentioned. I shall limit myself to a few points bearing on fields of recent interest to myself and my colleagues.

The materials field steadily assumes increasing importance in all kinds of engineering endeavor. The need to work at higher temperatures, in nuclear and cosmic ray environments, and under high mean stress coupled with severe fatigue loadings has engendered seemingly impossible requirements for materials. The empirical routes of materials development, dating from the Bronze Age, although they have served well in the past, seem no longer sufficient for current technology. Application of the rational techniques of modern physics and mechanics to materials problems certainly seems to have been slower than the importance of the problem warrants. The study of X-ray spectra produced by electron beams for analysis of materials, which is discussed in the paper, can be a valuable step, not only for introducing new methods of microanalysis, but also for more intimately acquainting materials engineers with fundamental physical processes in solids. Hopefully, this could lead to larger benefits in the understanding of material properties. A development with parallel implications in this country has been the recent application of electron paramagnetic resonance measurements to studies of polymerization and depolymerization of plastics.[2] It is clear that there is much more of this sort of thing to be done, and that it will be done in many countries.

The very high frequency fatigue machine reported on in the paper is an interesting development. Yet one cannot avoid suspecting that there must be high-frequency effects on fatigue properties, at least for some materials, so that such a machine cannot be used uncritically. On the other hand, the discovery and interpretation of such effects cannot but provide valuable information on the basic microscopic prop-

erties of materials, and is all to the good. The comprehensive survey of high-frequency phenomena in metals by Zener[3] suggests that this may become a most important tool in the hands of metal technologists.

The studies of crackling of cobalt during its phase changes have been paralleled in this country and Germany by investigations of sounds emitted by metals under stress.[4, 5] In the latter studies, attempts were made to analyze the results on a quantitative basis, with very limited success thus far. Yet here again is evidence of whole worlds of phenomena, either partly or wholly outside the range of human senses, but easily observable with modern instruments, entirely unexplored as to their engineering significance.

It is interesting that flight flutter testing, long viewed with fear and suspicion, following Von Schippe's ill-fated experiments, has now been generally accepted in France as it has been in this country. The French equipment for such work, displayed in the Figures, is indeed impressive even in the light of our own very considerable accomplishments in this field.

The energy method for the prediction of flutter speeds when a large number of degrees of freedom are involved, if I understand it correctly, cannot be more than a first improvement to the primitive energy method, since the modes are considered only in pairs for determination of relative amplitude and phase. Although such a method may have important specific applications it does not appear to be possible to violate the fundamental axiom of flutter analysis—that is, there is no royal road to the answer. When making flutter analyses by any method whatever,one always feels sure he is missing something, and the more approximate the method the worse this feeling becomes. The only relief for this unhappy feeling in difficult cases is recourse to wind-tunnel or flight tests.

In wind-tunnel techniques, I am willing to make something of an international trade with Professor Roy. I will buy his magnetic balance, and will sell him in return some of our automatic digital read-out equipment for pressure measurement, which eliminates the manometer photographs from the picture entirely.

The progress in three-dimensional boundary-layer theory and particularly its application to leading-edge separation on delta wings was especially interesting to me, since the subject has engaged our attention at Cornell Aero. Lab. for over 10 years now. Our first attempts to describe forces and moments on the basis of cross-flow theory were empirical and tentative, but remarkably successful for so small an effort. Subsequent efforts[6] to refine the concepts quickly led to the need for a choice between amassing vast quantities of empirical data and working up a detailed picture of the viscous flow around the leading edge. Under the press of other programs we actually did neither, but have favored the latter course. It is therefore gratifying that ONERA, and particularly Professor Roy, have undertaken this investigation and have made substantial progress. It is impossible to leave this subject without remarking on the flow visualization technique employed in these tests. Here one feels that the French talent for the esthetic component in science and technology has come to the fore. I have seen many methods for flow visualization, each having its own special utility and some producing rather striking pictures. But rarely have I seen such beautiful pictures which at the same time provided valuable new information on the details of the flow.

Viewing the lecture as a whole, it is difficult to escape the feeling that there is far less information exchange and cooperation between ourselves and the French than there should be. In some respects, the connections have been good, particularly where AGARD has been involved, but in other things we are working on the same problems, but might as well be on different planets. The barriers of geography, language, national pride, and military security are formidable, but not insurmountable. No one who has heard this lecture can go away with the feeling that we have a monopoly on scientific and technical ingenuity this side of the Iron Curtain. It should be clear to all that, in the difficult and exciting days which are ahead, all the talents which we and our friends can command will be needed. This paper has not only exposed what has been done in the past but has also pointed up how valuable the French contribution might be in the future.

References

[1] Kelly, Fred C., *The Wright Brothers*, Harcourt, Brace & Co., New York, 1943.

[2] Jain, P. L., *Paramagnetic Resonance in High Polymers*, J. Polymer Sci., Vol. 31, p. 210, 1958.

[3] Zener, C., *Elasticity and Anelasticity of Metals*, University of Chicago, 1948.

[4] Mason, W. P., McSkimin, H. J., and Shockley, W., *Ultrasonic Observation of Twinning in Tin*, Physical Review, Vol. 73, No. 10, p. 1213–1214, May, 1948.

[5] Schofield, B. H., Bareiss, R. A., and Kyrala, A. A., *Acoustic Emission Under Applied Stress*, WADC TR 58-194, April, 1958.

[6] Bartlett, G. E., and Vidal, R. J., *Experimental Investigation of Influence of Edge Shape on the Aerodynamic Characteristics of Low Aspect Ratio Wings at Low Speeds*, Journal of the Aeronautical Sciences, Vol. 22, No. 8, pp. 517–533, 588, August, 1955.

John J. Green, Defence Research Member, Canadian Joint Staff, and Defence Research Attaché, Canadian Embassy: I was most pleased and honored to be invited to join with Dr. Dryden and Mr. Flax in discussing this Twenty-Second Wright Brothers Lecture. Professor Roy and I have been associated in the work of AGARD ever since its creation in 1951, and I like to think that some of the work of ONERA which Professor Roy has discussed today had its inspiration in the panels and committees of AGARD. If this is indeed the case, then it is most appropriate that Professor Roy should be giving the Wright Brothers Lecture this year because much of the inspiration generated by AGARD stems from the great support given to it by the United States.

This is the first time that a Frenchman has been chosen to deliver this most important lecture. This

too is appropriate, for when the great accomplishments of the Wright brothers became known, France was soon in the forefront of development and achievement, and the early history of aviation is bright with the names of famous French pioneers. These men too were no doubt inspired by the triumph of the Wright brothers and especially by the demonstration flights and record-breaking performances of Wilbur Wright at Le Mans in 1908, to which Professor Roy has referred in his lecture.

The history of French aeronautics reveals much more than the flair for aircraft design possessed by French engineers. There is an unorthodoxy—an individualism if you will—which suggests the search for elegant solutions free of compromise. The lecture we have heard today suggests very strongly to me that this same imaginative, unconventional approach is manifest in French aeronautical science. Throughout Professor Roy's talk there are many examples of this search for new techniques to replace traditional methods. At the risk of being considered indiscriminate, I will mention one or two examples which appealed to me particularly. The elegant approach employed in flight research into aircraft structural vibration and damping is most commendable, as are the various aerodynamic techniques for the investigation of problems both in the wind tunnel and in flight. I was intrigued, too, by the unique magnetic suspension for wind-tunnel models, which perhaps should be named the "hobo" method—it has no visible means of support.

Professor Roy referred to the "unceasing development of wind tunnels of all types" at ONERA. I should perhaps caution him here that he might find himself in the position in which G. W. Lewis of the NACA found himself a number of years ago. The story goes that Dr. Lewis was escorting a distinguished British visitor around Langley Field, showing him one wind tunnel after another. Since the visitor made no comments and maintained what was becoming an awkward silence, Dr. Lewis at length ventured to ask him what he thought of it all, to which, so the story goes, the visitor replied, "A vulgar display of wind tunnels."

It is significant to me that Professor Roy's lecture concludes with a discussion of some of the French work on STOL/VTOL aircraft, for, to my mind, practical progress in this aspect of flight is the greatest challenge today to the aeronautical engineer. There is no shortage of power, but to apply this efficiently, sagaciously, and perhaps quietly in order to shorten the take-off and landing run of aircraft would have a more profound effect on aviation than almost any other development has had in a history brief in years but studded with brilliant achievement. All countries with aeronautical capability seem to be taking up the challenge, and I am glad to say that my own country, Canada, is making some contributions. On December 10, 1958, a Canadian designed aircraft, the De Havilland "Caribou," the fully loaded weight of which is about 25,000 lbs., was demonstrated at Fort Myer—landing and taking off from the same place that Orville Wright had flown from in September, 1908, to which Professor Roy referred in his opening remarks. Your newspapers said it "stopped on a dime." This may be a slight exaggeration. Flying at about 22,000 lbs. gross weight, it appeared to me to take-off and land in a distance of about 250 ft.

It would seem that the short take-off and landing aircraft has arrived and that it now remains for us to press on towards even more ambitious performances. There is room here for great ingenuity and much research effort, and neither of these are lacking on this continent or in Europe. The work at ONERA and elsewhere in France is excellent in this regard.

It is a pleasure to thank Professor Roy and to compliment him on his distinguished address.

Advances in Aeronautical Science

Proceedings of the First International Congress of the Aeronautical Sciences, Madrid, 1958 (2 Vols.)

In these two volumes are published the 46 papers presented by the world's outstanding specialists in the field of aeronautics and astronautics at the First International Congress of the Aeronautical Sciences held in Madrid in September, 1958, under the leadership of Prof. Theodore von Kármán. Some 600 delegates from 25 countries, including an official delegation from the U.S.S.R., attended, and the meeting was so successful that it was decided to hold similar congresses at 2-year intervals in future.

The volumes will have a full author and subject index and number 1,200 pages. The *Proceedings*, edited by Th. von Kármán, A. M. Ballantyne, H. Blenk, R. R. Dexter, M. Roy, and H. L. Dryden, are of special interest to aerodynamicists, aeronautical engineers, rocketry research workers, and propulsion engineers.

The *Proceedings* (price, $25.00) may be obtained by writing to: *Sales Director, Pergamon Press, Inc., 122 East 55 St., New York.*

Thermal Stresses and Deflections in Rectangular Sandwich Plates†

P. P. BIJLAARD*

Bell Aircraft Corporation

SUMMARY

Assuming the temperature of the upper surface of a rectangular sandwich plate to be T°F. higher than that of the lower one, equations are developed for bending and torsional moments and transverse shear forces. Special attention is paid to the required edge reactions.

Except for cases where all edges are clamped or all edges are simply supported, transverse shear forces occur, so that the shear deformation of the core has to be considered. Plates with two opposite edges simply supported and the other two free or clamped are dealt with. Also, the case where three edges are simply supported and the fourth edge is free is computed. Graphs of some numerical results are presented.

SYMBOLS

a	= length of plate in the X-direction
b	= length of plate in the Y-direction
m	= integer number
p_m	= given by Eq. (42)
t	= total thickness of sandwich plate
t_c	= thickness of core
t_f	= thickness of faces
w	= deflection, positive if downwards
x, y	= coordinates
$A_m, B_m, C_m, D_m, E_m, F_m$	= constants
B_1	= upward force to be exerted by corner bolt
D	= flexural rigidity of sandwich plate
$D_{Q_n, t, x, y}$	= shear stiffness of sandwich plate with respect to shear force $Q_{n, t, x, y}$
E	= elastic modulus of faces
G	= modulus of rigidity of core
I	= moment of inertia
$M_{n, t, x, y}$	= bending moment per unit width
M_{xy}	= torsional moment per unit width
$M_{\mathrm{I, II}}$	= moment per unit width in Sections I and II
$\bar{M}_{\mathrm{I, II}}$	= average moment per unit width
$Q_{n, t, x, y}$	= transverse shear force per unit width
R	= concentrated reactions at corners of plate
T	= excess temperature of upper with respect to lower surface if thermal gradient is T/t; equal to $[t/(t_c + t_f)]T_a$ if gradient is arbitrary
T_a	= difference between average temperatures in the two faces
T_2	= tensile force in attaching bolt
$V_{x, y}$	= statically equivalent reaction per unit length of edge
X, Y	= coordinate axes
Y_m, Y_{xm}, Y_{ym}	= functions of y only
α	= coefficient of thermal expansion
α_m	= $m\pi b/2a$
β_m	= $m\pi b/a$
γ_m	= $p_m b/2$
δ_m	= $p_m b$
λ_m	= $m\pi/a$
ν	= Poisson's ratio

Subscripts

x, y	refers to the X- and Y-directions
n, t	refers to the directions normal and tangential to edge

INTRODUCTION

THE TEMPERATURE of the upper surface is assumed to be T°F. higher than that of the lower one, but it is assumed not to vary in the X- and Y-directions. The thermal gradient in the faces is assumed as T/t. The gradient in the core is immaterial, since the normal stresses σ_x and σ_y in the core are neglected, as are those perpendicular to the middle surface. In cases where the transverse thermal gradient in the faces is different from T/t, T can be considered to be equal to $[t/(t_c + t_f)]\ T_a$, where T_a is the difference between the average

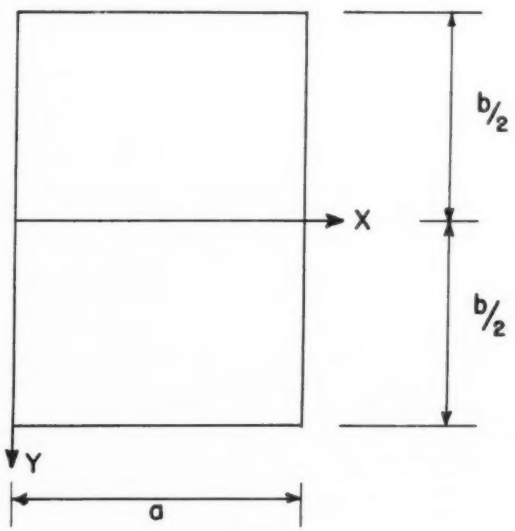

FIG. 1.

Presented at the Structures—High-Temperature Effects Session, 26th Annual Meeting, IAS, New York, January 27–30, 1958.

† This is part of a study undertaken by the author at the request of Bell Aircraft Corp. The author wishes to thank Bell Aircraft Corp. for permission to publish these results; Arthur Schnitt, then Assistant Manager, Development Analysis Department, Special Weapons Division, for clearly defining the problem and for his helpful advice; and Alexander Krivetsky, Head, Internal Research Group of the Structures Research Section, for supplying the graphs in Figs. 5 and 6.

* Consultant. Also, Professor of Mechanics, Cornell University.

temperatures in the two faces. The plate is assumed to be free to expand in its plane. The proper flexural rigidities of the faces are neglected.

The sign convention is similar to that in reference 1. The cases where all edges are clamped or simply supported lead to similar results as for homogeneous plates,[1] where deflections from transverse shear are neglected, since here the transverse shear forces appear to be zero. However, these results are considered in more detail, and it is shown that for all edges simply supported the concentrated corner reactions R are infinite. A method is given for computing the actual, finite force in the attaching corner bolt. In the other three cases, with two opposite edges simply supported and the other two edges free, or clamped, and that with three edges simply supported and the fourth one free, the shear deflections are taken into account, and formulas are derived for all important magnitudes, especially the edge reactions and the concentrated corner reactions.

Plate Clamped at Four Edges

A similar case for homogeneous plates is treated in reference 1, p. 54. The equally distributed clamping moments at all sides are

$$M_n = \alpha T D(1 + \nu)/t \tag{1}$$

so that the curvature produced by the nonuniform heating is eliminated over the entire plate. This leads to bending moments

$$M_x = M_y = M_n \tag{2}$$

over the entire plate (see Fig. 1), and twisting moments M_{xy} and transverse shear forces Q_x and Q_y equal to zero.

From reference 2, for a clamped sandwich plate three boundary conditions have to be satisfied. Assuming the sandwich plate to be supported over the entire thickness, they are

$$w = 0, \quad (\partial w/\partial n) - (Q_n/D_{Q_n}) = 0, \quad Q_t/D_{Q_t} = 0 \tag{3}$$

Since $Q_n = Q_t = 0$, for the homogeneous plate these conditions are also satisfied, and, since over the entire plate $Q_x = Q_y = 0$, a clamped sandwich plate will behave exactly as a homogeneous one. The bending moments are given by Eqs. (1) and (2), where D is now the flexural rigidity of the sandwich plate (shown in cross section in Fig. 2), so that

$$D = Et_f(t_c + t_f)^2/2(1 - \nu^2) \tag{4}$$

Plate Simply Supported at Four Edges

The same case for a homogeneous plate is treated in reference 1, pp. 176–180. It is found that for the deflection w the following differential equation holds:

$$\nabla^2 w = (\partial^2 w/\partial x^2) + (\partial^2 w/\partial y^2) = \alpha T(1 + \nu)/t \tag{5}$$

Hence, the transverse shear forces are

$$\left.\begin{aligned} Q_x &= -D(\partial/\partial x)\nabla^2 w = 0 \\ Q_y &= -D(\partial/\partial y)\nabla^2 w = 0 \end{aligned}\right\} \tag{6}$$

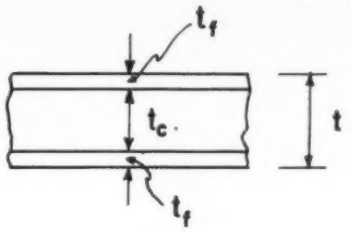

Fig. 2.

For a simply supported sandwich plate, the three boundary conditions are

$$M_n = 0, \quad w = 0, \quad Q_t = 0 \tag{7}$$

which are also satisfied for the homogeneous plate. Hence, for the sandwich plate, $Q_x = Q_y = 0$ also, so that it behaves as a homogeneous plate. Therefore, from Eq. (j) on p. 178 of reference 1,

$$w = -\frac{4\alpha T(1 + \nu)a^2}{\pi^3 t} \sum_{m=1,3,5,\ldots}^{\infty} \frac{\sin(m\pi x/a)}{m^3} \times \left[1 - \frac{\cosh(m\pi y/a)}{\cosh \alpha_m}\right] \tag{8}$$

and, from Eqs. (k) on p. 179,

$$\left.\begin{aligned} M_x &= \frac{4\alpha T(1 - \nu^2)D}{\pi t} \times \sum_{m=1,3,5,\ldots}^{\infty} \frac{\sin(m\pi x/a)\cosh(m\pi y/a)}{m \cosh \alpha_m} \\ M_y &= \frac{\alpha T(1 - \nu^2)D}{t} - \frac{4\alpha T(1 - \nu^2)D}{\pi t} \times \sum_{m=1,3,5,\ldots}^{\infty} \frac{\sin(m\pi x/a)\cosh(m\pi y/a)}{m \cosh \alpha_m} \end{aligned}\right\} \tag{9}$$

where D is now given by Eq. (4). The bending moments are maximum at the edges,

$$(M_x)_{y=\pm b/2} = (M_y)_{x=0,\, x=a} = \alpha T(1 - \nu^2)D/t = Et_f(t_c + t_f)^2\alpha T/2t \tag{10}$$

For practical applications, it is important to find the required strength of the attachments that connect the edges of the plate to its supports. From Eq. (8), the twisting moments are

$$M_{xy} = (1 - \nu^2)D\frac{\partial^2 w}{\partial x \partial y} = \frac{4\alpha T(1 - \nu^2)D}{\pi t} \times \sum_{m=1,3,5,\ldots}^{\infty} \frac{\cos(m\pi x/a)\sinh(m\pi y/a)}{m \cosh \alpha_m} \tag{11}$$

M_{xy} is maximum at the corners. For example,

$$(M_{xy})_{x=0,\, y=b/2} = [4\alpha T(1 - \nu^2)D/\pi t] \times \sum_{m=1,3,5,\ldots}^{\infty} (\tanh \alpha_m/m) \tag{12}$$

so that M_{xy} becomes infinite in the corners. Assuming that the plate is supported such that the attachments (bolts) can only transmit forces perpendicular to its middle plane, concentrated reactions R are exerted at

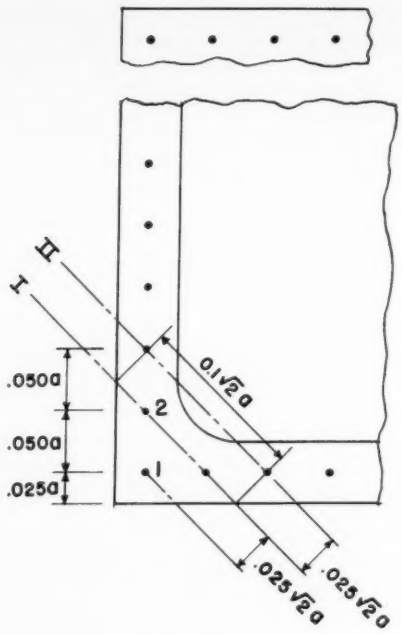

FIG. 3.

the corners, for example,

$$(R)_{x=0,\ y=b/2} = 2(M_{xy})_{x=0,\ y=b/2} \tag{13}$$

and these reactions are directed upwards. Hence, the forces R are infinite. From Eqs. (6) and (11), for example, for the edge $x = 0$, the statically equivalent reactions, continuously distributed along the edge and considered positive if acting upwards, are

$$(V_x)_{x=0} = [Q_x - (\partial M_{xy}/\partial y)]_{x=0} = -[4\alpha T(1-\nu^2)D/at] \sum_{m=1,3,5,\ldots}^{\infty} \times [\cosh(m\pi y/a)/\cosh\alpha_m] \tag{14}$$

Their minimum absolute value occurs at $y = 0$. For $b = a$ and using Eq. (4),

$$(V_x)_{x=0,\ y=0} = -[2Et_f(t_c+t_f)^2\alpha T/at] \times \sum_{m=1,3,5,\ldots}^{\infty} [1/\cosh(m\pi/2)] = -0.84[Et_f(t_c+t_f)^2\alpha T/at] \tag{15}$$

At the corners, say at $y = b/2$,

$$(V_x)_{x=0,\ y=a/2} = -[2Et_f(t_c+t_f)^2\alpha T/at] \times \sum_{m=1,3,5,\ldots}^{\infty} (\cosh\alpha_m/\cosh\alpha_m) \tag{16}$$

which is infinite.

Actually, in practical cases, R and V_x will not lead to infinite forces in the attachments. For a square plate ($b = a$) let the attachment be effected by bolts as shown in the neighborhood of the corner $x = 0$, $y = b/2 = a/2$ in Fig. 3. Then the force in the corner, which can be concentrated in the corner bolt and is compressive, has to be in equilibrium with the total downward load exerted by the tensile force in the bolts from $y = 0$ to $y = 0.45\,b = 0.45\,a$ and from $x = 0.05\,a$ to $x = 0.50\,a$. Hence the upward force to be exerted by bolt 1 (Fig. 3) is

$$B_1 = -\int_0^{0.45a} (V_x)_{x=0}\,dy + \int_{0.05a}^{0.50a} (V_y)_{y=0.50a}\,dx \tag{17}$$

where, since $M_{yx} = -M_{xy}$,

$$\int_0^{0.45a} (V_x)_{x=0}dy = -\int_0^{0.45a} (\partial M_{xy}/\partial y)_{x=0}\,dy = -(M_{xy})_{x=0,\ y=0.45a}$$

$$\int_{0.05a}^{0.50a} (V_y)_{y=0.50a}\,dx = \int_{0.05a}^{0.50a} (\partial M_{yx}/\partial x)_{y=0.50a}\,dx = (M_{xy})_{\substack{y=0.50a\\x=0.05a}} - (M_{xy})_{\substack{y=0.50a\\x=0.50a}}$$

Hence, from Eqs. (11) and (17),

$$B_1 = \frac{4\alpha T(1-\nu^2)D}{\pi t} \times \left[\sum_{m=1,3,5,\ldots}^{\infty} \frac{\sinh 0.45m\pi}{m\cosh 0.5m\pi} + \sum_{m=1,3,5,\ldots}^{\infty} \frac{\cos 0.05m\pi\tanh 0.5m\pi}{m}\right] \tag{18}$$

$$= 9.48\alpha T(1-\nu^2)D/\pi t = 1.51[Et_f(t_c+t_f)^2\alpha T/t] \tag{19}$$

The tensile forces in the other bolts can be calculated assuming that they take the downward forces $-(V_x)_{x=0}$ or $(V_y)_{y=0.50a}$. For example, bolt 2 in Fig. 3 has to exert a tensile force

$$T_2 = -\int_{0.40a}^{0.45a} (V_x)_{x=0}\,dy = (M_{xy})_{x=0,\ y=0.45a} - (M_{xy})_{x=0,\ y=0.40a} \tag{20}$$

where M_{xy} is given by Eq. (11).

Also, M_{xy} does not actually become infinite in the corners. The highest moments occur in sections I or II in Fig. 3. In section I the total moment is $0.025\sqrt{2}aB_1$, or per unit width an average

$$\bar{M}_{\mathrm{I}} = 0.025\sqrt{2}\,aB_1/0.1\sqrt{2}\,a = (1/4)B_1 = 0.38[Et_f(t_c+t_f)^2\alpha T/t] \tag{21}$$

which is smaller than M_x or M_y from Eq. (10). From Eq. (20), $T_2 = 0.22[Et_f(t_c+t_f)^2\alpha T/t]$. Hence, the average bending moment in section II is, from Fig. 3,

$$\bar{M}_{\mathrm{II}} = [0.05\sqrt{2}aB_1 - 0.025\sqrt{2}\,a(2T_2)]/0.15\sqrt{2}\,a = 0.43[Et_f(t_c+t_f)^2\alpha T/t] \tag{22}$$

Further sections get smaller average moments. The moments M_x and M_y from Eq. (10) cause at the ends of section II bending moments $M_{\mathrm{II}e}$ of half the value given in Eq. (10). Assuming a parabolic moment distribution in section II, the maximum moment $M_{\mathrm{II}\,max}$ in its center follows from the condition

$$M_{\mathrm{II}e} + (2/3)(M_{\mathrm{II}\,max} - M_{\mathrm{II}e}) = \bar{M}_{\mathrm{II}}$$

or

$$\left.\begin{aligned} M_{\mathrm{II}\,max} &= (1/2)(3\bar{M}_{\mathrm{II}} - M_{\mathrm{II}e}) = (1/2) \times (1.29 - 0.25)[Et_f(t_c+t_f)^2\alpha T/t] \\ &= 0.52[Et_f(t_c+t_f)^2\alpha T/t] \end{aligned}\right\} \tag{23}$$

being practically equal to the maximum bending moments M_x or M_y from Eq. (10).

Plate Simply Supported at Two Opposite Edges and Free at the Other Two Edges

In a similar way as for a homogeneous plate, for a plate clamped at all sides the equally distributed clamping moments would be given by Eq. (1). For a sandwich plate D is determined by Eq. (4). To obtain the case where in Fig. 1 the edges $x = 0$, $x = a$ are simply supported and the edges $y = \pm b/2$ are free, edge moments $M_n = -\alpha TD(1 + \nu)/t$ have to be superimposed along all edges, so that, for the case superimposed upon that of the plate clamped at all sides, for the edges $x = 0$, $x = a$ the boundary conditions are

$$M_x = -\alpha TD(1 + \nu)/t, \quad w = 0, \quad Q_y = 0 \tag{24}$$

while, for the edges $y = \pm b/2$,

$$M_y = -\alpha TD(1 + \nu)/t, \quad M_{yx} = 0, \quad Q_y = 0 \tag{25}$$

The expressions, given in reference 2 for the bending and twisting moments, contain the shear stiffness D_{Qx} and D_{Qy}. From reference 3, for a sandwich plate with an isotropic core,

$$D_{Q_x} = D_{Q_y} = G[(t_c + t_f)^2/t_c]$$

Since $t_f \ll t_c$, this can be written as

$$D_{Q_x} = D_{Q_y} = G[(t_c^2 + 2t_c t_f)/t_c] = G(t_c + 2t_f) = Gt \tag{26}$$

Using this expression, from p. 27 of reference 2,

$$\left.\begin{aligned} M_x &= -D\{(\partial^2 w/\partial x^2) + \nu(\partial^2 w/\partial y^2) - (1/Gt)\,[(\partial Q_x/\partial x) + \nu(\partial Q_y/\partial y)]\} \\ M_y &= -D\{(\partial^2 w/\partial y^2) + \nu(\partial^2 w/\partial x^2) - (1/Gt)\,[(\partial Q_y/\partial y) + \nu(\partial Q_x/\partial x)]\} \\ M_{xy} &= [(1 - \nu)/2]D\{2(\partial^2 w/\partial x \partial y) - (1/Gt)\,[(\partial Q_x/\partial y) + (\partial Q_y/\partial x)]\} \end{aligned}\right\} \tag{27}$$

Inserting Eqs. (27) in the equation of equilibrium

$$(\partial^2 M_x/\partial x^2) - 2(\partial^2 M_{xy}/\partial x \partial y) + (\partial^2 M_y/\partial y^2) = 0 \tag{28}$$

one obtains

$$\nabla^4 w = 0 \tag{29}$$

as for a homogeneous plate. Eq. (29) is in accordance with Eq. (79) of reference 4, since in the present case $q = m_x = m_y = 0$.

In order to satisfy, besides Eq. (29), the first condition (24), the deflection w is assumed as

$$w = -[\alpha T(1 + \nu)/t]\,[x(a - x)/2] + \sum_{m=1,3,5,\ldots}^{\infty} Y_m \sin \lambda_m x \tag{30}$$

where

$$\lambda_m = \pi m/a \tag{31}$$

Eq. (30) satisfies the second condition (24). At $x = 0$ and $x = a$, from Eq. (24) $\partial^2 w/\partial y^2 = 0$ and $\partial Q_y/\partial y = 0$, so that from Eqs. (27) and (30), at these edges,

$$M_x = -[\alpha TD(1 + \nu)/t] + (D/Gt)\,(\partial Q_x/\partial x) \tag{32}$$

Since Q_x is antisymmetrical with respect to the line $x = a/2$, let

$$Q_x = \sum_{m=1,3,5,\ldots}^{\infty} Y_{xm} \cos \lambda_m x \tag{33}$$

so that

$$\partial Q_x/\partial x = -\sum_{m=1,3,5,\ldots}^{\infty} Y_{xm}\lambda_m \sin \lambda_m x$$

Hence, at $x = 0$ and $x = a$, $\partial Q_x/\partial x = 0$, so that from Eq. (32) the first condition (24) is indeed satisfied. With

$$Q_y = \sum_{m=1,3,5,\ldots}^{\infty} Y_{ym} \sin \lambda_m x \tag{34}$$

the third condition (24) is also satisfied.

Since the first term of Eq. (30) vanishes after applying the operation ∇^4 to it, insertion of Eq. (30) in the differential equation (29) leads in the usual way (see reference 1, p. 127) to the solution

$$Y_m = A_m \cosh \lambda_m y + B_m \lambda_m y \sinh \lambda_m y + C_m \sinh \lambda_m y + D_m \lambda_m y \cosh \lambda_m y \tag{35}$$

From symmetry about the X-axis $C = D = 0$, so that

$$w = -[\alpha T(1 + \nu)/t]\,[x(a - x)/2] + \sum_{m=1,3,5,\ldots}^{\infty} (A_m \cosh \lambda_m y + B_m \lambda_m y \sinh \lambda_m y) \sin \lambda_m x \tag{36}$$

To find expressions for Y_{xm} and Y_{ym} it is observed that

$$Q_y = (\partial M_y/\partial y) - (\partial M_{xy}/\partial x) \tag{37}$$

Further, since the transverse load $q = 0$,

$$(\partial Q_x/\partial x) + (\partial Q_y/\partial y) = 0 \tag{38}$$

Using Eqs. (27) and (38), Eq. (37) becomes, after rearranging,

$$Q_y - [(1 - \nu)D/2Gt]\,[(\partial^2 Q_y/\partial x^2) + (\partial^2 Q_y/\partial y^2)] = -D(\partial/\partial y)\,[(\partial^2 w/\partial x^2) + (\partial^2 w/\partial y^2)] \tag{39}$$

whence, after insertion of Eqs. (34) and (36),

$$(d^2 Y_{ym}/dy^2) - \{\lambda_m^2 + [2Gt/(1 - \nu)D]\}\,Y_{ym} = [4Gt/(1 - \nu)]\lambda_m^3 B_m \sinh \lambda_m y \tag{40}$$

Letting $Y_{ym} = e^{py}$ and taking account of the fact that Q_y, and therefore Y_{ym}, is antisymmetrical about the X-axis, the solution of the homogeneous part of Eq. (40) becomes

$$Y_{ym1} = E_m \sinh p_m y \tag{41}$$

where

$$p_m = \{\lambda_m^2 + [2Gt/(1 - \nu)D]\}^{1/2} \tag{42}$$

The particular integral is found by assuming

$$Y_{ym2} = F_m \sinh \lambda_m y \tag{43}$$

which, after insertion into Eq. (40), gives

$$F_m = -2\lambda_m^3 DB_m \tag{44}$$

so that

$$Y_{ym} = E_m \sinh p_m y + F_m \sinh \lambda_m y \qquad (45)$$

With Eqs. (44) and (45), Eq. (34) becomes

$$Q_y = \sum_{m=1,3,5,\ldots}^{\infty} (E_m \sinh p_m y - 2\lambda_m{}^3 D B_m \sinh \lambda_m y) \sin \lambda_m x \qquad (46)$$

Inserting Eqs. (33) and (34) into Eq. (38) leads to

$$\left.\begin{aligned} Q_x &= \sum_{m=1,3,5,\ldots}^{\infty} (1/\lambda_m)\,(dY_{ym}/dy) \cos \lambda_m x \\ &= \sum_{m=1,3,5,\ldots}^{\infty} [E_m(p_m/\lambda_m) \cosh p_m y - 2\lambda_m{}^3 D B_m \cosh \lambda_m y] \cos \lambda_m x \end{aligned}\right\} \qquad (47)$$

The constants A_m, B_m, and E_m in Eqs. (36), (46), and (47) have to be determined from the boundary conditions (25). From the third condition (25) and from Eq. (46),

$$E_m = (2\lambda_m{}^3 D \sinh \alpha_m / \sinh \gamma_m) B_m \qquad (48)$$

where

$$\alpha_m = \lambda_m(b/2); \quad \gamma_m = p_m(b/2) \qquad (49)$$

From the second condition (25) and from Eq. (27), at $y = b/2$,

$$2(\partial^2 w/\partial x \partial y) - (1/Gt)\,[(\partial Q_x/\partial y) + (\partial Q_y/\partial x)] = 0$$

so that, after using Eqs. (36), (46), and (47),

$$2\lambda_m{}^2[(A_m + B_m) \sinh \alpha_m + B_m \alpha_m \cosh \alpha_m] = (1/Gt\lambda_m)\,[E_m(p_m{}^2 + \lambda_m{}^2) \sinh \gamma_m - 4\lambda_m{}^5 D B_m \sinh \alpha_m]$$

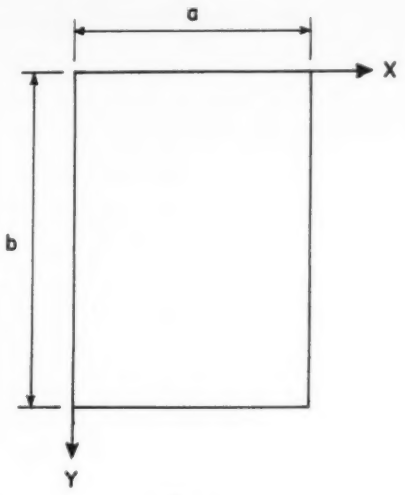

FIG. 4.

Expressing E_m in terms of B_m from Eq. (48), A_m can be expressed in terms of B_m, which gives

$$A_m = \{[(1 + \nu)/(1 - \nu)] - \alpha_m \coth \alpha_m\} B_m \qquad (50)$$

Finally, using Eqs. (27) and (38), the first condition (25) requires that, for $y = b/2$,

$$-D\{(\partial^2 w/\partial y^2) + \nu(\partial^2 w/\partial x^2) - [(1 - \nu)/Gt]\,(\partial Q_y/\partial y)\} = -[\alpha T D(1 - \nu)/t]$$

Using Eqs. (36) and (46) and expressing $\alpha TD(1 + \nu)/t$ as

$$\alpha TD(1 + \nu)/t = (4/\pi)\,[\alpha TD(1 + \nu)/t] \sum_{m=1,3,5,\ldots}^{\infty} (\sin \lambda_m x/m) \qquad (51)$$

results in the condition

$$\lambda_m{}^2\{(1 - \nu)A_m + \{2 + [2(1 - \nu)/Gt]\lambda_m{}^2 D\} B_m\} \cosh \alpha_m + \lambda_m{}^2(1 - \nu)\alpha_m B_m \sinh \alpha_m - [(1 - \nu)/Gt]E_m p_m \cosh \gamma_m = [4(1 - \nu)/\pi m]\,[\alpha T(1 + \nu)/t]$$

Since from Eqs. (48) and (50) E_m and A_m can be expressed in terms of B_m, with the use of Eq. (42) this yields

$$B_m = \frac{8\alpha(1 - \nu^2)T}{\lambda_m{}^3 at} \times \frac{\sinh \alpha_m}{\left[3 + \nu + 2(1 - \nu)\lambda^2{}_m \dfrac{D}{Gt}\right] \sinh 2\alpha_m - 2(1 - \nu)\alpha_m - \dfrac{2\lambda_m(1 - \nu)D}{Gt}\left[\lambda_m{}^2 + \dfrac{2Gt}{(1 - \nu)D}\right]^{1/2} \coth \gamma_m(\cosh 2\alpha_m - 1)} \qquad (52)$$

Taking account of the original moments $M_x = M_y = M_n$ from Eqs. (1), and using Eqs. (36), (38), (46), and (47), the resulting bending and twisting moments are

$$\begin{aligned} M_x &= [\alpha TD(1 + \nu)/t] - D\{(\partial^2 w/\partial x^2) + \nu(\partial^2 w/\partial y^2) - [(1 - \nu)/Gt]\,(\partial Q_x/\partial x)\} \\ &= D \sum_{m=1,3,5,\ldots}^{\infty} \big(\lambda_m{}^2\{[(1 - \nu)A_m - 2\nu B_m] \cosh \lambda_m y + (1 - \nu)B_m \lambda_m \sinh \lambda_m y\} + \\ &\qquad [(1 - \nu)/Gt]\,(E_m p_m \cosh p_m y - 2\lambda_m{}^4 D B_m \cosh \lambda_m y)\big) \sin \lambda_m x \qquad (53) \end{aligned}$$

$$\begin{aligned} M_y &= [\alpha TD(1 + \nu)/t] - D\{(\partial^2 w/\partial y^2) + \nu(\partial^2 w/\partial x^2) + [(1 - \nu)/Gt]\,(\partial Q_x/\partial x)\} \\ &= [\alpha TD(1 - \nu^2)/t] - D \sum_{m=1,3,5,\ldots}^{\infty} \big(\lambda_m{}^2\{[(1 - \nu)A_m + B_m] \cosh \lambda_m y + (1 - \nu)B_m \lambda_m y \sinh \lambda_m y\} - \\ &\qquad [(1 - \nu)/Gt]\,(E_m p_m \cosh p_m y - 2\lambda_m{}^4 D B_m \cosh \lambda_m y)\big) \sin \lambda_m x \qquad (54) \end{aligned}$$

$$M_{xy} = [(1 - \nu)/2]D\{2(\partial^2 w/\partial x\partial y) - (1/Gt)\,[(\partial Q_x/\partial y) + (\partial Q_y/\partial x)]\}$$

$$= (1 - \nu)D \sum_{m=1,3,5,\ldots}^{\infty} \{\lambda_m{}^2[(A_m + B_m)\sinh \lambda_m y + B_m\lambda_m y \cosh \lambda_m y] -$$

$$(1/2\lambda_m Gt)\,[E_m(p_m{}^2 + \lambda_m{}^2)\sinh p_m y - 4\lambda_m{}^5 DB_m \sinh \lambda_m y]\} \cos \lambda_m x \quad (55)$$

From Eqs. (25), at the free edges $M_{yx} = 0$, so that at all corners the concentrated reactions $R = \pm 2\,M_{yx}$ are zero. Using Eqs. (47) and (55) the tensile forces per unit length along the edges $x = 0$ and $x = a$ that have to be transferred by the attaching bolts are, for example, for $x = 0$,

$$-(V_x)_{x=0} = -[Q_x - (\partial M_{xy}/\partial y)]_{x=0}$$

$$= (1 - \nu)D \sum_{m=1,3,5,\ldots}^{\infty} \lambda_m{}^3[(A_m + 2B_m)\cosh \lambda_m y + B_m\lambda_m y \sinh \lambda_m y] +$$

$$2 \sum_{m=1,3,5,\ldots}^{\infty} B_m D\lambda_m{}^3\{[(1 - \nu)D/Gt]\lambda_m{}^2 + 1\}\cosh \lambda_m y -$$

$$\sum_{m=1,3,5,\ldots}^{\infty} E_m(p_m/\lambda_m)\{[(1 - \nu)D/Gt]\lambda_m{}^2 + 2\}\cosh p_m y$$

or, using Eqs. (48) and (50),

$$-(V_x)_{x=0} = D \sum_{m=1,3,5,\ldots}^{\infty} B_m\lambda_m{}^3\,(\{5 - \nu - (1 - \nu)\alpha_m \coth \alpha_m + [2(1 - \nu)D\lambda_m{}^2/Gt]\}\cosh \lambda_m y +$$

$$(1 - \nu)\lambda_m y \sinh \lambda_m y - (2p_m \sinh \alpha_m/\lambda_m \sinh \gamma_m)\{[(1 - \nu)D\lambda_m{}^2/Gt] + 2\}\cosh p_m y) \quad (56)$$

Plate Simply Supported at Two Opposite Edges and Clamped at the Other Two Edges

If, in Fig. 1, the edges $x = 0, x = a$ are simply supported and the edges $y = \pm b/2$ are clamped, after assuming first all edges to be clamped, so that M_x and M_y become equal to M_n from Eq. (1), moments $M_x = -\alpha TD(1 + \nu)/t$ are superimposed along the edges $x = 0, x = a$. Then, for the superimposed case, the boundary conditions along these edges are given by Eq. (24), and along the edges $y = \pm b/2$, from Eq. (3),

$$w = 0, \quad (\partial w/\partial y) - (Q_y/Gt) = 0, \quad Q_x = 0 \quad (57)$$

From the boundary conditions (24) along $x = 0, x = a$, and symmetry of w about the X-axis, w, Q_y, and Q_x are given again by Eqs. (36), (46), and (47). Then, from the last condition (57),

$$E_m = (2\lambda_m{}^4 D \cosh \alpha_m/p_m \cosh \gamma_m)B_m \quad (58)$$

From the second condition (57) one obtains

$$A_m = \{[(2\lambda_m{}^3 D/p_m Gt)\tanh \gamma_m - \alpha_m]\coth \alpha_m - (2\lambda_m{}^2 D/Gt) - 1\}B_m \quad (59)$$

and finally from the first condition (57), with the substitution (51),

$$B_m = \frac{4\alpha(1 + \nu)T}{\lambda_m{}^3 at} \frac{1}{\{(2\lambda_m{}^3 D/p_m Gt)\,[\tanh \gamma_m \coth \alpha_m - (p_m/\lambda_m)] - 1\}\cosh \alpha_m - (\alpha_m/\sinh \alpha_m)} \quad (60)$$

With these constants M_x, M_y, M_{xy}, and $(V_x)_{x=0}$ follow from Eqs. (53)–(56). Using Eqs. (58) and (59), from Eq. (56)

$$-(V_x)_{x=0} = D \sum_{m=1,3,5,\ldots}^{\infty} B_m\lambda_m{}^3\,(\{(1 - \nu)\,[(2\lambda_m{}^3 D/Gtp_m)\tanh \gamma_m - \alpha_m]\coth \alpha_m + (3 - \nu)\}\cosh \lambda_m y +$$

$$(1 - \nu)\lambda_m y \sinh \lambda_m y - (2\cosh \alpha_m/\cosh \gamma_m)\{[(1 - \nu)D\lambda_m{}^2/Gt] + 2\}\cosh p_m y) \quad (61)$$

The tensile forces per unit length along the edges $y = b/2$ that have to be transferred by the attaching bolt are, using Eqs. (46), (55), (58), and (59),

$$(V_y)_{y=b/2} = [Q_y - (\partial M_{xy}/\partial x)]_{x=b/2} = -2D \sum_{m=1,3,5,\ldots}^{\infty} B_m\lambda_m{}^2 \sinh \alpha_m \sin \lambda_m x \quad (62)$$

The required downward concentrated forces R at the corners, for example, for $x = 0$, $y = b/2$, are

$$(R)_{x=0,\,y=b/2} = -2(M_{xy})_{x=0,\,y=b/2} = 4D \sum_{m=1,3,5,\ldots}^{\infty} B_m(\lambda_m{}^3/p_m)\cosh \alpha_m \tanh \gamma_m \quad (63)$$

From Eqs. (54), (58), and (59), the clamping moments along the edge $y = b/2$ are

$$(M_y)_{y=b/2} = [\alpha TD(1 - \nu^2)/t] - D \sum_{m=1,3,5,\ldots}^{\infty} (\lambda_m{}^2 B_m/\sinh \alpha_m)\{2(1 - \nu)\,(\lambda_m{}^3 D/p_m Gt)\tanh \gamma_m \cosh^2 \alpha_m -$$

$$(1 - \nu)\alpha_m + [1 + \nu - 2(1 - \nu)\,(\lambda_m{}^2 D/Gt)]\sinh \alpha_m \cosh \alpha_m\} \sin \lambda_m x \quad (64)$$

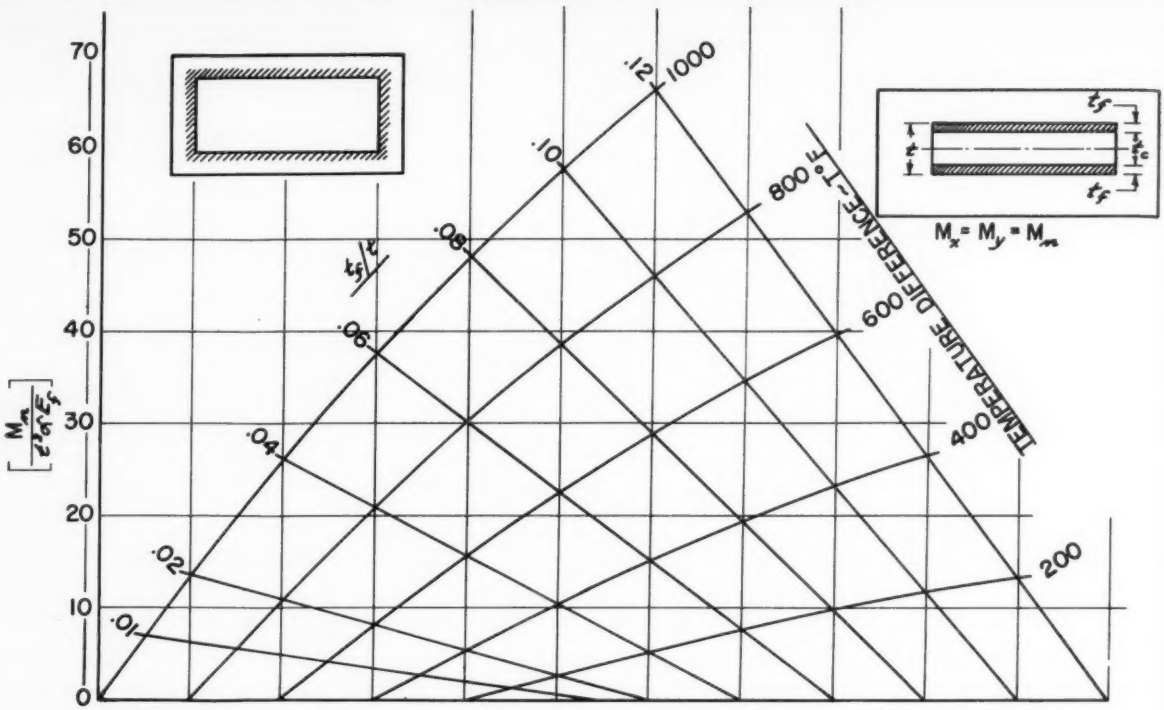

FIG. 5. Moment loading per unit width due to a difference T in face temperatures (sandwich panel with all edges clamped).

PLATE SIMPLY SUPPORTED AT THREE EDGES AND FREE AT THE FOURTH EDGE

In Fig. 4 let the edge $y = b$ be the free one. Then the boundary conditions for the superimposed case are again given by Eq. (24) for $x = 0$, $x = a$. For the edge $y = 0$,

$$M_y = -\alpha TD(1 + \nu)/t, \quad w = 0, \quad Q_x = 0 \tag{65}$$

and for the edge $y = b$,

$$M_y = -\alpha TD(1 + \nu)/t, \qquad M_{yx} = 0, \qquad Q_y = 0 \tag{66}$$

From Eq. (24) w can again be represented by Eq. (30), where Y_m is given by Eq. (35). Similarly, Q_x and Q_y can again be assumed as Eqs. (33) and (34). Since presently C_m and D_m are not zero, Eq. (39) now leads to

$$(d^2Y_{ym}/dy^2) - \{\lambda_m{}^2 + [2Gt/(1 - \nu)D]\}\, Y_{ym} = [4Gt/(1 - \nu)]\lambda_m{}^3(B_m \sinh \lambda_m y + D_m \cosh \lambda_m y) \tag{67}$$

instead of to Eq. (40), so that the solution of the homogeneous equation becomes

$$Y_{ym1} = E_m \sinh p_m y + F_m \cosh p_m y \tag{68}$$

where p_m is given by Eq. (42). The solution of the complete equation (67) gives

$$\left.\begin{aligned} Q_y &= \sum_{m=1,3,5,\ldots}^{\infty} Y_{ym} \sin \lambda_m x \\ &= \sum_{m=1,3,5,\ldots}^{\infty} [E_m \sinh p_m y + F_m \cosh p_m y - 2\lambda_m{}^3 D(B_m \sinh \lambda_m y + D_m \cosh \lambda_m y)] \sin \lambda_m x \end{aligned}\right\} \tag{69}$$

By inserting Eqs. (33) and (34) into Eq. (38),

$$\left.\begin{aligned} Q_x &= \sum_{m=1,3,5,\ldots}^{\infty} (1/\lambda_m)\,(dY_{ym}/dy) \cos \lambda_m x \\ &= \sum_{m=1,3,5,\ldots}^{\infty} (1/\lambda_m)\,[E_m p_m \cosh p_m y + F_m p_m \sinh p_m y - 2\lambda_m{}^4 D(B_m \cosh \lambda_m y + D_m \sinh \lambda_m y)] \cos \lambda_m x \end{aligned}\right\} \tag{70}$$

The constants A_m, B_m, C_m, and D_m in Eq. (35) and E_m and F_m in Eqs. (69) and (70) follow from the six boundary conditions in Eqs. (65) and (66). They are

$$D_m = \frac{4\alpha(1-\nu^2)T}{\lambda_m{}^3 at} \times \frac{\cosh \beta_m - 1}{(1-\nu)\beta_m + [3+\nu+2(1-\nu)\lambda_m{}^2(D/Gt)]\sinh\beta_m\cosh\beta_m - [2(1-\nu)D/Gt]\lambda_m p_m \tanh\delta_m\cosh^2 p_m} \quad (71)$$

where

$$\beta_m = \lambda_m b; \quad \delta_m = p_m b \quad (72)$$

$$\left.\begin{aligned} &A_m = 4\alpha T(1+\nu)/\lambda_m{}^3 at, \qquad B_m = 0 \\ &C_m = D_m\{[(1+\nu)/(1-\nu)] - \beta_m \tanh\beta_m\} - [4\alpha T(1+\nu)/\lambda_m{}^3 at]\tanh\beta_m \\ &E_m = 0, \qquad F_m = 2D_m\lambda_m{}^3 D\cosh\beta_m/\cosh\delta_m \end{aligned}\right\} \quad (73)$$

M_x, M_y, and M_{xy} can be calculated from the second members of Eqs. (53), (54), and (55) where w is given by Eqs. (30) and (35) and Q_x and Q_y by Eqs. (70) and (69), respectively. For the tensile forces along the edges that have to be transferred by the attaching bolts, one obtains

$$-(V_x)_{x=0} = D\sum_{m=1,3,5,\ldots}^{\infty} D_m\lambda_m{}^3\left(\{5-\nu-(1-\nu)\beta_m\tanh\beta_m + [2(1-\nu)D\lambda_m{}^2/Gt]\}\sinh\lambda_m y + (1-\nu)\lambda_m y\cosh\lambda_m y - 2(p_m/\lambda_m)\{[(1-\nu)D\lambda_m{}^2/Gt]+2\}(\cosh\beta_m/\cosh\delta_m)\sinh p_m y\right) - [4\alpha(1-\nu^2)TD/at]\sum_{m=1,3,5,\ldots}^{\infty}(\tanh\beta_m\sinh\lambda_m y - \cosh\lambda_m y) \quad (74)$$

$$-(V_y)_{y=0} = D\sum_{m=1,3,5,\ldots}^{\infty}\lambda_m{}^3\left(\{(1-\nu)\beta_m\tanh\beta_m + [2(1-\nu)D\lambda_m{}^2/Gt][(\cosh\beta_m/\cosh\delta_m)-1]\}D_m - [4\alpha(1-\nu^2)T/\lambda_m{}^3 at]\tanh\beta_m\right)\sin\lambda_m x \quad (75)$$

The concentrated downward force R at the corner $x = 0$, $y = 0$ is

$$(R)_{x=0,\,y=0} = 2(M_{xy})_{x=0,\,y=0} = 2(1-\nu)D\sum_{m=1,3,5,\ldots}^{\infty}\lambda_m{}^2\left(\frac{2}{1-\nu} - \beta_m\tanh\beta_m - \frac{2D\lambda_m{}^2}{Gt}\left\{\left[1+\frac{Gt}{(1-\nu)D\lambda^2{}_m}\right]\frac{\cosh\beta_m}{\cosh\delta_m} - 1\right\}\right)D_m - \frac{8\alpha(1-\nu^2)TD}{at}\sum_{m=1,3,5,\ldots}^{\infty}\frac{\tanh\beta_m}{\lambda_m} \quad (76)$$

Since at the free edge $M_{yz} = 0$, at the corners $x = 0$, $y = b$ and $x = a$, $y = b$ the forces R are zero.

Some Numerical Results

Alexander Krivetsky of Bell Aircraft computed some numerical results and presented them in the chart and graph given in Figs. 5 and 6. Fig. 5 gives the bending moments $M_x = M_y = M_n$ from Eq. (1) for a plate clamped at all edges, as a function of the difference in temperature T and the ratio t_f/t. If the temperature varies linearly through the thickness t, the bending stresses in the outer fibers can be calculated directly as

$$\sigma_x = \sigma_y = (M_n/I)(t/2) = \alpha TD(1+\nu)/2I = \alpha TE/2(1-\nu) \quad (77)$$

If the thermal gradient in the faces differs from T/t, where T for this case is defined in the Symbols, the stresses in the outer fibers are

$$\sigma_x = \sigma_y = \alpha T_0 E/2(1-\nu) \quad (78)$$

where T_0 is the temperature difference between the outer fibers.

Fig. 6 shows the bending moments at the clamped edge from Eq. (64) for a square plate of 24 by 24 in., as sketched in the insert, simply supported at two opposite edges and clamped at the others, if $t = 0.5$ in., $t_f = 0.02$ in. and $T = 200°$F. It shows the distribution of the clamping moment M_y between $x = 0$ and $x = 12$

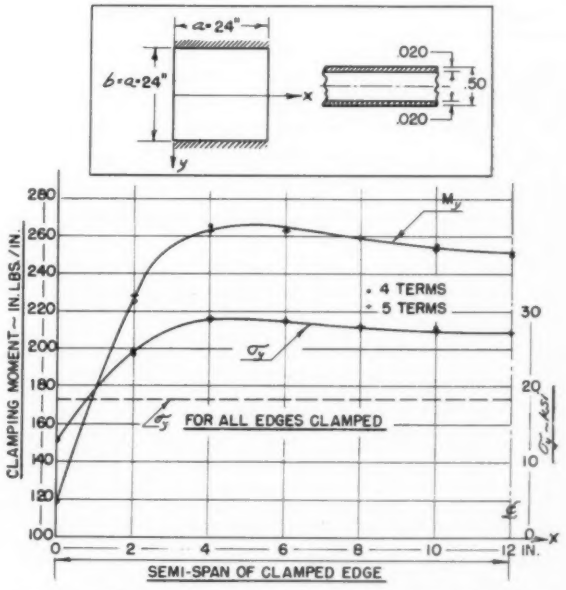

Fig. 6. Moments and stresses along clamped edge (plate simply supported at two opposite edges and clamped at the others).

in. It also shows the distribution of the stresses σ_y from M_y at the outer fibers, assuming a thermal gradient T/t in the faces. At the corner $x = 0$, $y = 12$ in., where σ_x is zero, obviously $\sigma_y = (1/2)\alpha ET$, so that with $\alpha = 0.000028$, $E = 10^7$ psi and $T = 200°$F., $\sigma_y = 12{,}800$ psi in accordance with Fig. 6.

For a square plate, clamped at all edges, from Eq. (77) $\sigma_y = 12{,}800/(1 - 0.3) = 18{,}300$ psi along the entire length of the clamped edges (as well as everywhere else), as indicated by the dashed line in Fig. 6. Hence, for the case with two opposite edges clamped, and simply supported at the other ones, as considered in Fig. 6, the maximum clamping moments are larger.* This is understandable, since canceling of the clamping moments at the edges $x = 0$ and $x = a$ will cause excess clamping moments along the edges $y = \pm b/2$ in order to keep the slopes $\partial w/\partial y$ along these edges equal to zero. This effect will become smaller if one moves farther from the edges $x = 0$ and $x = a$, which explains why the maximum stresses σ_y occur close to the edges $x = 0$ and $x = a$ and not in the center of the clamped edges.

It should be noted also that, for a thermal gradient T/t in the faces, in general, the stresses σ_y in the outer fibers are not completely given by the formula

$$\sigma_y = (M_y/I)\,(t/2) = [Et/2(1 - \nu^2)]\,(M_y/D) \quad (79)$$

M_y depends on the curvature of the plate as far as it is caused by the deformation from bending only. From Eq. (27) this effect is given by that of the total curvatures

$$-[(\partial^2 w/\partial y^2) + \nu(\partial^2 w/\partial x^2)]$$

diminished by the curvatures caused by the change of the shear deformation with x and y,

$$-(1/Gt)\,[(\partial Q_y/\partial y) + \nu(\partial Q_x/\partial x)]$$

or, from Eq. (38),

$$[(1 - \nu)/Gt](\partial Q_x/\partial x)$$

However, the curvature of the faces, of which the proper flexural rigidity is neglected throughout, is equal to the total curvature. Therefore, to the bending stresses from Eq. (79) excess bending stresses

$$\sigma_y = [E/(1 - \nu^2)]\,(t_f/2)\,[(1 - \nu)/Gt]\,(\partial Q_x/\partial x) = (G_f t_f/Gt)\,(\partial Q_x/\partial x) \quad (80)$$

have to be added, where G_f is the modulus of rigidity of the faces. However, in the present case, since at the clamped edge, from Eq. (57), Q_x, and therefore $\partial Q_x/\partial x$, are zero, σ_y from Eq. (80) is zero.

If the thermal gradient in the faces differs from T/t, the stresses σ_y from Eq. (79) have to be diminished by stresses

$$\sigma_y = E\alpha(T - T_0)/2(1 - \nu) \quad (81)$$

where T_0 has the same meaning as in Eq. (78) and T is defined in the Symbols.

* This is analogous to what happens in the case of a square plate with edges a, under equally distributed transverse loading q, where, with all edges clamped, the maximum clamping moment is $-0.0513\,qa^2$, whereas, with two opposite edges clamped and the other two simply supported, the maximum clamping moment is $-0.070\,qa^2$.

References

[1] Timoshenko, S., *Theory of Plates and Shells*, McGraw-Hill Book Co., New York, 1940.

[2] Libove, C., and Batdorf, S. B., *A General Small Deflection Theory for Flat Sandwich Plates*, NACA TN 1526, April, 1948.

[3] Bijlaard, P. P., *On the Elastic Stability of Sandwich Plates*, I–II, Proc. Royal Netherlands Academy of Sciences, Amsterdam, Nos. 1 and 2, 1947.

[4] Reissner, E., *Small Bending and Stretching of Sandwich-Type Shells*, NACA TN 1832, March, 1949.

Tenth International Congress of Applied Mechanics

Stresa, Italy, August 31–September 7, 1960

Apart from a number of invited general lectures, the technical sessions of the Congress will be held in two sections: Fluid dynamics (hydrodynamics and aerodynamics); and Mechanics of solids (rigid body dynamics, vibrations, elasticity, plasticity, and theory of structures).

It should be noted that thermodynamics and computational methods as such are not included, although specific applications of computational methods to pertinent problems of one of the two sections stated above are acceptable subjects for presentation.

Abstracts should be submitted before January 1, 1960 to: *The Secretary of the International Committee, Prof. Mekelweg 2, Delft, Netherlands.* Abstracts, in four copies, should not exceed two typewritten pages (double-spaced). It is recommended that abstracts be in two of the official Congress languages (English, French, German, and Italian).

All correspondence, apart from submission of papers, should be addressed to: *The Italian Organizing Committee, Consiglio Nazionale delle Ricerche, Ufficio relazioni internazionali, Piazza delle Scienza 7, Roma.*

The Tailored-Interface Hypersonic Shock Tunnel†

CHARLES E. WITTLIFF,* MERLE R. WILSON,** AND ABRAHAM HERTZBERG***

Cornell Aeronautical Laboratory, Inc.

SUMMARY

The "tailored-interface" hypersonic shock tunnel provides a means for producing the high Mach Number, high stagnation temperature flow conditions encountered in hypersonic flight. Various gasdynamic phenomena associated with shock tunnels are discussed, and experimental evidence of the successful application of this technique is presented. As an indication of its research application, the results of heat-transfer experiments on a hemisphere-cylinder model are presented and compared with theory.

INTRODUCTION

IN RECENT YEARS considerable attention has been focused on problems associated with hypersonic flight. This interest, for the most part, can be attributed to the high-temperature phenomena behind strong shock waves. At flight Mach Numbers above 6, the temperature behind a normal shock exceeds 1,500°K. and increases to about 10,000°K. at Mach 22. In this temperature range, the thermal energy of the air is sufficient to excite the higher rotational and vibrational states of the molecules, cause dissociation and ionization, and produce chemical reaction of the constituents. Since these real gas effects may alter the flow field about a body, it is important to have an understanding of this interaction.

In this relatively unexplored flow region, one of the primary needs has been for laboratory facilities capable of reproducing the high-temperature and high Mach Number conditions encountered in hypersonic flight. The shock tube offers a means by which the high temperature conditions can easily be created and maintained in a nearly steady state for brief periods of time.[1] In addition, the equilibrium state of the gas, which is homogeneously heated by the shock wave without contamination, can be precisely determined. These and other features of the shock tube have led to its widespread use in the fields of aerodynamic,[2–4] physical,[5–8] and chemical research.[9–13] However, the maximum flow Mach Number which can be obtained in air in the conventional shock tube is approximately three.[14] This Mach Number limitation has, in the field of hypersonic research, restricted the application of the shock tube to studies of flow problems which are not Mach Number sensitive.[15, 16] Thus, the conventional shock tube has been successfully used to simulate the very high stagnation-point heat-transfer rates encountered in the hypersonic re-entry of a ballistic missile.[17]

However, there are many hypersonic problems in which Mach Number simulation is necessary. In order to meet this requirement, development of the hypersonic shock tunnel began at the Cornell Aeronautical Laboratory in 1950 with the addition of a simple divergent nozzle to the downstream end of a conventional shock tube.[18] This nozzle expanded the supersonic flow behind the shock wave to hypersonic speeds, so that flow Mach Numbers up to 10 with full stagnation temperature simulation were obtained for about 1 millisecond. However, in order to obtain this flow duration, a relatively long shock tube was necessary. Because of viscous attenuation in this slender tube, the strength of the shock wave was found to be much less at the entrance of the nozzle than it was initially. Thus, total enthalpy was lost, and flow conditions in the test section became unsteady. Detailed results of these measurements have been reported in reference 19.

A study of more sophisticated shock tunnel designs showed that an increase in testing time per foot of shock tube of 8 to 60 times that of the conventional shock tube could be obtained.[20, 21] Such a large increase in testing time per foot would permit use of a shorter shock tube giving the same, or longer, test period relatively free of attenuation effects. The "tailored-interface" method, which resulted from this study, has recently been incorporated in the C.A.L. hypersonic shock tunnel.

A description of this technique and experimental verification of its usefulness are presented in this paper. In addition, some of the gasdynamic phenomena which are especially important in the design and operation of the tailored-interface shock tunnel are discussed. To illustrate the research application of this shock tunnel, measurements of heat-transfer rates on a hemisphere-cylinder body are presented, and the results are compared with theoretical predictions.

THE TAILORED-INTERFACE METHOD

In the "tailored-interface" modification, the incident shock wave is reflected at the downstream end of the

Presented at the ASME-ARS Aviation Conference, Dallas, Texas, March 16–20, 1958. Received April 17, 1958. Revised and received January 8, 1959.

† This paper is based on research supported by the United States Air Force through the Air Force Office of Scientific Research, ARDC, under Contract No. AF 18(603)-10. The Mechanics Division was the monitoring agency for this research.

The authors gratefully acknowledge the contributions of H. S. Glick for his ideas and discussions during the early portion of this work and of T. C. Golian for supervising most of the calculations.

* Research Aeronautical Engineer.

** Assistant Mechanical Engineer.

*** Assistant Head, Aerodynamic Research Dept.

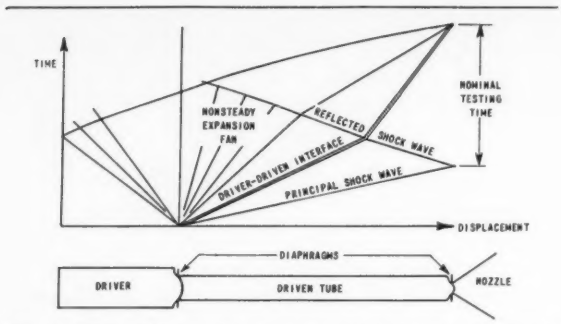

FIG. 1. Wave diagram for the tailored-interface shock tunnel (unsteady configuration).

shock tube, and conditions of the driver and driven gases at the interface are matched (or "tailored") so that no additional waves are created by the interaction of the reflected shock and the interface. A discussion of this procedure is provided below.

Shock-Wave Reflection

The reflection of the shock wave in the tailored-interface shock tunnel occurs at a convergent-divergent nozzle (see Fig. 1). The ratio of the nozzle throat area to the shock tube cross-sectional area is such that the shock wave is almost completely reflected, creating a region of almost stagnant, compressed air at the end of the shock tube. The strength of the reflected shock wave adjusts itself to provide a constant pressure at the nozzle entrance, even though air is flowing out of the shock tube. Flow entering the nozzle will be steady until either all the air is consumed or unsteady waves propagate into the stagnant air region. Such waves will, in general, result from the interaction of the reflected shock wave and the interface. In this case, the duration of steady flow would not be greatly different from that of the nonreflected shock method; however, it could be greatly increased if the shock wave could be made to pass through the interface without generating additional waves.

Tailoring Conditions

Following passage of the incident shock wave, both the driver and driven gases will be at equal and constant pressure and velocity in the absence of attenuation.[22–24] The interface between the two gases marks a discontinuity in temperature and density. If the reflected shock wave is to pass through the interface without creating any additional waves, the driver and driven gases must be at equal pressure and velocity behind the reflected shock. Therefore, the condition for tailoring is that the pressure ratio and velocity change across the reflected shock be the same in the two gases.

Assuming that the interaction of the reflected shock and the interface results only in transmitting the shock wave into the driver gas, and that no additional waves are created (Fig. 1), the procedure for calculating the tailoring conditions can be given. The pressure ratio and velocity change across the reflected shock wave in the driven gas can be easily calculated, taking into account real gas effects,[9, 14] if the velocity behind the reflected shock is assumed to be negligible. Since the interface is "tailored," the pressure ratio and velocity change across the reflected shock in the driver gas are

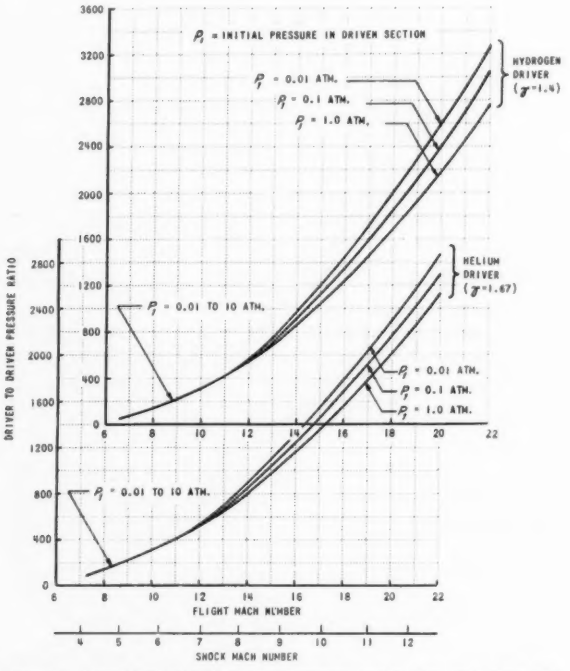
P_1 = INITIAL PRESSURE IN DRIVEN SECTION
P_1 = 0.01 ATM.
P_1 = 0.1 ATM.
P_1 = 1.0 ATM.
HYDROGEN DRIVER (γ=1.4)
HELIUM DRIVER (γ=1.67)
P_1 = 0.01 TO 10 ATM.
DRIVER TO DRIVEN PRESSURE RATIO
FLIGHT MACH NUMBER
SHOCK MACH NUMBER

FIG. 2. Required diaphragm pressure ratio for tailoring at various Mach Numbers (unsteady configuration).

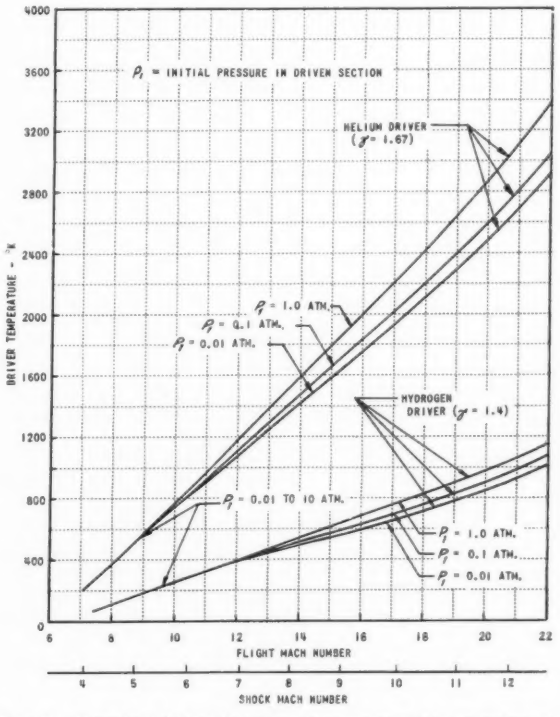
P_1 = INITIAL PRESSURE IN DRIVEN SECTION
HELIUM DRIVER (γ = 1.67)
P_1 = 1.0 ATM.
P_1 = 0.1 ATM.
P_1 = 0.01 ATM.
HYDROGEN DRIVER (γ = 1.4)
P_1 = 0.01 TO 10 ATM.
DRIVER TEMPERATURE - °K
FLIGHT MACH NUMBER
SHOCK MACH NUMBER

FIG. 3. Required initial driver gas temperature for tailoring at various Mach Numbers (unsteady configuration).

the same as in the driven gas. This information plus the specific heat ratio of the driver gas are sufficient to determine, first, the temperature of the driver gas ahead of the reflected shock, and, finally, the initial temperature and pressure of the driver gas.[1, 22] Thus, when the initial pressure and temperature of the driven gas, the desired Mach Number, and the driver gas composition are specified, the required driver gas pressure and temperature to achieve tailoring can be determined. These quantities have been calculated for helium and hydrogen driver gases, initial air pressures from 0.01 to 10 atmospheres, and flight Mach Numbers from 6 to 22. The results, presented in Figs. 2 and 3, are plotted, for convenience, against both shock wave Mach Number and the flight Mach Number corresponding to an equivalent stagnation enthalpy at an ambient temperature of 218°K.; i.e., in the stratosphere.

These Figures show that helium at room temperature (300°K.) will tailor at an equivalent flight Mach Number of 7.5, and room-temperature hydrogen will tailor at Mach 10.6. Tailoring at intermediate Mach Numbers can easily be achieved using a mixture of these two gases. To obtain stagnation enthalpies corresponding to flight Mach Numbers above 10.6 using the tailored-interface technique, a heated helium or hydrogen driver gas is necessary. This heating can be accomplished by various methods; for example, by an electrical heating unit or a heat exchanger, by an adaptation of the double driver or "buffer" gas technique,[25–27] by combustion,[1] or by an electric arc discharge.[1] Using helium heated to about 3,000°K. or hydrogen at 1,000°K., the tailored-interface shock tunnel should permit temperature simulation at flight Mach Numbers up to 22.

Testing Time

The maximum available testing time is determined by the interaction of the reflected shock wave and the unsteady expansion wave propagating downstream from the primary diaphragm station, provided the driver is long enough so that the expansion waves propagating upstream into the driver do not overtake the downstream propagating waves after reflecting from the end of the driver (Fig. 1). Calculation of the testing time, based on the wave diagram in Fig. 1, indicates values approximately 8 to 12 times greater, depending on the Mach Number, than can be achieved with a conventional nonreflected shock tunnel of the same length.

By placing a supersonic convergent-divergent nozzle at the primary diaphragm station, the supersonic portion of the unsteady expansion fan (Fig. 1) can be replaced by a steady flow expansion and the testing time thereby increased to the entire time it takes the reflected shock wave to travel from the hypersonic nozzle to the diaphragm station and return (Fig. 4). This "steady" configuration provides a test period from 14 to 60 times greater than the nonreflected method, depending on the Mach Number. However, the steady configuration requires that the area ratio of the steady

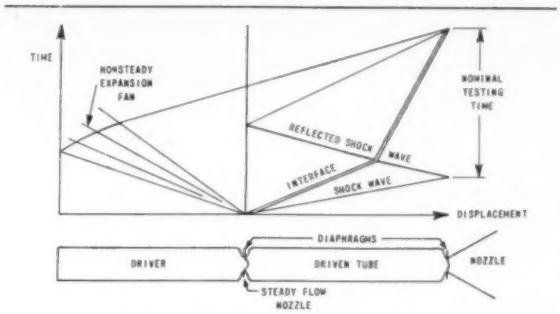

FIG. 4. Wave diagram for the tailored-interface shock tunnel (steady configuration).

flow nozzle at the diaphragm station be changed for each Mach Number. The required driver gas pressures and temperatures for tailoring are approximately the same as those for the unsteady configuration (Figs. 2 and 3).

The variation of testing time per foot of shock tube length with equivalent flight Mach Number is presented in Fig. 5 for these two configurations. It is important to note that, although the testing time decreases appreciably with increasing Mach Number, the number of model lengths of flow remains relatively constant because of the increased velocity. For example, in the C.A.L. shock tunnel using the unsteady configuration, over the Mach Number range from 6 to 18, the number of model lengths of flow decreases from 74 to 38, for a 6-in. model, while the testing time decreases from 6 to 1 milliseconds.

Test Section Conditions

The test section Reynolds Number per foot for flight Mach Numbers from 6 to 22 is presented in Fig. 6.

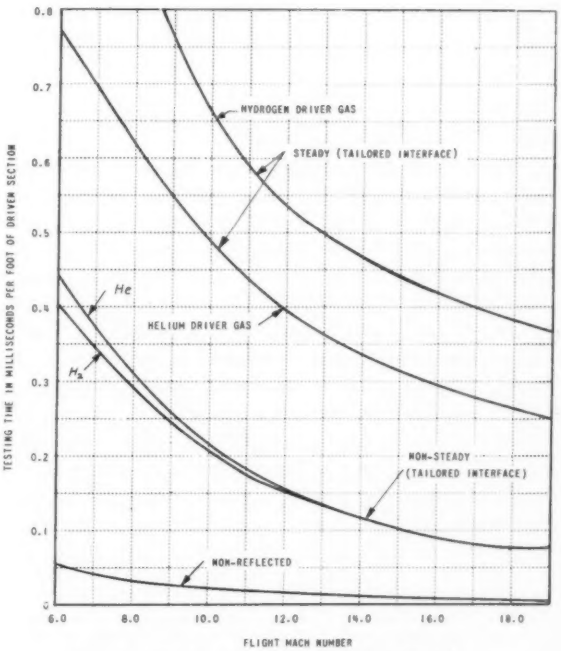

FIG. 5. Testing time vs. flight Mach Number.

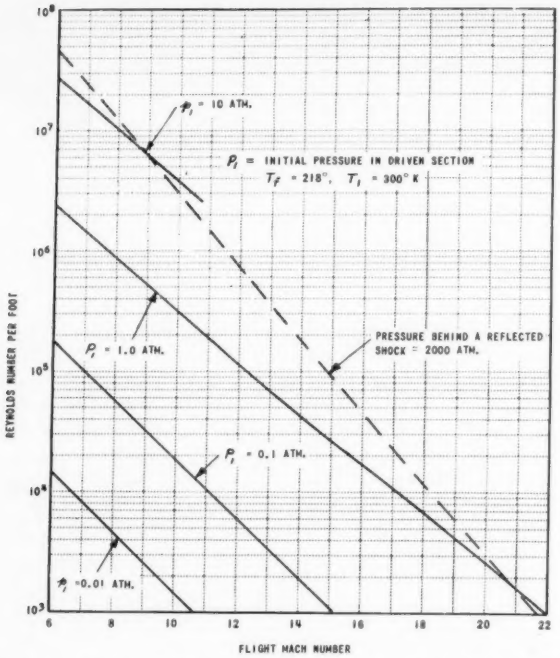
REYNOLDS NUMBER PER FOOT
FLIGHT MACH NUMBER
p_1 = 10 ATM.
p_1 = INITIAL PRESSURE IN DRIVEN SECTION
T_F = 218°, T_1 = 300° K
PRESSURE BEHIND A REFLECTED SHOCK = 2000 ATM.
p_1 = 1.0 ATM.
p_1 = 0.1 ATM.
p_1 = 0.01 ATM.

FIG. 6. Variation of Reynolds Number per foot with flight Mach Number.

These values were calculated using real gas properties for air[28–31] in thermodynamic equilibrium.* The test section conditions shown apply to any tailored-interface shock tunnel when stagnation enthalpy and Mach Number are simulated at an ambient temperature of 218°K. Any shock tunnel will have some pressure limitation which will restrict its range of full simulation of Mach Number and altitude. Such a restriction is shown in Fig. 6 by the curve indicating a pressure of 2,000 atmospheres behind the reflected shock wave, which is the pressure limit of the present C.A.L. shock tunnel.

Special Gasdynamic Considerations

There are a number of gasdynamic effects that have an important bearing on the design and performance of shock tunnels in general, and that warrant special consideration. Included in these are interaction of the reflected shock wave and the boundary layer on the walls of the shock tube, mixing at the interface between the driver and driven gases, the Taylor instabliity of the interface, loss of stagnation enthalpy by radiation, convective heat transfer at the throat of the hypersonic nozzle, thermodynamic nonequilibrium in the nozzle, and adequacy of the available test time. Although these phenomena do not introduce any problems in the present operation and performance of the C.A.L. tailored-interface shock tunnel, some of them may present difficulties if the range of operation is extended to higher Mach Numbers.

Interaction of Reflected Shock and Boundary Layer

The interaction of the reflected shock wave with the boundary layer behind the incident shock has been studied analytically and experimentally by H. Mark,[32] who showed that a large scale shock-boundary-layer effect exists when low energy flow in the boundary layer does not have sufficient total pressure to pass through the reflected shock without separating. However, it has been observed that, at high densities in which the boundary layer behind the incident shock undergoes early transition from laminar to turbulent, this interaction is not very pronounced. The turbulent boundary layer feeds energy into the low energy portion, increasing the total pressure and inhibiting separation. In the C.A.L. tailored-interface shock tunnel, which operates at high densities, no effects of this shock-boundary-layer interaction have been found in the test air.

Interface Mixing

In all of the tailoring calculations it has been assumed that the interface between the driver and driven gases represents a discontinuity in temperature and density. In reality, the interface is a constant pressure mixing region, the extent of which is believed to depend on the opening process of the diaphragm, the speed of the shock, and the geometry of the shock tube. Mixing between the hot air and cold driver gas would be expected to reduce the amount of air available for testing. The experimental results obtained thus far, however, do not indicate any noticeable effect of this sort.

It should be noted that interface mixing would be enhanced by any strong Taylor instability[33] relating to the deceleration of two gases of different density by the reflected shock wave. For the "tailored-interface," the air density is always greater than that of the driver gas, and this represents a stable system.

Radiation Losses

If the almost stagnant air behind the reflected shock wave remains in the shock tube at a high temperature for longer than a few milliseconds, it is possible for it to lose a significant portion of its energy by radiation to the walls of the shock tube. For example, if the testing time were 20 milliseconds, which could easily be obtained in the steady configuration, the radiation loss at 2,000 atm. would be about 6 per cent at a stagnation temperature of 6,000°K. and 15 per cent at 8,000°K. This loss would increase to about 40 per cent at 100 milliseconds for 8,000°K., and would be even greater for lower stagnation pressures. The above values are based on an emissivity of unity selected on the basis of the available data.[12, 13] Calculations indicate, however, that radiation losses never exceed 5 per cent of the stagnation enthalpy over the operating range of the C.A.L. tailored-interface shock tunnel. Any facility which heats a fixed mass of air in a closed chamber will

* The authors wish to thank C. Beckett for making available the latest NBS calculations of the equilibrium properties of argon-free air at densities up to 316 times sea level density.[31] These tables were necessary in order to calculate the $p_1 = 10$ atm. curve in Fig. 6.

experience similar radiation losses. Hence, it is desirable to obtain the data in the shortest possible testing time in order to minimize the uncertainty in the stagnation enthalpy.

Nozzle Throat Heat Transfer

Another heat-transfer problem that is important in the design of a tailored-interface shock tunnel is the convective heat transfer at the throat of the nozzle. The results of an analysis that considered both the compressible laminar[34] and incompressible turbulent[35] boundary-layer cases indicate that the nozzle heating problem can be very serious for testing times greater than several milliseconds for both cases. For example, at a stagnation temperature of 6,000°K., an uncooled stainless steel nozzle would begin to melt after 11 milliseconds. The testing time in the present tailored-interface shock tunnel is not long enough for the nozzle surface to reach the melting point, and, in fact, after some 200 tests no damage due to heating or erosion has been observed.

Thermodynamic Nonequilibrium

Since the temperature and density decrease rapidly through the hypersonic nozzle, it is possible that thermodynamic nonequilibrium conditions may occur in the nozzle because of relaxation effects. Nonequilibrium conditions will exist if the local flow time becomes short compared to the local relaxation times for such phenomena as molecular vibration, dissociation, ionization, and chemical reaction between the different gas species. Criteria for predicting such behavior have been given by Penner[36] and Bray.[37]

Although Penner's criterion is for determining whether the exhaust gases from a rocket engine will be near thermodynamic equilibrium or nearly frozen after adiabatic expansion through a nozzle, it has been used to predict nonequilibrium effects in a hypersonic nozzle.[38] More recently, Bray has proposed a criterion that appears to be more applicable to hypersonic wind-tunnel nozzles having large expansion ratios. Applied to the case of oxygen dissociation, for example, Bray's criterion states than nonequilibrium, or "freezing," will occur when the equilibrium rate of change of the degree of dissociation is of the order of the atom recombination rate.

Because of the complexity of the chemical kinetics of a real gas at high temperatures, Bray utilizes Lighthill's model for an ideal dissociating gas[39] to obtain relatively simple mathematical expressions for the changes of state. A calculation has been made for air using Bray's approach and the recent chemical-kinetic data for oxygen reported by Byron.[40] A pressure and temperature behind the reflected shock wave of 1,000 atm. and 4,500°K., respectively, were selected, because at these conditions the relaxation effects of oxygen dissociation should predominate over oxygen and nitrogen vibration and nitrogen dissociation. For example, Logan[38] shows that, at a temperature of 4,500°K. and a density of one-tenth sea level density, oxygen dissociation contains 40 per cent of the total internal energy, nitrogen vibration about 10 per cent, nitrogen dissociation about 2 per cent, and oxygen vibration only a negligible amount. The remaining internal energy is contained in the active degrees of freedom, which have very fast relaxation times. Even if the relaxation time for nitrogen vibration were much slower than that for oxygen dissociation, the latter would predominate in the overall effect on the flow because of its greater percentage of the internal energy.

In this calculation two different assumptions were made regarding the effectiveness of nitrogen molecules in the recombination of the oxygen atoms; first, that the nitrogen was completely ineffective and served only as a diluent, and, second, that the nitrogen was completely effective. These two extreme cases bracket the actual conditions. These calculations for the C.A.L. shock tunnel nozzle indicate that freezing will occur at nozzle area ratios of 45 and 100 for the respective assumptions regarding nitrogen. Although these area ratios are quite small compared to the overall area ratio of several thousand, indicating freezing early in the nozzle, the temperature, density, and degree of dissociation decrease so rapidly that very little energy of dissociation is locked in the frozen state. In the calculated example, at an area ratio of 45, the ratios of the temperature and density to their stagnation values are 0.36 and 0.0052, respectively, and the percentage of dissociation is 0.08. The amount of "frozen" energy in dissociation is about 0.8 per cent of the total enthalpy, and the assumption of thermodynamic equilibrium for the test section calculations appears justified for these conditions. However, for much lower pressures a significant amount of the total enthalpy may be frozen out, and the assumption of thermodynamic equilibrium would not then be valid.

Adequacy of Available Test Time

In view of the brief testing times available in shock tubes and shock tunnels, it is appropriate to inquire whether or not the flow duration is adequate for aerodynamic investigations. Flow phenomena about a body may be broadly classified into three groups—the external flow field, the boundary layer, and the wake. The establishment of quasi-steady states for each of these phenomena will be by wave processes, diffusion, and mixing, respectively.

The external flow field generally should achieve quasi-steadiness within a few body lengths of flow, since the wave processes propagate at a sonic speed or greater. This has been well substantiated by schlieren photographs.

The unsteady growth of a boundary layer can also be related to body lengths of flow, and can be expected to become quasi-steady about as quickly as the external flow field. Of course, changes in a boundary layer take place by molecular or turbulent diffusion, which is a much slower process than wave propagation. How-

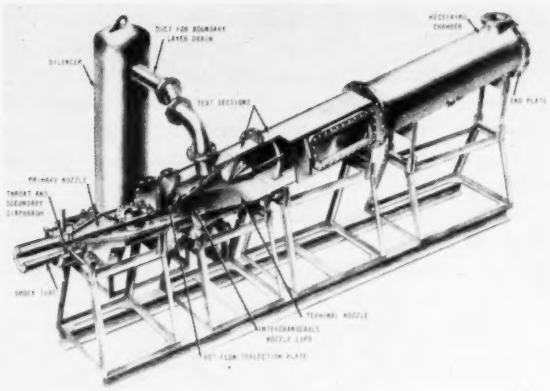

FIG. 7. Cornell Aeronautical Laboratory 11-in. by 15-in. Hypersonic Shock Tunnel.

ever, except on the leeside, the boundary layer will be relatively thin, so that the adjustment of the boundary layer to flow changes is very rapid.

The time required to establish the quasi-steady situation in the wake is not well understood. Wave processes are involved in establishing the overall shape, and the edge is a layer of high shear, as is a boundary layer. These two aspects of the wake suggest early flow establishment. If the circulation within the wake is established by a diffusion process, a very long time would be required, since the wake size is of the same order as the body diameter. However, the pumping action responsible for the circulation may well involve wave processes within the wake, in which case establishment times would be short. This is supported by recent shock tube experiments[41, 42] which indicate that the wake of a hemisphere-cylinder becomes quasi-steady in less than 100 microseconds, or about 15 body lengths of flow.

In view of these considerations, the testing time in the C.A.L. tailored-interface shock tunnel should be adequate since, as previously mentioned, it provides flow durations in excess of 30 body lengths.

APPARATUS

Description of Tunnel

The C.A.L. tailored-interface shock tunnel consists of a high-pressure driver section 14 ft. long with a 3.5-in. inside diameter and a low-pressure driven section, also 14 ft. long, with a 3-in. inside diameter. These sections are designed for a working pressure of 2,000 atm. Located at the downstream end of the low-pressure tube is a convergent-divergent nozzle having a contraction ratio of 18.9:1, which is sufficient to ensure almost complete reflection of the incident shock wave.

The divergent portion of the nozzle has a two-stage bilateral expansion. This arrangement permits an initial expansion in the horizontal plane ending in a 1.5 by 12.25 in. cross section, and a terminal expansion in the vertical plane to a test section size of 15 by 11 in. The opening of the terminal nozzle is variable in order to change the test section Mach Number, and is smaller than the exit of the primary nozzle in order to provide for a boundary-layer bleed.

A thin secondary diaphragm of Mylar, separating the shock tube from the nozzle and test section, permits the nozzle, test section, and dump tank to be evacuated to very low pressures (on the order of 1 micron Hg absolute) prior to each test. This procedure is necessary to minimize the nozzle starting time.[43] A starting time from 0.5 to 1.0 millisecond is obtained in this nozzle. The high pressure behind the shock wave easily ruptures this diaphragm so that its presence does not affect the flow establishment. However, it was found that minute Mylar fragments eroded blunt models and resulted in flow disturbances when they rebounded from the model.[44]

In order to avoid this particle damage, a simple deflection nozzle was inserted between the two expansion nozzzles. This deflector section has a two-dimensional wedge which spans the width of the flow and is mounted at a negative angle of attack. The flow passing below the wedge is turned upward 10° through a Prandtl-Meyer expansion. The terminal nozzle and test section are then mounted behind the wedge also at a 10° inclination. The entrance of this nozzle is thus shielded from diaphragm particles which are effectively centrifuged out of the test flow, and no further erosion of the models has been observed. Air passing above the wedge, plus the unused air below, is dumped into a large tank. A drawing of the nozzle and test section region is shown in Fig. 7.

Data Measurements and Instrumentation

The data measured in the shock tube during each run are the initial pressure in the low-pressure (driven) tube, the driver pressure at which the primary diaphragm bursts, the pressure history in the driven tube behind the incident and reflected shock waves, and the speed of the incident and reflected shocks. These data are used to calculate, taking into account the real gas effects, the flow conditions behind the reflected shock which are the stagnation conditions for the nozzle flow.

Local heat-transfer rates on a model in the test section are determined from measurements of transient surface temperatures by means of a thin film resistance thermometer.[45] The theory for the heat conduction in the body is then used to relate these measured temperatures to the heat-transfer rate.[45]

Rayleigh pitot pressure measurements in the test section are made using both a Statham pressure transducer (Model PM222b $\pm$ 25-200)[46] and a Kistler SLM gage (PZ-14). The test section static pressure is measured at the sidewall using an Altec-Lansing Model 21BR-200-2 microphone as a pressure transducer. All of these pressure transducers are suitably shock mounted for vibration isolation.

Schlieren photographs of the flow about models are obtained using a multiple spark light source[47] and a rotating drum camera. With this equipment, five

schlieren photographs can be taken during each run at preset time intervals varying from 50 to 1,000 microseconds.

Experimental Results

Shock Tunnel Performance

The first experiments that were made in the tailored-interface shock tunnel were aimed at verifying the predicted tailoring conditions. During these initial tests, in which helium was used as the driver gas, pressure histories were recorded at three stations along the low-pressure tube, and schlieren pictures were taken of the flow around a blunted cone using the multiple spark light source. The pressure measurements showed a constant pressure behind the reflected shock for about 4 milliseconds, an indication of successful tailoring. Further evidence that the test section flow was steady during this period was presented by the schlieren photographs.

Fig. 8(a) shows the pressure records taken during one of these runs. The incident shock Mach Number for the run shown was 3.78, which is slightly less than the theoretical value of 4.1. Flashing of the multiple light source is indicated by the pips appearing on the traces. The 4 millisecond period of constant pressure is in good agreement with the predicted testing time (see Fig. 5). The available testing time in the test section will be somewhat less than this because of the nozzle starting phenomenon. Tests were continued over a range of shock Mach Numbers from 3.4 to 4.2 and the results show that room temperature helium successfully tailors over this range. Fig. 8(b) shows another pressure history for a run where the shock Mach Number was almost identical to the theoretical value. These results indicate that it is not necessary to maintain the theoretical conditions precisely in order to achieve tailoring.

Another significant point is that the attenuation of the shock wave is truly negligible over the last half of the shock tube where the wave speed is measured. This can, for the most part, be attributed to the low value of the length-to-diameter ratio ($L/D = 56$) of the driven section.[19]

Following the experiments with helium, several tests

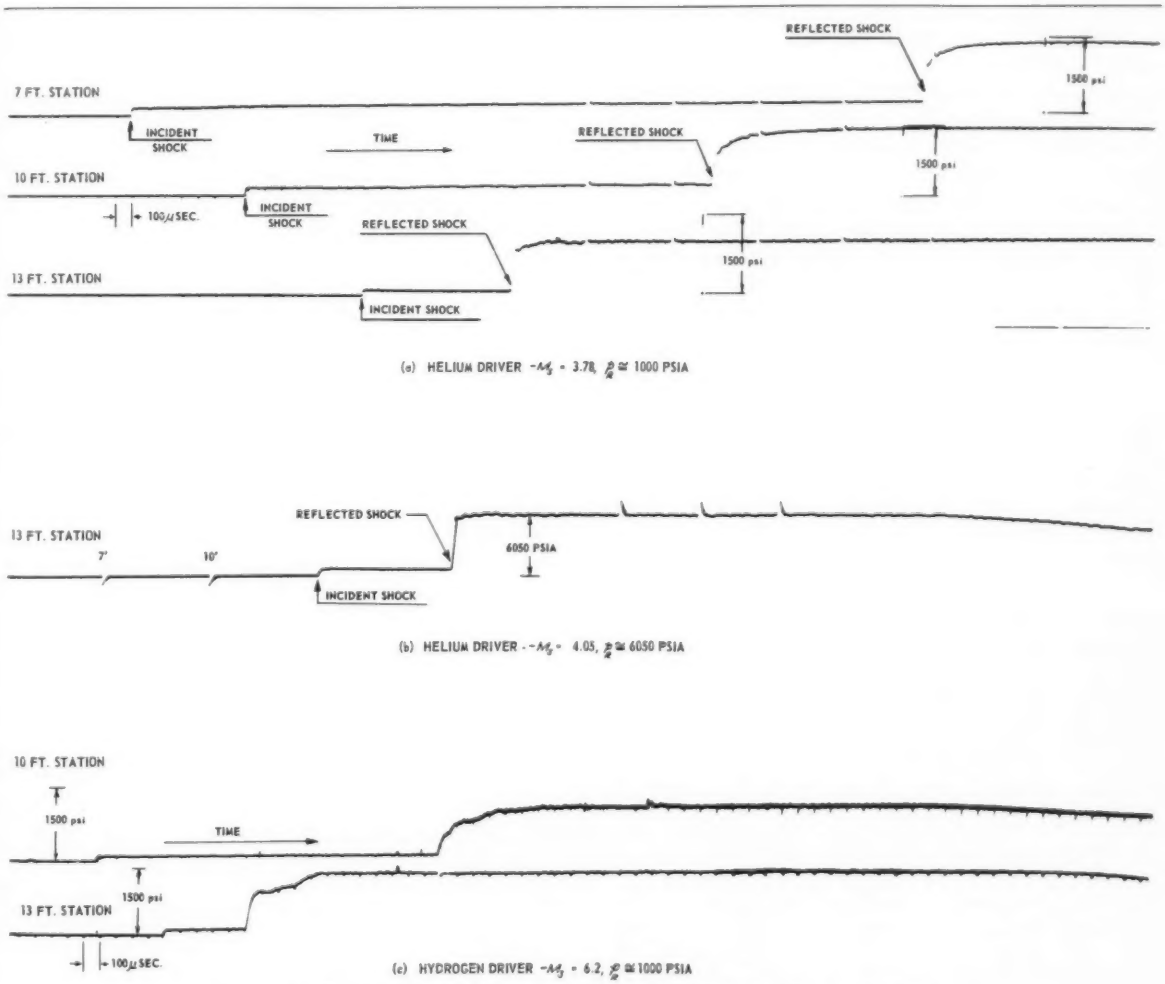

Fig. 8. Oscillograph record of pressure histories in the tailored-interface shock tunnel.

TABLE 1
Summary of Mach Number Measurements

Driver Gas	Test Gas	Nominal Stagnation Pressure (psia)	Nominal Stagnation Temp. (°K.)	Nominal Static Temp. (°K.)	Pitot Pressure Mach No.	Static Pressure Mach No.
Helium	Air	1,000–10,000	2,000	50–75	13.4 ± 0.5	12.3 ± 0.5
Hydrogen	Air	5,000	4,000	220°	11 ± 1	—

were made using hydrogen at room temperature as the driver gas. For this case, the theoretical calculations predict tailoring at a shock Mach Number of 6.14, corresponding to a flight Mach Number of 10.6. The pressure histories at the 10-ft. and 13-ft. stations are shown in Fig. 8(c). For this test the shock Mach Number was 6.20. The arrival of the incident and reflected shock waves at the 7-ft. station appears as a pip on the upper trace. Although the pressure behind the reflected shock ultimately achieves a constant value, it does not attain this value as quickly as in the helium driver tests [see Fig. 8 (a), (b)]. A comparison of the records from many hydrogen driver gas tests indicates that this type of pressure history is present in all the runs. Since these tests indicate that it is not a function of either shock Mach Number or pressure level, this effect does not appear to be associated with either the tailoring process or the interaction of the reflected shock wave and the boundary layer. In addition, wave speed measurements indicate very little attenuation. Combustion at the hydrogen-air interface is a possible explanation of this phenomenon. To check this possibility, several tests were made using nitrogen as the driven gas and a hydrogen driver, since this combination would tailor at nearly the same conditions as hydrogen and air. These tests exhibit a pressure history behind the reflected shock similar to that of the helium-air tests [Fig. 8 (a), (b)], adding additional weight to the interface-combustion explanation.

Having established the tailored-interface modification of the shock tunnel as a practical technique, a series of experiments was made to measure the test section Mach Number. Using the pressure transducers previously described, the Rayleigh pitot and the wall static pressure were measured in the test section. Mach Numbers have been computed from the ratios of these pressures to the pressure behind the reflected shock wave, assuming that the flow is isentropic. The resulting Mach Numbers are shown in Table 1. The plus and minus variations represent the scatter from run to run as well as the variation with stagnation pressure. For the helium tests, the two methods of determining Mach Number give values that consistently differ by about one Mach Number. It is not known at this time whether this is due to instrumentation error or a stagnation pressure loss from either viscous effects in the primary nozzle or wave phenomena in the deflection nozzle. The lower Mach Number measured during the hydrogen tests results from increased real gas effects at the higher stagnation temperature.

The effective nozzle area ratios, inferred from the pitot pressure Mach Numbers, are about 3,000 and 2,500 for the helium and hydrogen tests, respectively, compared to the geometrical area ratio of 5,000. This reduction, which is attributed to boundary-layer growth, is comparable to that of other hypersonic tunnels.

Aerodynamic Experiments

The first aerodynamic tests made in the tailored-interface shock tunnel were a series of experiments with both helium and hydrogen drivers to measure heat-transfer rates on a hemisphere-cylinder model. The temperature histories at several angular positions are shown in Fig. 9(a), and the variation of the stagnation-point heat-transfer rate with time is shown in Fig. 9(b) for a typical run. The stagnation heat-transfer rate is relatively constant from 0.8 to 4.0 milliseconds at an average value of 52 B.t.u./ft.^{2}-sec. In calculating the heat-transfer rate from the temperature histories, the temperature records are read at 100 microsecond intervals. This accounts for the discrete points shown in Fig. 9(b). Although the maximum variation in the heat transfer is approximately ±18 per cent of the average value, 80 per cent of the data points, in this time interval, lie within ±10 per cent of the average. This scatter includes the experimental errors as well as the effects of flow fluctuations and electrical noise.

A comparison of the experimental stagnation-point heat-transfer rates with theoretical predictions of Fay and Riddell[18] has yielded additional information regarding the test section Mach Number. Typical results are summarized in Table 2.

The experimental stagnation-point heat-transfer rates for hydrogen/air tests agree very well with the values predicted theoretically for a Mach Number of 11.2. This Mach Number value agrees with that determined from the pitot pressure measurements with the hydro-

TABLE 2
Comparison of Experimental and Theoretical Stagnation-Point Heat-Transfer Rates

Driver Gas	Test Gas	Shock Mach. No.	Stag. Pres. (psia)	Stag. Temp. (°K.)	Exper. Heat Transfer (B.t.u./ft.^{2}-sec.)	Theoretical Heat Transfer (B.t.u./ft.^{2}-sec.) M_∞ = 13.4	M_∞ = 12.0	M_∞ = 11.2
He	Air	3.85	2,860	1,880	52.0	39.8	51.3	
He	Air	3.93	2,970	1,930	53.6	41.2	53.3	
H_2	Air	6.55	3,000	4,140	128.7			125.7
H_2	Air	6.45	3,640	4,050	157.5			154 2

gen driver. In the case of the helium driver gas tests, however, the experimental data agree with the theory at a Mach Number of 12, which is consistent with the static pressure measurements rather than the pitot pressure measurements. It should be noted that, when the differences in the test conditions between runs are accounted for in the theoretical heat-transfer calculations, the differences in the experimental data from run to run are satisfactorily resolved.

A comparison of the experimental heat-transfer distribution over the nose of the model with Lees' theoretical prediction[49] for a laminar boundary layer is shown in Fig. 10. The data include tests in air using both helium and hydrogen drivers as previously tabulated plus one test in nitrogen using a hydrogen driver. The theoretical curve is for $\gamma = 1.4$ and $M_\infty = 10$. The agreement with the theory is quite good for all the tests, which include a range of stagnation temperatures from 1,700°K. to 4,100°K. in air and a value of 6,300°K. in nitrogen. The variation of the data during a typical run is indicated by the vertical bars alongside the data points.

Recent research in the C.A.L. tailored-interface shock tunnel has included a study of the hypersonic shock-boundary-layer interaction on a flat plate and also of the heat transfer on a slender yawed cone.[50] It should be noted that it is in research of this type, where high Mach Number and high stagnation temperature conditions are required, that the shock tunnel is most valuable.

Concluding Remarks

The tailored-interface shock tunnel offers a means whereby the high Mach Number and high stagnation temperature flows necessary to simulate hypersonic flight conditions can be easily produced. An important feature of this type of shock tunnel is that it provides a longer testing time than a conventional shock tunnel and, hence, a means of alleviating flow unsteadiness in the test section caused by shock-wave attenuation. In addition, there appear to be no unusually difficult problems related to its design and operation.

In its present state of development as a hypersonic test facility, the shock tunnel is particularly well suited to heat-transfer studies. Recent advances in force and pressure measuring techniques, however, promise to extend its application to a wider range of investigations.

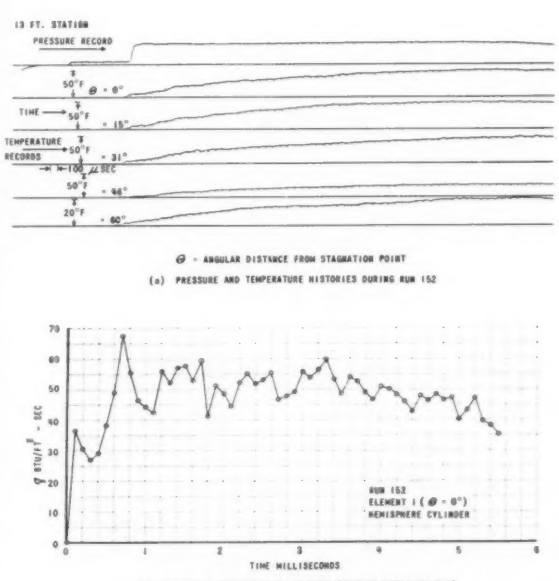
13 FT. STATION
PRESSURE RECORD
TIME
TEMPERATURE RECORDS
θ = ANGULAR DISTANCE FROM STAGNATION POINT
(a) PRESSURE AND TEMPERATURE HISTORIES DURING RUN 152
RUN 152
ELEMENT 1 (θ = 0°)
HEMISPHERE CYLINDER
TIME MILLISECONDS
(b) RECORD OF STAGNATION POINT HEAT TRANSFER RATE WITH TIME

Fig. 9. Experimental data from typical heat-transfer test.

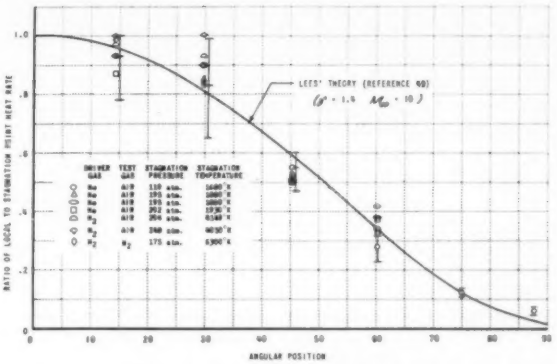

Fig. 10. Comparison of heat-transfer distribution with high Mach Number laminar theory for a hemisphere.

References

[1] Resler, E. L., Lin, S. C., and Kantrowitz, A., *The Production of High Temperature Gases in Shock Tubes*, J. Appl. Phys., Vol. 23, No. 12, pp. 1390–1399, December, 1952.

[2] Geiger, F. W., Martz, C. W., and Hollyer, R. N., *The Shock Tube as an Instrument for the Investigation of Transonic and Supersonic Flow Patterns*, Univ. of Michigan, Engineering Research Institute Project 720–4, June, 1949.

[3] Hertzberg, A., and Kantrowitz, A., *Studies With an Aerodynamically Instrumented Shock Tube*, J. Appl. Phys., Vol. 21, No. 9, pp. 874–875, September, 1950.

[4] Rabinowicz, J., *Aerodynamic Studies in the Shock Tube*, GALCIT Hypersonic Research Project, Memorandum No. 38, June, 1957.

[5] Lin, S. C., *Electrical Conductivity of Thermally Ionized Air Produced in a Shock Tube*, AVCO Research Laboratory, Research Rept. No. 5, February, 1957; also, Lamb, L., and Lin, S. C., J. Appl. Phys., Vol. 28, No. 7, pp. 754–759, July, 1957.

[6] Blackman, V. H., *Vibrational Relaxation in O_2 and N_2*, J. Fluid Mech., Vol. 1, No. 1, pp. 61–85, May, 1956.

[7] Glick, H. S., and Wurster, W. H., *Shock Tube Study of Dissociation Relaxation in Oxygen*, J. Chem. Phys., Vol. 27, No. 5, November, 1957.

[8] Penner, S. S., Harshbarger, F., and Vali, V., *An Introduction to the Use of the Shock Tube for the Determination of Physico-Chemical Parameters*, Cal Tech Jet Propulsion Center Rept. AD-95210, AFOSR TN 56-344, June, 1956.

[9] Glick, H. S., Klein, J. J., and Squire, W., *Single-Pulse Shock Tube Studies of the Kinetics of the Reaction $N_2 + O_2 \rightleftarrows 2\ NO$ Between 2,000–3,000°K.*, C.A.L. Rept. No. AD-959-A-1, AFOSR TN 57-407, September, 1957; also, J. Chem. Phys., Vol. 27, No. 4, pp. 850–857, October, 1957.

[10] Carrington, T., and Davidson, N., *Shock Waves in Chemical Kinetics: The Rate of Dissociation of N_2O_4, I_2*, J. Phys. Chem., Vol. 57, No. 4, pp. 418–427, April 16, 1953.

[11] Feldman, S., *The Chemical Kinetics of Air at High Temperatures: A Problem in Hypersonic Aerodynamics*, AVCO Research Rept. No. 4, February, 1957.

[12] Wurster, W. H., Glick, H. S., and Treanor, C. E., *Radiative Properties of High Temperature Air*, C.A.L. Rept. No. QM-997-A-1, September, 1957.

[13] Keck, J., Kivel, B., and Wentink, T., *Emmissivity of High Temperature Air*, AVCO Research Rept. No. 8, February, 1957.

[14] Squire, W., Hertzberg, A., and Smith, W. E., *Real Gas Effects in a Hypersonic Shock Tunnel*, C.A.L. Rept. No. AD-789-A1,-AEDC 55-14, March, 1955.

[15] Lees, L., *Hypersonic Flow*, Proceedings of the Fifth International Aeronautical Conference, IAS-RAeS, June, 1955.

[16] Li, Ting-Yi, and Geiger, R. E., *Stagnation Point of a Blunt Body in Hypersonic Flow*, IAS Preprint No. 629, January, 1956.

[17] Rose, P. H., and Stark, W. I., *Stagnation Point Heat-Transfer Measurements in Dissociated Air*, AVCO Research Rept. No. 3, April, 1957; also, Journal of the Aeronautical Sciences, Vol. 25, No. 2, pp. 86–97, February, 1958.

[18] Hertzberg, A., *Shock Tubes for Hypersonic Flow*, C.A.L. Rept. No. AF-702-A-1, May, 1951.

[19] Wittliff, C. E., and Wilson, M. R., *Shock Tube Driver Techniques and Attenuation Measurements*, C.A.L. Rept. No. AD-1052-A-4, AFOSR TN 57-546, AD 136531, August, 1957.

[20] Hertzberg, A., Smith, W. E., Glick, H. S., and Squire, W., *Modifications of the Shock Tube for the Generation of Hypersonic Flow*. C.A.L. Rept. No. AD-789-A-2, AEDC TN 55-15, March, 1955.

[21] Glick, H. S., *The Tailored-Interface Hypersonic Shock Tunnel* C.A.L. Memorandum for the Record, June, 1956.

[22] Lukasiewicz, J., *Shock Tube Theory and Applications*, Rept. 15, National Aeronautical Establishment, Canada, 1952.

[23] Rudinger, G., *Wave Diagrams for Nonsteady Flow in Ducts*, D. Van Nostrand Co., Inc., New York, 1955.

[24] Glass, I. I., and Patterson, G. N., *A Theoretical and Experimental Study of Shock-Tube Flow*, Journal of the Aeronautical Sciences, Vol. 22, No. 2, pp. 73–100, February, 1955.

[25] Russo, A., and Hertzberg, A., *A Method for Improving the Performance of Shock Tubes*, Jet Propulsion, Vol. 27, No. 11, pp. 1191–1193, November, 1957.

[26] Henshall, B. D., *The Use of Multiple Diaphragms in Shock Tubes*, N.P.L. (England) ARC CP 291, December, 1955.

[27] Dolder, K., *Multiple-Chamber Shock Tubes*, United Kingdom Atomic Energy Research Establishment Rept. A.E.R.E. GP/R2238, May, 1957.

[28] Feldman, S., *Hypersonic Gas Dynamic Charts for Equilibrium Air*, AVCO Research Laboratory, January, 1957.

[29] Hilsenrath, J., et al., *Tables of Thermal Properties of Gases*, NBS Circular 564, November, 1955.

[30] *Handbook of Supersonic Aerodynamics*, NAVORD Rept. 1488, Vol. 5, 1953.

[31] Beckett, C., *Equilibrium Properties of Argon Free Air—Extension of Hilsenrath-Beckett Tables to High Densities*, NBS calculations obtained by private communication.

[32] Mark, H., *The Interaction of a Reflected Shock Wave With the Boundary Layer in a Shock Tube*, AFOSR TN 57-345, Cornell Univ., June, 1957; also, Readers' Forum, Journal of the Aeronautical Sciences, Vol. 24, No. 4, pp. 304–306, April, 1957.

[33] Taylor, G. I., *The Instability of Liquid Surfaces When Accelerated in a Direction Perpendicular to Their Planes*, Proc. Roy. Soc., A201, pp. 192–196, March 22, 1950.

[34] Libby, P., and Visich, M., Jr., *Laminar Heat Transfer in Two-Dimensional Subsonic Effusors*, Journal of the Aeronautical Sciences, Vol. 22, No. 6, pp. 425–430, June, 1955.

[35] Sibulkin, M., *Heat Transfer to an Incompressible Turbulent Boundary Layer and Estimation of Heat-Transfer Coefficients at Supersonic Nozzle Throats*, Journal of the Aeronautical Sciences, Vol. 23, No. 2, pp. 162–172, February, 1956.

[36] Penner, S. S., *Introduction to the Study of Chemical Reactions in Flow Systems*, AGARDograph No. 7, Butterworth Sci. Pub. (London), 1955.

[37] Bray, K. N. C., *Departure from Dissociation Equilibrium in a Hypersonic Nozzle*, ARC 19,983, March, 1958.

[38] Logan, J. G., *Relaxation Phenomena in Hypersonic Aerodynamics*, paper presented at the Aerodynamics—III Session, 25th Annual Meeting, IAS, New York, January, 1957.

[39] Lighthill, M. J., *Dynamics of a Dissociating Gas, Part I—Equilibrium Flow*, J. Fluid Mech., Vol. 2, Part 1, January, 1957.

[40] Byron, S. R., *Interferometric Measurement of the Rate of Dissociation of Oxygen Heated by Strong Shock Waves*, Cornell University Graduate School of Aeronautical Engineering.

[41] Rabinowicz, J., *Measurement of Turbulent Heat Transfer Rates on the Aft Portion and Blunt Base of a Hemisphere-Cylinder in the Shock Tube*, California Institute of Technology Hypersonic Research Project Memo. No. 41, November, 1957.

[42] Powers, W. E., Stetson, K. F., and Adams, M. C., *A Shock Tube Investigation of Heat Transfer in the Wake of a Hemisphere-Cylinder With Application to Hypersonic Flight*, AVCO Research Rept. 30, August, 1958.

[43] Glick, H. S., Hertzberg, A., and Smith, W. E., *Flow Phenomena in Starting a Hypersonic Shock Tunnel*, C.A.L. Rept. No. AD-789-A-3, AEDC TN 55-16, March, 1955.

[44] Hertzberg, A., *The Shock Tunnel and Its Applications to Hypersonic Flight*, C.A.L. Rept. No. AD 1052-A-5, AFOSR TN 57-268, AD 126567, June, 1957; also, AGARD Rept. 144, July, 1957.

[45] Vidal, R. J., *Model Instrumentation Techniques for Heat Transfer and Force Measurements in a Hypersonic Shock Tunnel*, C.A.L. Rept. No. AD-917-A-1, WADC TN 56-315, February, 1956.

[46] Reece, J. W., and Stevenson, L. M., *Tests of a Stagnation Pressure Probe Using a Miniature Statham Transducer*, C.A.L. Rept. No. WTH-001, August, 1958.

[47] Wilson, M. R., and Hiemenz, R. J., *High Speed Multiple Spark Light Source*, Rev. Sci. Inst., Vol. 29, November, 1958.

[48] Fay, J. A., and Riddell, F. R., *Theory of Stagnation Point Heat Transfer in Dissociated Air*, AVCO Research Rept, No. 1, June, 1956; also, Journal of the Aeronautical Sciences. Vol. 25, No. 2, pp. 73–86, February, 1958.

[49] Lees, Lester, *Laminar Heat Transfer Over Blunt-Nosed Bodies at Hypersonic Flight Speeds*, Jet Propulsion, Vol. 26, No. 4, pp. 259–269, April, 1956.

[50] Wittliff, C. E., and Rudinger, G., *Summary of Instrumentation Development and Aerodynamic Research in a Hypersonic Shock Tunnel*, C.A.L. Rept. No. AD-917-A-2, WADC TR 58-401 Part I, August, 1958.

Midwestern Conference on Fluid and Solid Mechanics

University of Texas, September 9–11, 1959

Although the Conferences are held on a regional basis, there are no restrictions on attendance or on the residence of authors of technical papers.

Abstracts and titles of proposed papers should have been submitted before April 1, 1959, to the Chairman: *Dr. Milton J. Thompson, Professor of Aeronautical Engineering, University of Texas.* Complete manuscripts will be required by June 1, 1959, to make possible the distribution of the Proceedings at the opening of the Conference. Inquiries concerning other details of the Conference should also be addressed to Professor Thompson.

A number of technical societies and research organizations, including the IAS, have joined with The University of Texas in cosponsoring this Midwestern Conference.

The Smallest Height of Roughness Capable of Affecting Boundary-Layer Transition

A. M. O. SMITH* AND DARWIN W. CLUTTER**

Douglas Aircraft Company, Inc.

SUMMARY

An investigation was made to determine the smallest size of isolated roughness that will affect transition in a laminar-boundary layer. Critical heights for three types of roughness were found in a low-speed wind tunnel. The types were (1) two-dimensional spanwise wires, (2) three-dimensional discs, and (3) a sandpaper type. In addition to type of roughness, test variables included the location of roughness, pressure distribution, degree of tunnel turbulence, and length of natural laminar flow.

The most satisfactory correlation parameter was found to be the roughness Reynolds Number, based on the height of roughness and flow properties at this height. The value of this critical Reynolds Number was found to be substantially independent of all test variables except the shape of roughness. This parameter also correlates well other published data on critical roughness in low-speed flow. The value of the roughness Reynolds Number necessary to move transition forward to the roughness itself was also determined for the three types of roughness and was found to be approximately constant for a given type of roughness.

An investigation of the limited amount of available data on critical roughness in supersonic flow indicates that the effects of roughness may still be correlated by the roughness Reynolds Number. The value of this Reynolds Number depends primarily on the Mach Number at the top of the roughness. When this Mach Number is greater than 1.0, the roughness Reynolds Number based on conditions behind a shock is probably the characteristic parameter.

SYMBOLS

A = constant
a = speed of sound
c = chord of airfoil or test surface
d = diameter or width of roughness element
H = boundary-layer shape parameter δ^*/θ
k = roughness height
R = Reynolds Number, Ux/ν unless otherwise noted
R_c = chord Reynolds Number $U_\infty c/\nu$
R_k = roughness Reynolds Number $u_k k/\nu$
R_{δ^*} = Reynolds Number based on displacement thickness $U\delta^*/\nu$
R_θ = Reynolds Number based on momentum thickness $U\theta/\nu$
U = local velocity outside boundary layer
u = velocity within boundary layer in x direction
v_* = friction velocity $\sqrt{\tau_w/\rho}$
x = distance along surface measured from forward stagnation point
y = distance perpendicular to surface
α = angle of attack
β = shape parameter of Hartree boundary-layer profile, $U = Cx^{\beta/(2-\beta)}$
δ = boundary-layer thickness
δ^* = boundary-layer displacement thickness
θ = boundary-layer momentum thickness
λ = length of a wave in the surface
μ = dynamic viscosity
ν = kinematic viscosity
ρ = mass density

Subscripts

crit = evaluated at the critical roughness
H.W. = evaluated at the hot wire
k = evaluated at the roughness element
T = evaluated at transition
w = evaluated at the wall
0 = natural transition
∞ = conditions in undisturbed flow
δ = evaluated at edge of boundary layer
1 = evaluated ahead of normal shock
2 = evaluated aft of normal shock

Received June 30, 1958. Appendix received December 1, 1958.

* Supervisor, Aerodynamics Research, El Segundo Division.

** Aerodynamicist, Aerodynamics Research, El Segundo Division.

INTRODUCTION

THE PUBLISHED DATA on the effects of isolated roughness elements on transition fall primarily into two categories: (a) the effect of a roughness element on the transition point as a continuous function of all roughness heights, and (b) the more restricted problem of determining the largest height of roughness that does not affect the transition point. Category (b) is the principal subject of this paper.

Although the published data on critical roughness heights cover a large range of critical roughness Reynolds Numbers ($R_{k\,crit} = (u_k k/\nu)_{crit} = 60$ to 1,100), the data do not cover the range of relatively high velocity and small critical height. The test surfaces used in most of the investigations had rather low transition Reynolds Numbers. Moreover, the various investigators have presented their results in a variety of ways by means of a variety of correlation parameters, such as k/δ^*, R_{δ^*}, R_k, etc. Most of the data were obtained in low-speed flow.

The primary part [Part (I)] of this paper concerns itself with low-speed flow and is essentially a digest of reference 1.† Part (II) extends the results to high-speed flows.

PART (I) CRITICAL ROUGHNESS IN LOW-SPEED FLOW

The principal purpose of the present investigation was to determine the smallest or critical roughness height over a large range of Reynolds Numbers, as affected by (1) body pressure distribution, (2) roughness shape, (3) roughness height, (4) roughness location, (5) tandem

† This research was sponsored by the U.S. Navy Bureau of Aeronautics, under Contract NOa(s) 54-773c.

arrangement of roughness elements, and (6) wind-tunnel turbulence.

Of course, an immediate purpose was to establish, if possible, a general method for correlating the critical roughness heights with parameters of the flow (such as R_θ or R_k). Fulfillment of this objective was achieved partially by a general examination of already available test data and partially by creation of new data, as described later. Because of the variety of presentation made in the past, considerable effort was expended to bring most of the data, including our own, together into a consistent presentation.

Factors Affecting Transition Due to Roughness

Transition from laminar to turbulent flow is brought about by various types of disturbances in the laminar boundary layer. On flat or convex surfaces the magnitude or growth of disturbances is dependent on one or more of the following:

(a) Pressure gradient
(b) Free-stream velocity and viscosity
(c) Free-stream turbulence
(d) Internal flow disturbances, such as blowing into the boundary layer, thermal gradients, and vibrations
(e) Secondary-flow effects, as, for example, the effects of sweep
(f) Surface roughness

In this investigation we are primarily interested in disturbances introduced by the last-named factor—that is, roughness—but whether or not these disturbances affect transition will depend on both the static and the dynamic properties of the boundary layer, which are dependent on the other factors listed above.

Neglecting free-stream turbulence and pressure gradient, the transition point x_T due to a given shape of roughness is a function of the following variables:

k = height of roughness
x_k = position of roughness
u_k = velocity in the undisturbed boundary layer corresponding to the top of the roughness
U = velocity outside the boundary layer
$(\partial u/\partial y)_k$ = velocity gradient at top of roughness
ν = kinematic viscosity

The location of transition x_T can be written functionally as

$$x_T = f(k, x_k, u_k, U, \partial u/\partial y_k, \nu) \tag{1}$$

Obviously these variables are not independent of each other, for, in a particular flow,

$$u_k/U = f(k, x_k)$$

and also $$(\partial u/\partial y)_k = f(k, x_k)$$

Therefore, Eq. (1) can be reduced to

$$x_T = f(k, x_k, U, \nu) \tag{1a}$$

These variables may be grouped into various nondimensional parameters. One such parameter is the roughness Reynolds Number,

$$R_k = u_k k/\nu \tag{2}$$

If k is not large compared to the boundary-layer thickness, we know from the approximately linear nature of the bottom of the boundary-layer profile that

$$u_k/U = A\ k/\theta_k \tag{3}$$

where A is a constant.

The roughness Reynolds Number may now be written

$$R_k = (u_k k/\nu) = (U\theta_k/\nu)(u_k/U)(k/\theta_k) \doteq A\ R_{\theta_k}[k/\theta_k]^2 \tag{4}$$

Eq. (4) is a functional relation of three dimensionless parameters.

Eq. (4) is valid for small k only; if k is so great as to be outside the boundary layer,

$$u_k/U = 1$$

and

$$R_k = (k/\theta_k)R_{\theta_k} \tag{5}$$

That is, R_k varies linearly with k/θ_k for large k, whereas for small k it varies quadratically as k/θ_k.

Of course, there are other nondimensional parameters that could be obtained from the variables above; a relation involving R_k was chosen because a Reynolds Number is inferred as the critical parameter if it is assumed either that a wake is created or that vortices are shed from the roughness element at a certain critical Reynolds Number and that one or both of these disturbances either cause immediate transition or, when amplified, cause transition farther downstream. The criterion that $R_{k\,crit}$ = constant was first proposed by Schiller in 1932 (see reference 2, page 311).

Previous Investigations

Most previous investigators of the effect of roughness on transition have presented their results in the form of parameters similar to those of Eq. (4) above (see references 3 through 14). The parameters are similar in that they include a roughness Reynolds Number based either on the roughness height or on the boundary-layer thickness at the roughness and a roughness-height parameter such as k/θ_k or $k/\delta_k{}^*$. The investigations indicate that the shape of the roughness has a major effect on the values of the critical-roughness parameters, but, on the other hand, they indicate that surface curvature, history of the boundary layer, and free-stream turbulence have only minor effects on the values, even though these latter factors are major ones in establishing natural transition on a smooth surface.

The various investigations show disagreements on several points: (1) the effect of roughness shape on the critical roughness height, (2) the ratio of critical height to the height of the boundary layer at the roughness, and (3) whether or not the length of natural laminar flow greatly affects the value of critical roughness.

Although the previous investigations covered a wide range of types, heights, and positions of roughness, they did not give information on the case of a small roughness element close to the leading edge. This is perhaps the most important case in determining the tolerable roughness on a body. Part of the purpose of the investigation reported here is to fill this gap and reconcile the discrepancies in the existing data.

Test Facilities and Techniques

Wind Tunnel

All tests in the present investigation were made in the Douglas El Segundo 30- by 45-in. wind tunnel. Air speeds as high as 185 ft. per sec. were used during the tests. The settling chamber at the entrance of the contraction cone of the tunnel accommodates six removable screens, 40 mesh by 0.0065-in. wire, spaced 10 in. apart. For the majority of tests, all six screens were used, but, for the purpose of learning the effect of turbulence, a few tests were run with one screen and some with no screens. With all screens in place the turbulence is quite low; transition measurements on the model, which are described below, gave an amplification factor of $e^{8.7}$, which compares favorably with values obtained in other low-turbulence tunnels and in flight.[15]

The 108-In.-Chord Test Surface

The model was designed as a nearly constant-velocity, two-dimensional surface spanning the tunnel from top to bottom. The model profile began as a sharp 30° wedge, fairing into a flat-sided surface 25 in. aft of the leading edge, being so designed as to give a constant velocity over the curved portion.[16] The model is shown in Figs. 1 and 2. The flat section was 2.254 in. thick and extended aft from 25 in. to 96 in. from the leading edge. The last 12 in. of the chord was a simple, radius-nose, straight-sided flap, which could be deflected between −13° and +13°.

Surface joints could not be made to fair as smoothly as was desired on the test surface; therefore the entire test surface was covered with a single sheet of "Mylar" polyester film (manufactured by the Dupont Company). The "Mylar" film was 0.005 in. thick and had an average root mean square roughness of 2.5 and a maximum of 4 microinches. The film was folded around the nose and carried aft to the leading edge of the flap, being secured to the model surface with strips of pressure-sensitive tape (adhesive on both sides). This "Mylar" film proved satisfactory for fairing out the discontinuities of the metal surface, and the film stood up well for the duration of the tests.

Since the test section of the wind tunnel is only 4 ft. in length, the leading edge of the model extended 4.5 in. into the contraction cone of the tunnel and extended aft 55.5 in. into the diffuser. A profile of the tunnel wall is shown in Fig. 1, along with the model.

Types of Roughness

The roughness tested was primarily of three types: spanwise round wires, 1/16-in. diameter circular discs, and sandpaper. A few tests were made with the Mylar sanded at right angles to the direction of the airflow, but these will not be discussed in this paper; for further details, see reference 1. The wires may be thought of as representing spanwise skin joints; they are, of course, two-dimensional in nature. The discs may be considered as representing spots of dirt or incompletely countersunk flush rivets; they are a three-dimensional type of roughness. The sandpaper and scratched Mylar cannot very well be classified dimensionally. One or the other or both might represent roughness such as may arise from raindrop and dirt erosion, dust on the surface, mud spots, or the like.

Stretch-straightened lengths of brass or copper wires were stretched tightly spanwise across the test surface at the selected location. They were secured to the surface by taping the ends and by nitrate dope applied to the full span of the wire. The wires used in the tests varied from 0.002 in. to 0.043 in. in diameter. Tests were not confined to a single wire since, in addition, several runs were made with wires in tandem—that is, one located a few inches behind the other.

The second type of roughness tested consisted of spanwise rows of brass cylindrical discs of 1/16-in. diameter. The discs ranged in height from 0.0029 in. to 0.030 in. The spanwise spacing of the discs was 1.25 in. throughout, except for a few runs in which only a single disc cemented to the center was tested.

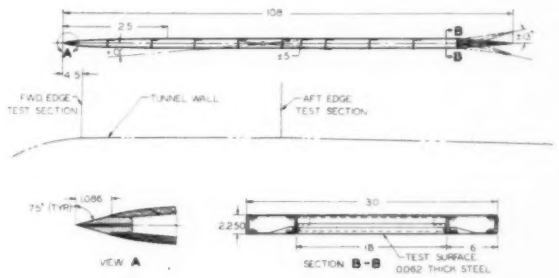

FIG. 1. Details of the two-dimensional test surface.

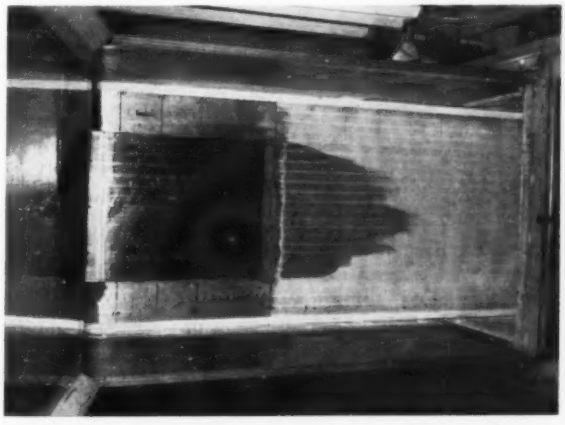

FIG. 2. Typical china-clay transition pattern on the two-dimensional test surface. The irregularity of the transition locus is due partly to transverse contamination from the tunnel walls and partly to irregularities in the roughness element. The rearmost point was always used in reduction of data.

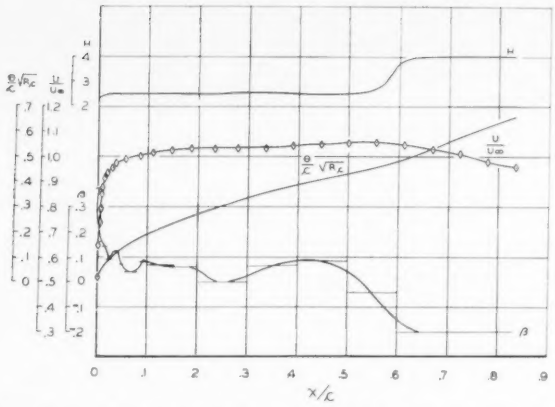

FIG. 3. Variation of velocity and boundary-layer parameters with chordwise position for $\alpha = 0°$.

Two materials were used to represent the sandpaper type of roughness—No. 100 grit Crystolon, an abrasive, and ground steel shot, a steel grit used in sandblasting. To apply the grit, the Mylar surface of the model was masked off locally to leave a 1/4-in.-wide spanwise gap. Nitrate dope was applied over the exposed strip and the grit was blown onto the wet dope. Before the dope had hardened, the masking tape was removed so that no rough edge was left in the dope by the tape. In this way satisfactory 1/4-in.-wide strips of roughness were made.

Measurement of Roughness Height

Heights of wire, disc, and sandpaper roughness were always measured on the model by means of a roughness gage consisting primarily of an Ames dial gage, reading to 0.0001 in. The measurement sought and used was maximum height of roughness along the entire span. For the wires, every inch of each wire was checked. For the rows of discs, the height of each individual disc was measured. For the sandpaper type of roughness, the entire area of roughness was searched to find the highest point. When measured this way the actual roughness heights were found to be appreciably greater than the nominal heights.

The maximum error in determining the roughness height was 7 per cent for the wires and discs, with the exception of the 0.002-in. wire, where the error was about 15 per cent. For the sandpaper type of roughness, the error was less than 12 per cent.

Methods of Determining Transition

Two methods were principally used to determine transition—the china-clay and the stethoscope techniques. These two techniques were checked with the hot-wire anemometer and surface pitot tube technique. Usually the various techniques indicated values of R_T that agreed with each other within 4 per cent.

RESULTS

Transition Measurements With and Without Roughness

The tests were made with the model at angles of attack of +1°, 0°, −1°, and −2°. The velocity distribution for the model at an angle of attack of 0° is shown in Fig. 3. The boundary-layer parameters needed in the data reduction are also shown. These parameters were determined by the method presented in reference 17.

Fig. 4(a) shows the variation of the natural transition Reynolds Number with chord Reynolds Number for four angles of attack. The highest transition Reynolds Number $R_T = 7.4 \times 10^6$ was obtained at an angle of attack of −2°. Fig. 4(b) shows the corresponding variation of R_{θ_T}, the Reynolds Number based on the momentum thickness at transition, with chord Reynolds Number.

Fig. 5 illustrates the effects on transition produced by the various types of roughness having the same height. It shows that, as the air speed is increased beyond the point where the roughness first begins to cause premature transition, the rate of forward movement of transition with speed increases rapidly until transition occurs at the element itself. The rate of this movement forward is greater for the three-dimensional disturbances than for the two-dimensional. A single disc has no effect on natural transition until it produces a wedge of turbulence whose apex is at the disc itself. Fig. 5 also exhibits the fact that three-dimensional roughnesses are less apt than two-dimensional to promote transition.

Transition Measurements With Several Values of Tunnel Turbulence

The effect of varying the degree of tunnel turbulence on the natural transition Reynolds Number is shown in Fig. 6. The Figure shows the decrease in transition Reynolds Number as the number of screens in the tunnel was reduced from six to one or none. The tunnel turbulence was not measured in this series of tests, but

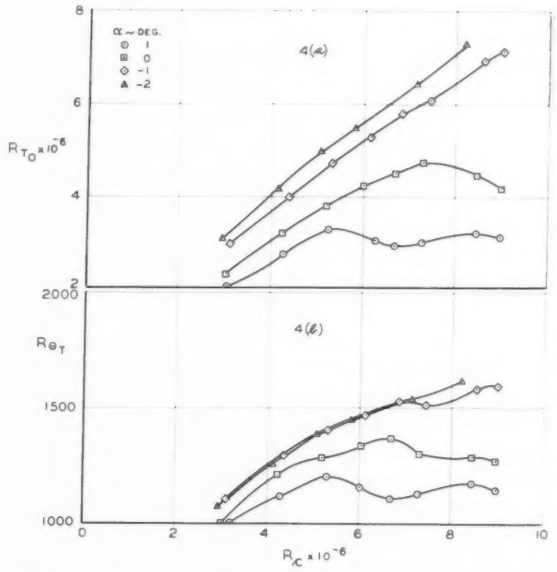

FIG. 4. Variation of the natural transition Reynolds Number and the Reynolds Number based on momentum thickness at transition with chord Reynolds Number for various angles of attack.

previous measurements and calculations indicated the following: for no screens,

$$100\sqrt{(u'^2 + v'^2 + w'^2)/3}/U \simeq 0.26 \text{ to } 0.30$$

for six screens,

$$100\sqrt{(u'^2 + v'^2 + w'^2)/3}/U \simeq 0.03$$

where u', v', and w' are root mean square values of the u, v, and w fluctuations, respectively.

Fig. 7 shows the effect of increased tunnel turbulence on the heights of roughness required to cause premature transition. There is a very slight increase in critical roughness with the increased tunnel turbulence.

Definition of Critical Roughness

Observation of plots of $(x/c)_T$ versus R_c shows that it is frequently difficult to determine exactly when a given roughness becomes effective in reducing the length of natural laminar flow. Therefore, a new definition has been used in the data reduction, and this definition is presented in this Section.

Plots can be made of the ratio of the transition Reynolds Numbers with and without roughness R_T/R_{T_0} versus the height parameter k/θ_k. Typical curves of such plots are shown in Fig. 8. As can be seen from these plots, it is difficult to determine exactly the value of k/θ_k at which the roughness becomes effective in reducing the natural transition Reynolds Number—that is, when the ratio of transition Reynolds Numbers R_T/R_{T_0} becomes just less than unity. *Therefore, the definition of critical roughness for a particular configuration was taken as the value of k for which R_T has decreased to 0.95 R_{T_0}.* Using this definition, the critical value of k/θ_k can be determined from the plots of k/θ_k versus R_T/R_{T_0} for a particular roughness height and location, as is shown in Fig. 8. This critical value of k/θ_k can then be used to determine the critical value of R_{θ_k}, R_{x_k}, etc. The same type of plot—that is, R_T/R_{T_0} versus k/θ_k—was used to determine the roughness values when transition reached the roughness element itself.

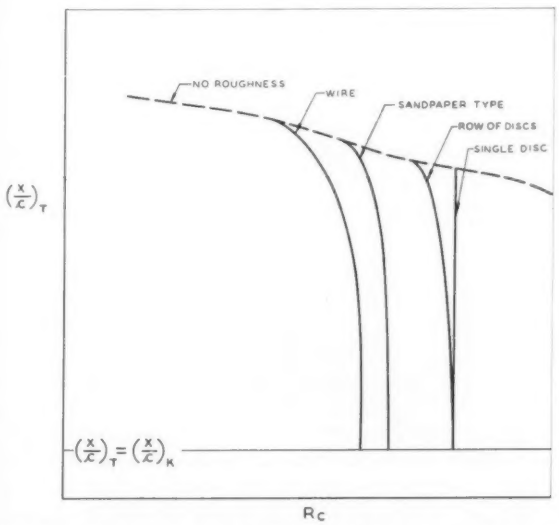

FIG. 5. Variation of transition point with chord Reynolds Number for various types of roughness having the same height

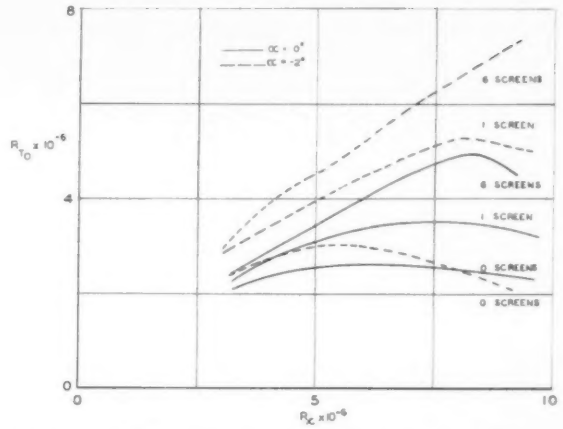

FIG. 6. Variation of natural transition Reynolds Number with chord Reynolds Number with six, one, or no turbulence screens installed in the tunnel.

The value of the critical roughness Reynolds Number can be determined from the relation

$$R_k = u_k k/\nu = (k/\theta_k)(u_k/U)R_{\theta_k}$$

where all variables are determined at critical conditions. The value of u_k/U can be determined from the known model velocity distribution (β from $U = Cx^{\beta/(2-\beta)}$) and the tables of u/U of reference 18.

Method of Presentation of Critical-Roughness Parameters

The results of this investigation will be presented on plots similar to that shown in Fig. 9, which shows the relation between R_k, R_{θ_k}, u_k/U, and k/θ_k for several boundary-layer profiles. Fig. 9 shows the relation between R_{θ_k}, k/θ_k, and R_k for $R_k = 200$ and various pres-

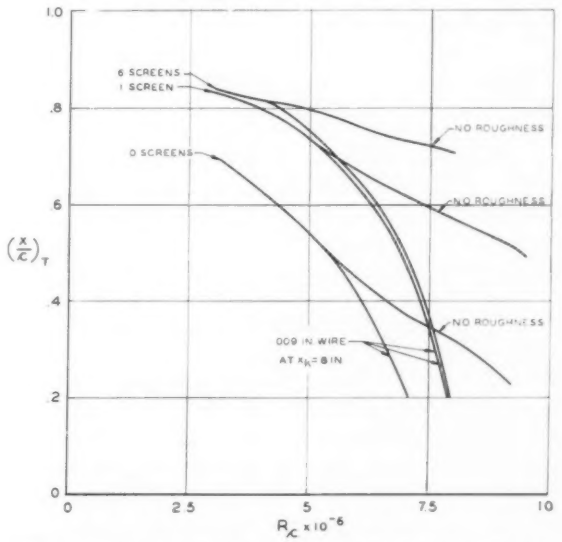

FIG. 7. Variation of transition point with chord Reynolds Number for single spanwise wires with six, one, or no turbulence screens installed in the tunnel, at $\alpha = -2°$.

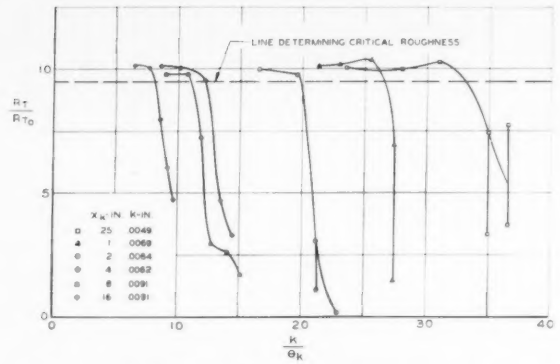

FIG. 8. Variation of ratio of transition Reynolds Number, with and without roughness R_T/R_{T_0}, with k/θ_k for single spanwise wires at $\alpha = 0°$.

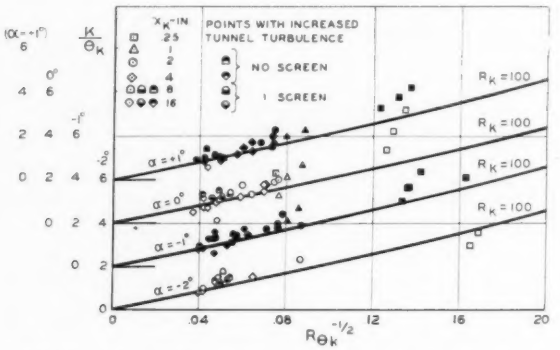

FIG. 10. Critical values of k/θ_k and $R_{\theta_k}{}^{-1/2}$ for single spanwise wires. Open symbols are for $\alpha = 0°$ and $-2°$. Solid symbols are for $\alpha = -1°$ and $+1°$. Half-solid symbols denote values at increased tunnel turbulence. Lines of R_k = constant represent Blasius boundary layer ($\beta = 0$).

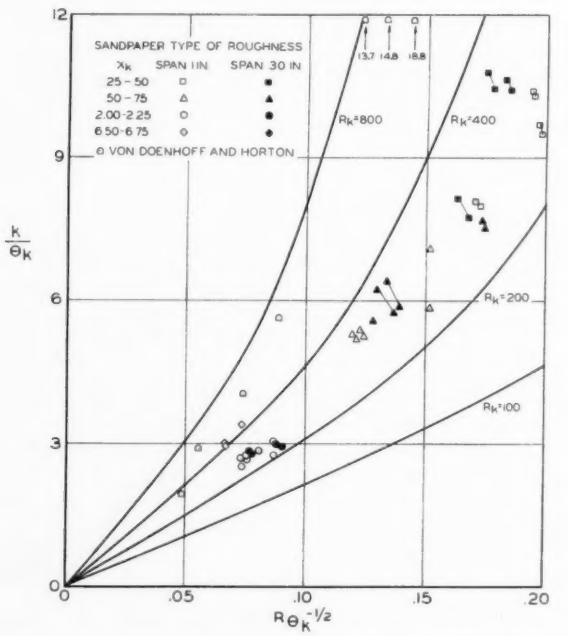

FIG. 12. Critical values of k/θ_k and $R_{\theta_k}{}^{-1/2}$ for 1/4-in. strips of sandpaper type of roughness. Values from reference 14 are also shown. Lines of R_k = constant represent Blasius boundary layer ($\beta = 0$).

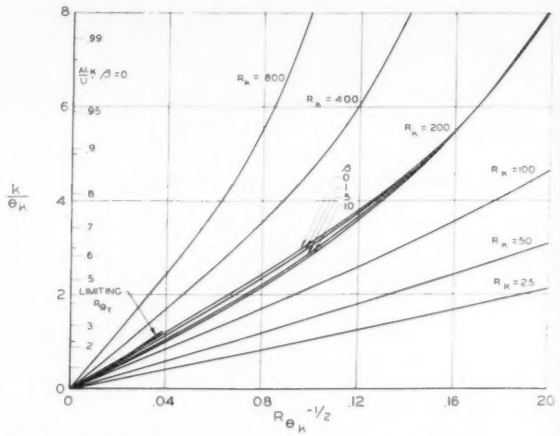

FIG. 9. The relation between R_k, R_{θ_k}, u_k/U, and k/θ_k for several boundary-layer profiles.

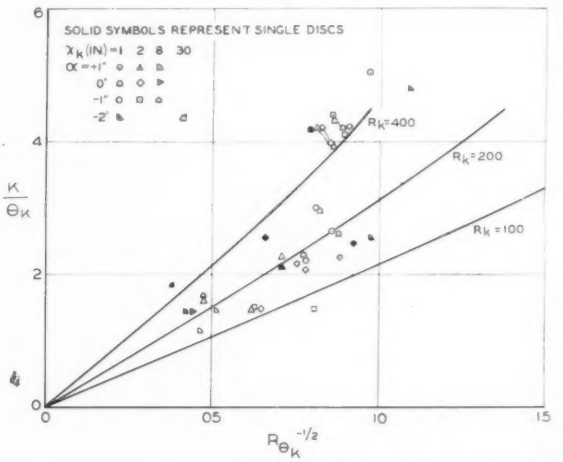

FIG. 11. Critical values of k/θ_k and $R_{\theta_k}{}^{-1/2}$ for spanwise rows of discs. Lines of R_k = constant represent Blasius boundary layer ($\beta = 0$).

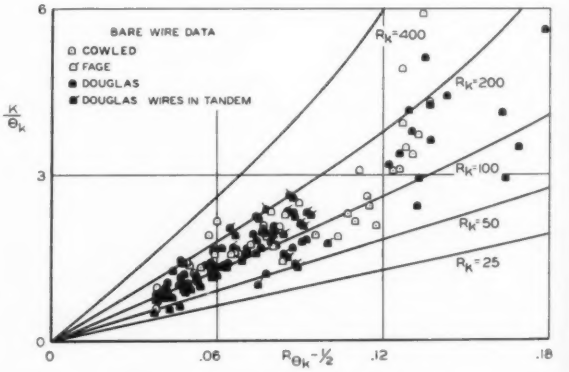

FIG. 13. Critical values of k/θ_k and $R_{\theta_k}{}^{-1/2}$ for spanwise wires of this and previous investigations. Lines of R_k = constant represent Blasius boundary layer ($\beta = 0$).

sure distributions ($\beta = 0$, 0.1, 0.5, and 1.0 from the Falkner-Skan family of velocity profiles). Over the range of β's shown, the shape of the boundary-layer profile has only a minor effect on the $k/\theta_k - R_{\theta_k}{}^{-1/2} - R_k$ relation. For the present investigation, β varied from 0.025 to 0.64 in the test region. Natural transition sets a lower limit for the values of critical $R_{\theta_k}{}^{-1/2}$, and this lower limit may be estimated from stability theory and experimental results.[15] The lower limit is shown in Fig. 9, for the curves of $R_k = 200$ and the various β's and a small-perturbation amplification factor of e^9; that is, $\int \beta_i dl = 9$ (reference 15). It should be noted that this lower limit of R_{θ_k} is a function of β only. Also shown in Fig. 9 is the relation between $R_{\theta_k}{}^{-1/2}$, k/θ_k, and R_k for R_k's equal to other constant values for $\beta = 0$; that is, flat-plate flow. The relation between u_k/U and k/θ_k for $\beta = 0$ is also presented.

The presentation of the data on a three-parameter plot with R_k, $R_{\theta_k}{}^{-1/2}$, and k/θ_k as the variables is consistent with the relation for R_k developed above,

$$R_k \simeq A(k/\theta_k)^2 R_{\theta_k} \qquad (k/\theta_k \text{ small}) \tag{4}$$

Critical-Roughness Data

Fig. 10 shows the values of critical roughness of wires of various sizes and locations at various angles of attack. The critical roughness points tend to follow the lines of $R_k = 100$ with a scatter of approximately 50 per cent, except at the most forward location of roughness—that is, at $x_k = 0.25$ in.—where the values of R_k were as high as 260. The values of critical roughness appear to be independent of angle of attack, with the possible exception that, for those wires located close to the leading edge ($x_k = 0.25$ in.), there is a trend for R_k and k/θ_k to decrease as α varies from 0 to $-2°$.

The increase of R_k as k approaches the leading edge is consistent with the observations presented by Preston in reference 19. Preston points out that there is a lower limit to the Reynolds number R_θ at which fully developed turbulent flow can occur. This limit can not only be predicted by theory but is also observed experimentally. The lower experimental limit is about $R_\theta = 320$. To cause transition at a point where $R_\theta < 320$, the device producing transition must add a drag to the boundary layer to raise R_θ to a value of 320. Clearly, any roughness has a drag and, consequently, increases the momentum thickness of the boundary layer. Of course, in addition to the criterion that $R_\theta > 320$, disturbances must be present and must be amplified, to establish turbulent flow. The amplification of the disturbance depends on both R_θ and the pressure gradient. In the present setup, as one approaches the leading edge, R_θ becomes small and the pressure gradient becomes more favorable. Both of these factors have a stabilizing effect on any disturbance in the boundary layer and, consequently, the roughness must produce larger and larger disturbances as it approaches the leading edge if it is to produce early transition.

In any case, the variation of $R_{k\,crit}$ with pressure distribution is small. The effect of tunnel turbulence on the values of critical roughness of the wire type is indicated in Fig. 10. There appears to be a slight increase in the values of $R_{k\,crit}$ and $(k/\theta_k)_{crit}$ with increased tunnel turbulence.

Fig. 11 gives the critical values of roughness for the spanwise rows of discs and for single discs. The Figure shows more scatter and higher critical values of R_k and k/θ_k than does the similar plot for the two-dimensional roughness. The scatter may be due to the effect of shape, which subject is discussed further below. The single discs show higher critical values of R_k than do rows of discs. This fact is not surprising, for the disturbance produced by a disc spreads in a wedge-shaped wake behind the disc and the interaction of several of these disturbance wedges produces earlier transition than that caused by a single disc. It is worth noting again that a single disc had no effect on the natural transition point until transition was produced at the disc itself.

The critical values for the sandpaper type of roughness are presented in Fig. 12. In the Figure the two symbols with a line joining them are for the same roughness configuration for which it was impossible to determine exactly the critical values—thus, the range. The critical values shown were calculated from conditions at the leading edge of the 1/4-in. strip of roughness. They generally fall in the range of R_k from 250 to 300. Fig. 12 shows that the span of the strip of the sandpaper type of roughness has little effect on the values of critical roughness.

Comparison and Discussion of the Results of This and Previous Investigations on Critical Roughness

Correlation of Data With Various Parameters

A study of various parameters for correlating the critical roughness values, including those parameters used by the previous investigators, resulted in the choice of $R_{k\,crit}$ as the most suitable parameter. In some instances, the parameters used previously give better correlation for particular conditions, such as a particular size, location, or shape of roughness, but have one or more of the following disadvantages: (a) they are valid over only a small range of Reynolds Numbers, (b) they are restricted to particular regions on a body, or (c) they depend on the length of natural laminar flow.

One of the parameters used previously will be compared with R_k for correlating the results of this investigation. Several investigators select k/δ^* or k/δ as one parameter for correlating the effect of roughness on transition. If the parameter is really fundamental, $k/\delta_k{}^*$ or k/δ_k should be a constant for critical roughness of a given shape. If $k/\delta_k{}^*$ or k/δ_k is constant, it follows that k_{crit} must approach zero at the leading edge of a flat plate; otherwise $k/\delta_k{}^*$ would become infinite. Experience indicates that the permissible roughness in

this example is something greater than zero. Hence $k/\delta_k{}^*$ is not fundamentally a sound parameter.

In the present investigation θ_k is chosen in preference to $\delta_k{}^*$ or δ_θ as the parameter to represent the boundary-layer thickness, because it is usually the most significant of the three common thickness parameters. The variation in the shape parameter $H = \delta^*/\theta$ is relatively small over the test region (H_k varies from 2.26 to 2.56). Thus, a plot of critical roughness in k/θ_k, ${R_{\theta_k}}^{-1/2}$ coordinates would look like one in $k/\delta_k{}^*$, ${R_{\delta^*{}_k}}^{-1/2}$ coordinates. Dryden,[3] using the results of several investigations on two-dimensional roughness, shows that a plot of R_T/R_{T_0} versus $k/\delta_k{}^*$ gives a single curve for the region where the roughness moves transition from its natural location x_{T_0} to the location of roughness itself x_k. A similar plot of the results of this investigation shows no such correlation. Fig. 8 is typical of the R_T/R_{T_0} versus k/θ_k plots of this investigation. The plot shows a wide variation of R_T/R_{T_0} with k/θ_k, the value of k/θ_k increasing as the roughness moves forward on the test surface. One explanation of this apparent discrepancy is offered. Dryden does not give the location of the roughness elements for all the data he presents, but a check of three of the four sets of data he used showed that the locations of the roughnesses vary from 20 to 67 in. from the leading edge. The present investigation dealt mostly with locations 16 in. or less from the leading edge. The curves of R_T/R_{T_0} versus k/θ_k tended to move closer together as the roughness was placed farther aft on the test surface. Moving the roughness even farther back would undoubtedly have restricted the variation of k/θ_k still more. This is physically plausible, for as x_k increases, the distance between the roughness location and natural transition (between x_k and x_{T_0}) decreases, and the range of θ_k, and thus of k/θ_k, for a given k correspondingly decreases for the movement of transition from x_{T_0} to x_k. Inspection of Figs. 9 and 10 shows that, as x_k increases, the critical parameters k/θ_k and ${R_{\theta_k}}^{-1/2}$ both decrease, and eventually R_{θ_k} would approach the limiting value given by stability theory for a "clean" surface.

Other investigations—that of Klebanoff et al.[4] on three-dimensional roughness and that of Brinich[20] on a wire type of roughness in supersonic flow—whose results are presented after the method of Dryden, show that moving the roughness position forward increases the values of $k/\delta_k{}^*$. The roughness positions for both of these investigations are closer to the leading edge than those presented by Dryden.

Comparison of Critical Roughness Data

Before comparing the values of critical roughness from previous investigations and those of our investigation, the definition of critical roughness will first be discussed. The previous investigators used one or more of the following techniques to define critical roughness: a hot wire placed just forward of the clean-airfoil transition point, the china-clay technique, or observation of the drag rise on an airfoil. With the data of this investigation, several calculations have been made for which critical roughness is defined as the height that reduces the transition Reynolds Number to 99 per cent of its natural value, that is, $R_T/R_{T_0} = 0.99$ instead of $R_T/R_{T_0} = 0.95$, as in the definition given earlier. A comparison of the critical values of roughness as determined by the two definitions shows that the maximum difference in k/θ_k determined by the two definitions is less than 8 per cent for wire type roughness and even less for three-dimensional elements, since for them the transition point moves forward more abruptly once the roughness has become critical.

The critical-roughness values observed for spanwise wires in this investigation and in the investigations of Cowled and Fage are presented for Comparison in Fig. 13. The several sets of data show similar variation of critical k/θ_k with ${R_{\theta_k}}^{-1/2}$; for example, the sharp rise in $(k/\theta_k)_{crit}$ and $R_{k\ crit}$ for the wires nearer the leading edge. The amount of scatter of the various results is about the same. The values of $R_{k\ crit}$ lie between 40 and 260, with a mean of about 125.

The critical values for wires in tandem are shown in Fig. 13 along with the single-wire data. The values shown are based on the wire that gave maximum value of $R_{k\ crit}$. The results help to verify Cowled's discovery that transition was dependent only on the most critical roughness when two wires were in tandem.

A study of the various investigations of three-dimensional roughness has shown greater values of $R_{k\ crit}$ than those for the two-dimensional roughness, and also a great deal more scatter. The study has shown that some of the scatter is due to the shape of the roughness. Fig. 14 shows the variation of $R_{k\ crit}$ with k/d for several investigations. The diameter of the roughness elements is d. There is a tendency for the values of $R_{k\ crit}$ to increase with an increase in k/d. The one exception is the work of Gregory and Walker, where single roughness elements rather than spanwise rows of elements were tested. In their tests on single roughness elements, $R_{k\ crit}$ increases with an increase in k or a decrease in x_k for a constant k/d ratio. It is also worth noting that as the value of k/d decreases, the three-dimensional type of roughness approaches a

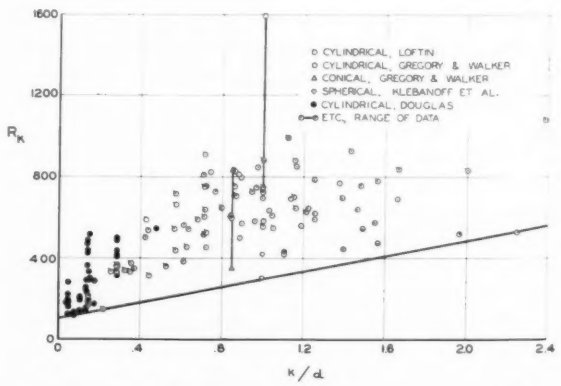

FIG. 14. Critical values of R_k and shape parameter k/d for various three-dimensional types of roughness of this and previous investigations. A limiting line of minimum $R_{k\ crit}$ is shown.

two-dimensional type and, thus, the lower values of $R_{k\ crit}$ follow.

No attempt has been made to determine the effect of spanwise spacing of the three-dimensional elements on the values of $R_{k\ crit}$. However, as was noted above, single discs gave higher values of $R_{k\ crit}$ than a row of such discs. Klebanoff et al.[4] present one example showing that a decrease in the spacing between elements gives a slightly lower value of $k/\delta_k{}^*$ for a given R_T. It is reasonable to expect that decreasing the spacing between elements would lower the values of $R_{k\ crit}$, because the row becomes more nearly two-dimensional in nature.

The critical roughness values observed for the sandpaper type of roughness in the present investigation and in an investigation by the NACA[14] are shown in Fig. 12. Both investigations were made on 1/4-in.-wide strips of roughness. The NACA investigation shows higher values of critical roughness than those obtained in the present investigation. One possible explanation of this difference is that the density of the grains of sand was greater in this investigation, and thus the strips of roughness acted more like a two-dimensional roughness than those used by the NACA.

One type of surface irregularity of major importance that was not investigated in the present wind-tunnel tests is surface waviness. Cowled[11] presents the results of such investigations. His report shows that waves give much higher critical values of R_k than the other types of roughness, values falling in the range of $R_{k\ crit}$ from 1,000 to 4,200. There is no consistent correlation shown on the k/θ_k versus $R_{\theta_k}{}^{-1/2}$ type of plot. An approximate single-curve correlation is obtained by plotting Cowled's data on a k/λ versus $R_{\theta_k}{}^{-1/2}$ plot, as is shown in Fig. 15. It should be noted that λ, the wavelength, is constant for Cowled's data. This plot suggests that, for the wave type roughness, thickness ratio rather than height alone is of importance in determining whether or nor the wave will precipitate premature transition.

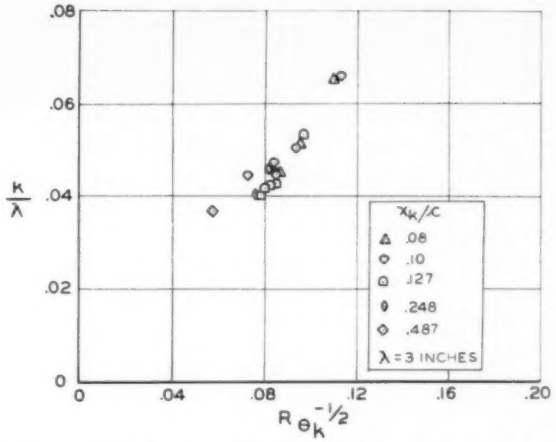

FIG. 15. Critical values of k/λ and $R_{\theta_k}{}^{-1/2}$ for surface waves of reference 11.

Effect of Pressure Gradient on Critical Roughness

The various investigations show that pressure-distribution effects are of minor importance in determining critical roughness. Critical values that have been obtained from the various investigations cover a wide range of pressure distributions. In the regions of laminar flow, the pressure distribution of the present investigation covers a range of Hartree's β from -0.2 to $+0.64$. The regions where roughness was located covers a range of β from 0.025 to 0.64. Cowled's roughness lay in a range of β from 0.4 to 0.6. Fage tested in a range from 0.02 to 0.1. As is shown in Figs. 10 and 13, the values of critical roughness are all in reasonable agreement.

The range in pressure distributions that has been covered by the various investigations should be sufficient for any practical application of the roughness data, such as the design of low-drag airfoils. The maximum value of β that is ever likely to occur on airfoils is about 0.55; e.g., an NACA 66,2-420 airfoil at an angle of attack of 16° gave a β of 0.57 on the lower surface in a wind-tunnel test. It is impossible to obtain values of β this high and simultaneously have laminar flow on both sides of an airfoil. Hence, the maximum β's of interest are even less.

Effect of Tunnel Turbulence on Critical Roughness

Two facts seem to indicate that the degree of tunnel turbulence has a minor effect on critical values of R_k. First, satisfactory correlation of the data from various investigations has been obtained for roughness of a given shape. These investigations were carried out in a variety of tunnels, in which it may be assumed that the level of tunnel turbulence varied widely. Second, tests made in this investigation show that increasing the turbulence level tenfold (from 0.03 per cent turbulent to 0.30 per cent) increases the value of $R_{k\ crit}$ approximately 50 per cent (see Fig. 10), that is, reducing the number of turbulence screens from six to one to none increases the average $R_{k\ crit}$ for the wire configuration tested from approximately 130 to 165 to 195, respectively.

The increase in the critical-roughness Reynolds Number with increased tunnel turbulence is consistent with small-perturbation theory. First, the length of natural flow is less for increased turbulence, and thus a perturbation introduced by the roughness element has less time to grow before it reaches natural transition. Second, premature transition may be caused not only by the perturbation introduced by the roughness but also by the sum of this perturbation and those present due to free-stream turbulence. If the level of free-stream turbulence is increased, the perturbation contributed by the roughness elements may have to be increased correspondingly to cause premature transition.

Composite Plot of All Critical-Roughness Data and Its Practical Utilization

The results of the various investigations for all types of roughness are presented in Fig. 16. The critical

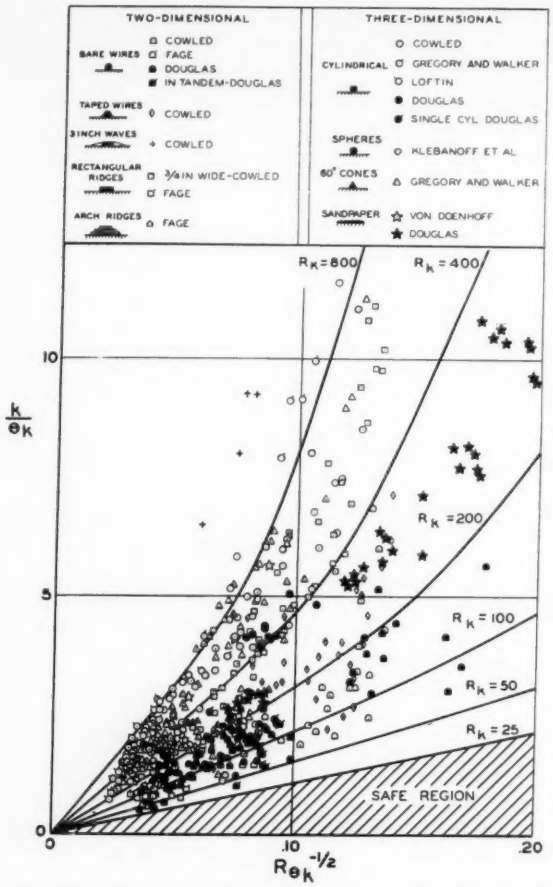

FIG. 16. Comparison of critical roughness values for various types of roughness of this and other investigations. Lines of R_k = constant represent Blasius boundary layer ($\beta = 0$).

values extend over a large range in R_k, but the values may be grouped according to type of roughness. The most critical types are the two-dimensional elements, which have R_k as low as 40 and which extend as high as $R_k = 400$, with a mean of 125. The second most critical elements are the three-dimensional elements, which fall in the range of $R_{k\ crit}$ from 100 to 800, with a mean of about 350. The least critical are surface waves, which have $R_{k\ crit}$ extending from 1,000 to 4,000.

Frequently, the predominant interest lies in the region where the roughness has no effect on transition. The limit for this region of tolerable roughness can be obtained from Fig. 16. The lowest observed roughness is $R_k = 40$, but to allow for a safety factor to account for shapes worse than those investigated, etc., the "safe region" of roughness is selected as that below $R_k = 25$. Using $R_k = 25$, the tolerable roughness was calculated for an airfoil and a body of revolution. Values for $M = 0.4$ are presented in Table 1. The values indicated are for the most critical positions on the bodies, a point slightly forward of 1 per cent chord.

At least one series of flight tests that has been made to determine the effect of isolated surface roughness on transition corroborates the values in Table 1. Johnson,[21] reporting the results of two flight tests made at

TABLE 1
Maximum Allowable Roughness for $M = 0.4$ at Most Critical Point on the Body

Configuration	Altitude 10,000 ft.	Altitude 35,000 ft.	Altitude 60,000 ft.
NACA 65-010 Airfoil, $C_L = 0$	0.00092 in.	0.0017 in.	0.0042 in.
Elliptical Body of Revolution of Fineness Ratio 9:1	0.00064 in.	0.0012 in.	0.0029 in.

an altitude of 1,000 ft. and a Mach Number of 0.62, states that "... near the leading edge at about $2^1/_2$ per cent chord, a pimple of about 1 thou. in height causes transition while further aft at 20 per cent chord a pimple 3 thou. high is needed."

It is interesting to compare the critical roughness for transition in laminar flow with the roughness necessary to cause a drag rise in turbulent flow. In turbulent flow a surface is considered to be hydraulically smooth if $kv_*/\nu \leq 5$ (see Schlichting[22]). We follow Schlichting's notation except to replace his k_s by k; v_* is the friction velocity defined as $\sqrt{\tau_0/\rho}$. Since $\tau_0 = \mu(\partial u/\partial y)_w$, we have, remembering that $u_k \simeq k(\partial u/\partial y)_w$,

$$kv_*/\nu = \sqrt{(k^2/\nu^2)(\mu/\rho)(\partial u/\partial y)_w} \simeq \sqrt{u_k k/\nu} \leq 5$$

The quantity $u_k k/\nu$ is our usual roughness Reynolds Number, and, thus, the long established criterion for a hydraulically smooth pipe—namely, $kv_*/\nu \leq 5$—is approximately the same as the lower limit of critical roughness Reynolds Number (arbitrarily chosen as 25 above), a most interesting coincidence. Goddard[23] also noted this similarity. In Part (II) we shall return to this similarity in discussing the effect of compressibility on critical roughness.

Roughness Used as a Tripping Device

In wind-tunnel and towing-tank tests it is often desirable to fix transition at a given location. Roughness is the most common means of accomplishing this result. Here the value of R_k necessary to bring transition right up to the roughness is of importance, for the roughness should be no larger than that necessary to trip the boundary layer because it adds to the form drag and may have other adverse effects. The roughness necessary to move transition to the roughness itself is presented in Fig. 17. The data of this and the other investigations show that the values of R_k necessary to trip the boundary layer are, approximately,

Roughness	Average R_k
Spanwise wire	300
Row of 1/16-in.-dia. discs	600
1/4-in. wide strip of sandpaper type	400

R_k increases above these values as the tripping device approaches very close to the leading edge, because of the criterion, noted earlier, that $R_\theta > 320$ for a fully turbulent flow. Preston[11] notes that, when the natural R_θ is so small that one must depend entirely on the drag

of the tripping device to produce $R_\theta > 320$, then the R_k of a wire-type tripping device required to trip the boundary layer is from 600 to 800.

Hama[13] presents "an efficient tripping device" that incorporates the favorable properties of both the two- and three-dimensional elements for producing turbulence immediately. The two-dimensional element is favorable in that, for the same size, it produces a larger perturbation in velocity. The three-dimensional element is favorable in that it produces vortices that will go turbulent quicker than will two-dimensional disturbances. Hama's device consists of a spanwise row of flat triangular patches lying on the surface with their apexes pointed upstream. Hama estimates the height Reynolds Number necessary to produce transition at this device to be 45. Values of k/θ_k and R_{θ_k} taken from a figure of reference 13, in which turbulence is shown behind the trip, are plotted in Fig. 17, along with the corresponding values for the other types of roughness. The values plotted are not necessarily the lowest values of k/θ_k and R_k producible by Hama's device.

Concluding Remarks on Critical Roughness in Low-Speed Flow

It has been shown that the effect of critical roughness on transition is primarily a function of the roughness Reynolds Number, and, in turn, its value has been found to depend greatly on shape. These findings are not inconsistent with that part of boundary-layer theory that deals with the growth of small perturbations and their development into turbulence. Briefly, the two-dimensional roughness is more critical than the three-dimensional because it introduces larger disturbances. But, because the two-dimensional element produces two-dimensional disturbances, which must evolve into three-dimensional vortices before producing turbulence, the rate of movement of transition forward is less for the two-dimensional elements. In the preceding discussion it has been shown that as the shape ratio k/d of three-dimensional elements becomes small, the effect of these elements on transition approaches that of two-dimensional elements. Now what about the other extreme, when k/d becomes very large—that is, what is the effect of a fine wire normal to the surface, extending through the boundary layer far into the free stream? Now, instead of a height parameter like R_k, the major parameter is undoubtedly $R_d = ud/\nu$, the local wire-diameter Reynolds Number. From the well-known behavior of wakes and vortex streets behind cylinders it is obvious that turbulence will be generated when R_d at any point along the wire exceeds a certain value. Because u is zero on the surface and increases to U outside the boundary layer, turbulence should first be generated outside the boundary layer.

When a wire is laid spanwise along the model, within the boundary layer, the disturbances it creates are amplified by the velocity distribution within the boundary layer, perhaps by the Tollmien-Schlichting amplification mechanism. Certainly the disturbance initially caused by the wire becomes stronger downstream.

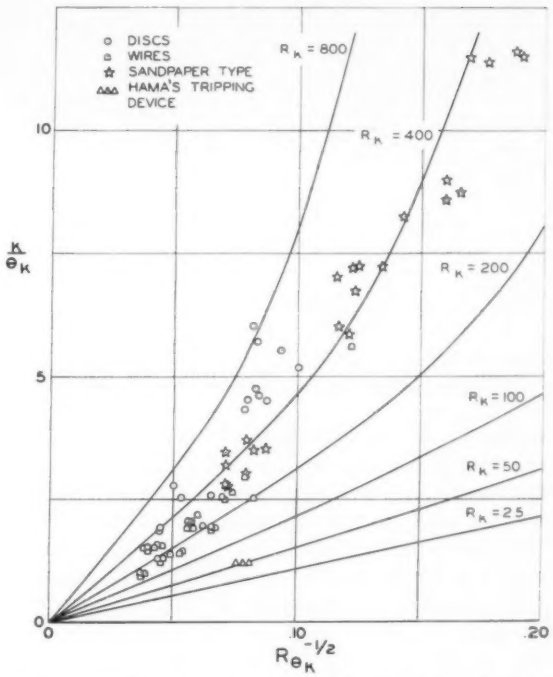

FIG. 17. Values of k/θ_k and $R_{\theta_k}^{-1/2}$ for various types of roughness when transition occurs at the roughness itself. Lines of R_k = constant represent Blasius boundary layer ($\beta = 0$).

But the disturbance created by a long thin wire perpendicular to the model acts in a quite different fashion. If the wire does create some turbulence, this turbulence is generated substantially outside the boundary layer and directly behind the wire. Unless the turbulence is developed immediately, it will not develop at all, because disturbances introduced by the wire will be damped in the free stream, more or less in accordance with well-known laws of turbulence decay.

This idealized example, together with that of a conventional two-dimensional wire type of roughness, helps to bound the types of effect caused by different kinds of roughness. On the one hand, for the perpendicular wire, if turbulence is present at a downstream point, it is obvious that stronger and stronger indications will be found forward of this point right to the wire. On the other hand, for the wire on the surface of the model and immersed in the boundary layer, turbulence may be present at a downstream point but not slightly forward of this point.

The downstream development of disturbances caused by other shapes of roughness will be somewhere between those of the examples above. The disturbed region caused by a three-dimensional roughness high in the boundary layer may be more similar to that behind the perpendicular wire. The disturbed region caused by a three-dimensional roughness that lies very low in the boundary layer may be more similar to that behind the conventional two-dimensional wire. In order to understand fully the effect of roughness on transition, a detailed research on the flow around and behind roughness elements is necessary. Some studies of the micro-

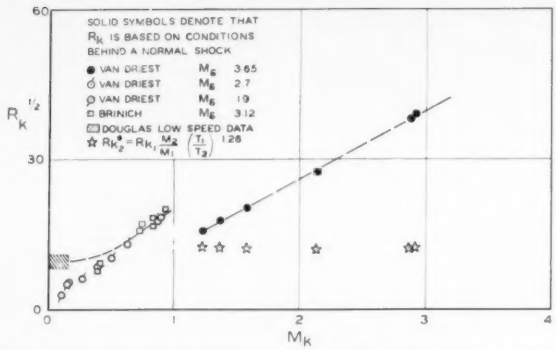

FIG. 18. Variation of critical roughness Reynolds Number with the local roughness Mach Number in supersonic flows.

mechanism of the disturbed flow behind an element have been made (see references 6, 7, 10, 12, and 24), but many questions still remain unanswered, particularly the dynamic aspects dealing with wave motion.

In retrospect, when a wide range of conditions is considered, it is clear that no better correlation parameter exists than R_k for determining the degree of roughness necessary to affect transition. While there is a great deal of scatter in experimental values of $R_{k\,crit}$, the value is not affected by the several variables considered in this investigation. The large spread of values is much less when considered in terms of $R_k^{1/2}$, a quantity more nearly proportional to the height of the roughness. In brief, R_k is a very sensitive parameter.

As was noted in the Introduction, Schiller was first to propose the criterion that $R_{k\,crit}$ = constant. Furthermore, purely from considerations of the wake behind cylinders in a uniform stream, Schiller proposed that $R_{k\,crit} = 50$ was about the value to be expected for a wire type of roughness.

PART (II) EFFECTS OF MACH NUMBER ON CRITICAL ROUGHNESS

Useful data on critical roughness at high Mach Numbers are extremely limited. From wind-tunnel tests, it is known that the height of a roughness trip or the roughness Reynolds Number defined as kU/ν_δ necessary to cause transition increases markedly with Mach Number.[25] This increase is not surprising for the following reasons: first, the boundary-layer thickness increases with Mach Number for a given U/ν; second, the wall temperature rises as M^2 (unless the wall is cooled), and thus the viscosity increases; and, third, the Reynolds Number above may be written as

$$R_{k_\delta} = kU/\nu_\delta = (1/0.663)(U/a)(k/\lambda)$$

where $\nu_\delta = 0.663\, a\lambda$ (by basic kinetic gas theory), a = speed of sound, and λ = mean free path of molecules. If R_{k_δ} were to remain constant for all Mach Numbers, k/λ could become quite small. This is not physically reasonable.

An approach to the effect of Mach Number on critical roughness is suggested by the work of Liepmann and Goddard.[23,26] They conducted tests to determine the effect of surface roughness on skin friction in turbulent flow and found that the "critical roughness" below which the surface is hydraulically smooth is a function of kv_*/ν_w only, just as in the incompressible case. Furthermore, the critical roughness below which the surface is hydraulically smooth is

$$k_{crit} \simeq 10\nu_w/v_*$$

and is independent of Mach Number. This is approximately equal to the thickness of the laminar sublayer for a smooth surface for both compressible and incompressible flows. As noted above in the Section "Composite Plot of All Critical-Roughness Data and Its Practical Utilization,"

$$kv_*/\nu \simeq \sqrt{u_k k/\nu}$$

for the low-speed flow. This fact and the work of Liepmann and Goddard on turbulent boundary layers suggest the local Reynolds Number,

$$R_k = u_k k/\nu_k$$

as the parameter to correlate the effect of Mach Number on critical roughness. Then, if there is any effect of Mach Number, it will be as a function of local Mach Number,

$$M_k = u_k/a_k$$

The local values of R_k and M_k must be based on properties in the neighborhood of the roughness. The top of the roughness is both a convenient and a logical reference point; therefore, hereafter the subscript "k" will denote properties at the top of the roughness.

CRITICAL ROUGHNESS AT SUPERSONIC SPEEDS

The only available sources of useful supersonic data on critical roughness that enable the determination of $R_k = u_k k/\nu_k$ are references 20, 27, and 28. The results of reduction of the data on wires are shown in Fig. 18. The calculations were made using the boundary-layer temperature and velocity profiles calculated by the Chapman and Rubesin method.[29] Sutherland's relation for the variation of viscosity with temperature was used. The data of reference 27 were obtained for wire-type roughness on a cone whose surface was either insulated or cooled. In the case of cooling, the roughness element was always in front of the region of maximum cooling, which caused relatively large temperature gradients at the roughness location. These temperature gradients were approximated from the data presented in reference 27 and used in the determination of the velocity and temperature profiles by the method of reference 29. The NACA data[20] were also obtained for wires but on an insulated surface. Fig. 18 shows the variation of R_k with M_k, where $M_k = u_k/a_k$. It should again be emphasized that the properties u_k, ν_k, and a_k are values calculated at a height k in the boundary layer when roughness is not present.

At roughness Mach Numbers equal to or greater than 1, one would expect a shock wave to occur in front of or

on the roughness element—e.g., see Fig. 18 of reference 27 and the various photographs presented in reference 32. If the shock wave produced by the roughness is of the form shown in Fig. 19—that is, the shock is normal at the top of the roughness, changing to an oblique shock above the roughness—then the flow conditions at the top of the roughness are those behind a normal shock. The characteristic roughness Reynolds Number is now $R_{k_2} = u_{k_2}k/\nu_{k_2}$, where the subscript 2 refers to conditions behind a normal shock at M_k. A calculation of R_{k_2} gives the broken line in Fig. 18 for $M_k > 1$. It should be pointed out that, in the supersonic region, R_k is plotted against M_{k_1}, not M_{k_2}. The latter would, of course, always be equal to or less than 1. Thus, assuming a normal shock when M_k is greater than 1, Fig. 18 shows that in the subsonic region $R_{k\ crit}$ increases nearly as $M_{k_1}^2$, dips at $M_{k_1} \geq 1$, then again increases as $M_{k_1}^2$.

It is of interest to note that a Reynolds Number $R_{k_2}{}^*$, based on velocity and temperature downstream of a normal shock and pressure upstream of the normal shock, has nearly a constant value for the limited amount of data on critical roughness at supersonic M_{k_1}. This is shown by the "star" points in Fig. 18, where $R_{k_2}{}^*$ is defined by

$$\frac{R_{k_2}{}^*}{R_{k_1}} = \frac{u_2}{u_1}\frac{\rho_2{}^*}{\rho_1}\frac{\mu_1}{\mu_2} = \frac{u_2}{u_1}\frac{T_1}{T_2}\left(\frac{T_1}{T_2}\right)^{0.76} = \frac{M_2}{M_1}\left(\frac{T_1}{T_2}\right)^{1.26}$$

It is known from experimental work on laminar flow over small steps or roughness elements (for example, see reference 32) that the pressure measured on the surface about the element does not necessarily change greatly even though shocks are observed at the step or roughness element. This would be expected both because the shock almost immediately evolves into a simple Mach line and because the extent of the shock is too small to cause a general pressure rise.

A still more nearly constant value of R_k throughout both the subsonic and supersonic regime is obtained if R_k is computed using (1) stagnation temperature, (2) static pressure upstream of any shock, and (3) a velocity u_{k_2} determined by normal shock relations. Use of upstream static pressure is plausible, as has already been noted. Furthermore, use of stagnation temperature is plausible because the fluid in contact with the roughness will be close to this temperature. Unfortunately, no

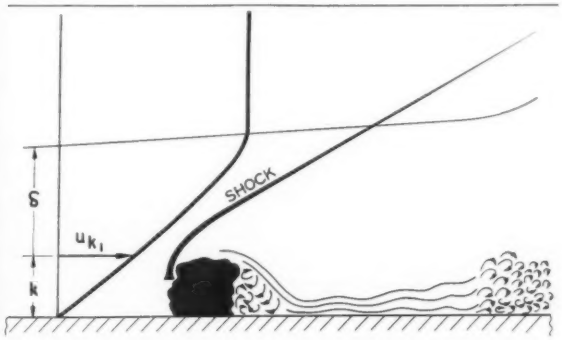

FIG. 19. The approximate physical process by which a roughness produces turbulence in a boundary layer.

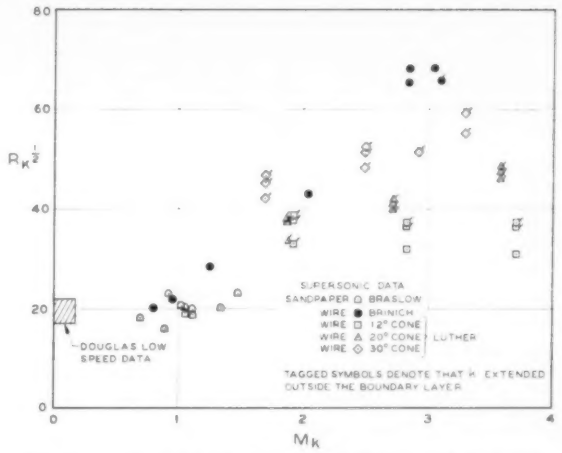

FIG. 20. The roughness Reynolds Number required to produce transition at the roughness, as a function of the local roughness Mach Number.

plausible physical justification for using a velocity u_k downstream of a normal shock has been found. These remarks and facts are included in the hope they will aid other investigators in studying the effect of Mach Number.

Fig. 18 shows that the critical values of R_k for M_k less than 0.5 fall below those values of R_k observed by the authors for low-speed flows. Possibly the explanation is as follows. Both Brinich and van Driest give the nominal heights of their roughness elements. The calculation of their R_k's was based on these heights. Our experience shows that the maximum height is undoubtedly higher than the nominal height. A greater height would cause the values of both R_k and M_k to increase; and the increase would follow closely the line of data points in Fig. 18, since the variation of local yu/ν and M in the boundary layer closely follows this line for the free-stream conditions of the points shown.

A similar variation of R_k with M_k is observed for roughness elements necessary to cause transition at the element. References 20, 28, and 30 present observations on such roughnesses at supersonic speeds. The variations of R_{k_1} or R_{k_2} with M_k for these observations are shown in Fig. 20. When the roughness element protrudes completely through the boundary layer, relatively large values of R_{k_2} were observed—for example, note Brinich's data in Fig. 20.

DISCUSSION

The concept that the roughness senses the purely local flow, which of course implies conditions downstream of a shock for supersonic flow, is in agreement with observations made with hot wires. In a study of heat transfer from fine wires in supersonic flows, Laufer and McClellan[31] found that the Nusselt Number was a unique function of the Reynolds Number when both of these parameters were based on properties behind a normal shock. In other words, heat-transfer properties of a small hot wire are independent of Mach Num-

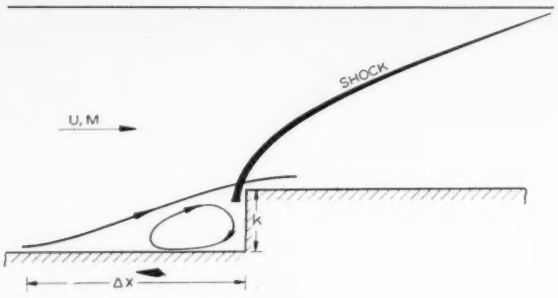

SKETCH.

ber when based on fluid properties downstream of a normal shock. This statement was well verified by the experimental data presented in reference 31.

If it is separation from the roughness that produces vortices or disturbances that cause transition, as was suggested above for low-speed flow, perhaps an idea of the effect of Mach Number on critical roughness Reynolds Number can be obtained by studying the effect of Mach Number on laminar separation on bodies at very low Reynolds Numbers or by studying separation caused by bumps or steps on a surface in supersonic flows. The authors know of no experiments which give the effect of Mach Number on separation from bodies at low Reynolds Numbers, but separation caused by bumps or steps on a surface have been studied by Chapman, et al.[32] and Greber, et al.[33] Reference 32 shows that the Reynolds Number $R_{\Delta X} = \Delta X\ U/\nu$, based on the length of the separated region ΔX in front of a bump (see Sketch), which is just large enough to cause turbulent reattachment, increases with the free-stream Mach Number, and that this increase is similar to the variation of critical R_{k_1} with M_{k_1} found for the roughness wires above. A calculation of $R_{\Delta X_2} = U_{k_2}\ \Delta X/\nu_2$ for points where $M_1 > 1$ shows that $R_{\Delta X_2}$ increases nearly as $M_{k_1}{}^2$ but dips at M_k close to 1. Although the Reynolds Number $R_{\Delta X_2}$ is much larger numerically than the roughness Reynolds Number R_k, the variation of the two Reynolds Numbers with local Mach Number is similar. It should be noted that the height of the steps of reference 32 was considerably greater than the boundary-layer thickness ahead of the separated region, and also that if a shock was caused by the step, it formed immediately in front of or on the step but behind the separated region. Since the separated region (of length ΔX) was in front of the shock, the only reason for discussing the variation of $R_{\Delta X_2} = \Delta X\ U_2/\nu_2$ with M_{k_1} is that the length of the separated region gives an idea of the magnitude of the disturbance.

Greber, et al.,[33] have made experimental and theoretical studies of the interaction of oblique shock waves with laminar boundary layers, and these studies may help to explain the dip in R_{k_2} at M_k slightly greater than 1. They have been able to predict the pressure rise that causes separation and also the length of the separated region. Furthermore, they point out that the conditions near separation are independent of the agency that induces separation—e.g., a shock wave or a step in the surface—and they also point out that the separation phenomena are essentially self-similar. That is, all significant parameters at separation are functions of the local Mach Number and Reynolds Number. The criterion for separation which they present can be written as

$$C_{p_s} = 2\sqrt{(C_{f_k})_s/(M^2 - 1)^{1/2}}$$

when C_{p_s} = pressure rise at separation and $(C_{f_k})_s = (\tau/q)_s$, where subscript s denotes values evaluated at the height of the separated region, or, in the case where separation is caused by a surface protuberance, the value of τ/q at the height of the protuberance. Clearly, this expresssion for C_{p_s} peaks at $M = 1$.

In the case of a normal shock at a surface protuberance of height k, it can be shown that

$$R_k = A M_k{}^4/(M_k{}^2 - 1)^{5/2}$$

where A is a constant.

Thus, we see that in supersonic flows—i.e., $M_k \geq 1$—the pressure rise necessary to cause separation gives a peak in R_k at $M_k = 1$. This, of course, does not explain the increase of R_k with Mach Number for subsonic or supersonic flows. It is known that the stability of a laminar separated region increases markedly with Mach Number.[32]

Before summarizing what is known of the effects of Mach Number on critical roughness, an illustration will be given in which the variation of R_k with M_k presented in Fig. 18 helps explain an observed phenomenon. The NACA has observed that, under conditions of extreme surface cooling, the transition Reynolds Number decreased with decreasing surface temperature.[34, 35] This is in disagreement with the prediction of stability theory and with what has been observed for moderate surface cooling. The authors of reference 34 question whether or not transition reversal can be attributed primarily to surface roughness, their reasoning being that cooling produces only a small change in k/δ. Calculations based on data presented in references 34 and 35 and an assumed k show that in one case in which cooling produced only a 50 per cent increase in k/δ, it produced a tenfold increase in R_k. It appears that if the criterion for critical roughness is R_k as presented in this Section, transition reversal due to extreme surface cooling can be attributed to surface roughness.

Summarizing, it can be said that the limited amount of data on critical roughness at high Mach Number is not inconsistent with the mechanism, suggested above, by which the roughness causes transition in low-speed flow—that is, critical roughness is that which first introduces local separation or vortices. Calculations based on this principle and the variation of R_k with M_k presented in Fig. 18 (the broken line) give tolerable roughness that would be encountered in flight. Such tolerable roughnesses are presented in Fig. 21, both for an insulated flat plate and for a flat plate with a wall-to-free-stream temperature ratio of 1. The curve of Fig.

18 was extended linearly to make the calculations at the higher Mach Numbers. The Figure shows that tolerable roughness first decreases with Mach Number and then increases because of aerodynamic heating, particularly because of the effect of temperature on viscosity. Also the Figure shows the effect of surface temperature on the tolerable roughness at 1 in. from the leading edge; as the Mach Number is increased in the subsonic region, the curves of tolerable roughness for the two surface temperatures (the insulated wall and $T_w = T_\delta$) diverge because of aerodynamic heating. At higher Mach Numbers further increases in temperature and a corresponding increase in viscosity are caused by the shocks produced by the roughness. The increase in viscosity along with the increasing Mach Number increases the tolerable roughness until eventually the roughness extends through the boundary layer into the free stream. When the roughness extends far enough R_k becomes independent of wall conditions, as is indicated in Fig. 21. Also, the tolerable roughness becomes independent of its position on the plate if it extends far enough out of the boundary layer. Further experimental data on critical roughness in supersonic flows is needed to validate the values of tolerable roughness presented in Fig. 21 and also to validate the mechanism on which the calculation of these tolerable roughness values was based.

Conclusions

This investigation to find the smallest height of roughness capable of affecting boundary-layer transition leads to the following conclusions.

Low-Speed Flow

(1) For a given shape of roughness, the value of $R_{k\ crit}$ has been found to be relatively constant and to be substantially independent of both height and location of roughness, the pressure distribution, and the degree of free-stream turbulence.

(2) The shape of roughness has a major effect on the values of $R_{k\ crit}$. The value of $R_{k\ crit}$ increases as the type of roughness changes from a three-dimensional type to a two-dimensional type. The present investigation established values of $R_{k\ crit}$ for three types of roughness as follows:

Roughness	Range of $R_{k\ crit}$
Spanwise wires	40–260
Row of 1/16-in.-dia. discs	100–550
1/4-in. wide strip of sandpaper type	178–330

(3) The results of the various investigations covering all types of roughness show that the smallest roughness that has any effect on boundary-layer transition is that corresponding to a roughness Reynolds Number of about 40.

(4) The values of R_k necessary to move transition to the roughness itself are, approximately,

Roughness	Average R_k
Spanwise wire	300
Row of 1/16-in.-dia. discs	600
1/4-in. wide strip of sandpaper type	400

High-Speed Flow

(5) The small amount of available, usable test data shows that R_k may be the characteristic parameter for correlating the effects of roughness on transition, just as in the subsonic case. The value of R_k varies with the local Mach Number M_k at the top of the roughness. For M_k greater than 1, the Reynolds Number R_{k_2}, based on conditions behind a shock, is perhaps the best characteristic parameter. The value of R_k increases with M_k and, if a normal shock is assumed, the value peaks at $M_k = 1$, decreases for M_k slightly greater than 1, then again increases for larger M_k, approximately as M_k^2, according to the sparse amount of data. The value of $R_{k\ crit}$ for a wire at supersonic M_k is lower than the corresponding value for a three-dimensional roughness, just as in the subsonic flows. Further studies of critical roughness in supersonic flow are needed.

The Physical Process—It is believed that the dominant process by which isolated, protruding types of surface roughness first affect transition is now essentially established, at least in the gross or first-order sense. Premature transition is caused when the roughness Reynolds Number becomes sufficient to develop a dead-water region and/or vortices behind the roughness. Three parameters seem to determine when this region will just begin to form—a Reynolds Number based on strictly local properties of the flow, a Mach Number based on the same local properties, and, finally, the shape of the roughness. All other factors, such as free-

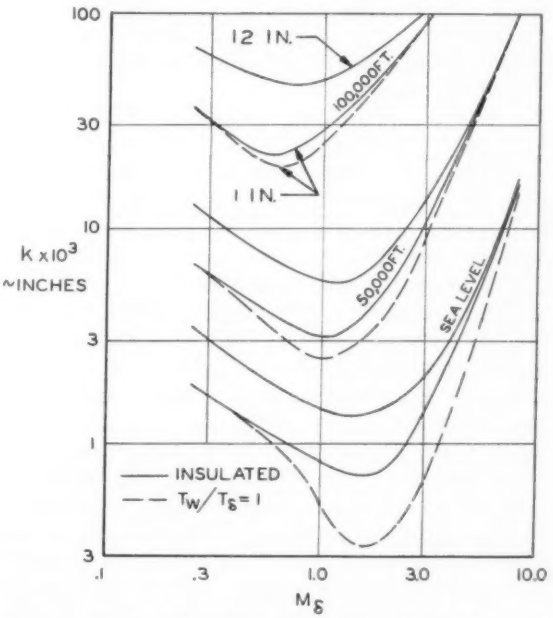

FIG. 21. The variation with Mach Number of tolerable roughness on a flat plate at 1 in. and 12 in. from the leading edge.

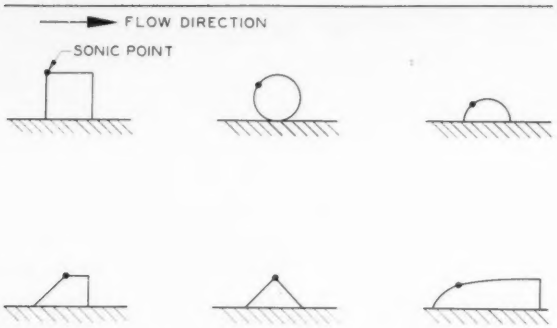

FIG. A-1. Approximate location of sonic point on several typical bodies.

stream Mach Number or pressure distribution, enter into consideration only to the extent that they determine the local fluid properties at the reference point on the roughness. To first order, none of the observed facts are inconsistent with this model. Flow pictures of separation behind rods at very small Reynolds Numbers, Laufer's observations on hot wires, Goddard's observations on roughness in compressible turbulent flow, and Chapman's and Greber's considerations on flow separation all reinforce the concept. The approximate physical model is illustrated by Fig. 19.

APPENDIX—AN IMPROVED PHYSICAL MODEL FOR THE COMPRESSIBLE FLOW PAST AN ISOLATED BIT OF ROUGHNESS

In the main body of this article, in the section of the effects of Mach Number, two methods of computing a roughness Reynolds Number were introduced. One used the height k and the density, velocity, temperature, and viscosity computed for conditions behind a normal shock, corresponding to the appropriate stream filament at the height k. The second used the velocity and temperature downstream of a normal shock but the pressure upstream.

Some criticisms of the first method are: (1) no normal shock is observed to exist near a roughness element low in the boundary layer, and (2) there is no observable pressure rise near a roughness element; in fact, the main effect of a small bit of roughness is to create a Mach line.

With respect to the second method, criticism (1) continues to apply, and, in addition: (3) the assumptions do not fit together into any known physical model or flow situation.

A model that is much nearer physical reality has since been conceived; it uses sonic velocity as the reference velocity and recognizes the fact that the roughness is a small bluff body. When M_{k_1} exceeds some high subsonic value, the flow becomes transonic and remains transonic as M_{k_1} is indefinitely increased. For a cone-cylinder body as well as a two-dimensional shape having the same profile, sonic velocity occurs at the intersection of the nose with the afterbody. Hence, at the maximum breadth of these bodies a characteristic velocity is the sonic velocity. This breadth can be thought of as corresponding to k. In general, in the transonic flow regime, for any type of nose the maximum velocity is approximately sonic, and this velocity occurs close to the top of the nose. Liepmann and Roshko[36] discuss the problem of bodies having wedge and conical noses. Fig. 5 of Bogdonoff[37] shows the sonic point for several axially symmetric and two-dimensional bodies. Lees[38] and Sibulkin[39] provide good source material for the theory of the sonic-point location and the flow in its vicinity.

The essence of these considerations is that, because of the blunt nature of the roughness, the sonic point will always be near the top of the roughness, as illustrated in Fig. A-1, and the maximum velocity never differs greatly from the sonic value, so that the sonic velocity appears to be a reasonably representative measure. Then a suitable characteristic Reynolds Number is one formed as follows: (a) the characteristic height is k, (b) the characteristic velocity is equal to sonic velocity appropriate to the streamline at the height k, (c) the pressure is equal to static pressure, and (d) the temperature is equal to the sonic temperature appropriate to the streamline at the height k. The viscosity is determined from the temperature (d). The density is determined by means of the perfect gas law and the pressure (c) and temperature (d). Because the roughness is very small and because it is in the boundary layer, the use of static pressure is believed justified. No large region of locally high pressure can exist, because pressures can be propagated by way of the bottom of the boundary layer. The formula for R_k so defined, designating sonic conditions by ( )*, is

$$R_k^* = \rho(p_1, T_k^*)a^*k/\mu(T_k^*) \qquad \text{(A-1)}$$

The symbol R_k^* should not be confused with $R_{k_2}^*$ in the main body of this article.

Fig. A-2 presents the data of Fig. 18 reduced according to Eq. (A-1). The dashed line is taken from Fig. 18 to indicate the previous normal-shock results. The critical Reynolds Number is indeed nearly constant. In addition, under the present hypothesis the high-speed data now appear more consistent with the low-speed results. Under the present system of data reduction we refer to a velocity (a^*) in the immediate

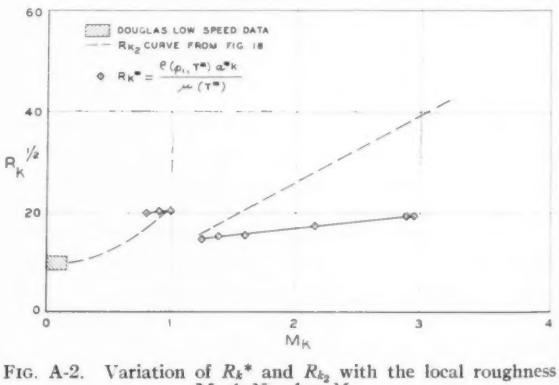

FIG. A-2. Variation of R_k^* and R_{k_2} with the local roughness Mach Number M_{k_1}.

vicinity of the top of the roughness. The low-speed results used u_k, a velocity at the correct height but far upstream of the roughness. Were we to use a local velocity in the immediate vicinity of the top of the roughness, considerations of the flow about circular cylinders adjacent to a wall indicate that the local velocity would be two to three times u_k. Then $R_k^{1/2}$ so evaluated would be some 50 per cent greater—that is, it would be in line with the high-speed data.

The differences in concept of this Appendix, that of the main report, and the older $u_\delta k/\nu_\delta$ formula are worthy of further explanation. The older $u_\delta k/\nu_\delta$ formula referred to properties in the free stream far away in both the x and y directions. Roughly speaking, the $u_k k/\nu_k$ correlation refers to properties at the correct y elevation in the boundary layer but still far away in the x direction. The present correlation refers to the properties of the flow in the immediate vicinity of the roughness—that is, at about the correct value of both x and y. The only reason a correlation of this sort becomes possible at all in such a complicated, viscous, transonic flow is that velocities near the top of the roughness are known not to differ greatly from a^*.

The flow that is actually in contact with the roughness has come from the wall upstream, and of course the roughness has both physical and thermal contact with the wall. Therefore, Eq. (A-1) is not the only one possible under the present concept. Recovery temperature, wall temperature for cooled walls, and total temperature are all possible characteristic temperatures. However, until more data are available there is no way to discriminate among the various possibilities.

An interesting deduction can be made from Eq. (A-1) for the special case of flow past an insulated plate of a gas whose Prandtl Number is unity. For these conditions T^* and a^* are constant on all streamlines and R_k as evaluated by Eq. (A-1) becomes independent of the shape of the boundary-layer velocity profile!

The roughness Reynolds Number defined as $R_k = u_\delta k/\nu_\delta$ is also independent of the shape of the velocity profile. Then, for the special case under consideration, assuming perfect gas relations and $\mu \backsim T^{0.76}$, it is easy to compute the ratio of R_k to $R_k{}^*$. When the Mach Number is great enough to develop sonic velocity at the roughness—that is, $M_k > 0.7$ approximately—we find

$$\frac{R_k}{R_k{}^*} = M_\delta \left[\frac{1 + [(\gamma - 1)/2] M_\delta{}^2}{[(\gamma + 1)/2]} \right]^{1.26} \qquad \text{(A-2)}$$

At Mach 5 with $\gamma = 1.4$ the ratio is about 38:1.

References

[1] Smith, A. M. O., and Clutter, Darwin, W., *The Smallest Height of Roughness Capable of Affecting Boundary-Layer Transition in Low-Speed Flow*, Douglas Aircraft Co., Inc., Report No. ES 26803, August 31, 1957.

[2] Goldstein, S. (Ed.), *Modern Developments in Fluid Dynamics*, Vols. I and II, Oxford, 1938.

[3] Dryden, H. L., *Review of Published Data on the Effect of Roughness on Transition from Laminar to Turbulent Flow*, Journal of the Aeronautical Sciences, Vol. 20, No. 7, pp. 477–482, July, 1953.

[4] Klebanoff, P. S., Schubauer, G. B., and Tidstrom, K. D., *Measurements of the Effect of Two-Dimensional and Three-Dimensional Roughness Elements on Boundary-Layer Transition*, Readers' Forum, Journal of the Aeronautical Sciences, Vol. 22, No. 11, pp. 803–804, November, 1955.

[5] Potter, J. L., *Subsonic Boundary-Layer Transition Caused by Single Roughness Elements*, Readers' Forum, Journal of the Aeronautical Sciences, Vol. 24, No. 2, pp. 158–159, February, 1957.

[6] Tani, I., and Sato, H., *Boundary-Layer Transition by Roughness Element*, Journal of the Physical Society of Japan, Vol. 11, No. 12, pp. 1284–1291, December, 1956.

[7] Liepmann, H., and Fila, G. H., *Investigations of Effects of Surface Temperature and Single Roughness Elements on Boundary-Layer Transition*, NACA TR 890, 1947.

[8] Fage, A., *The Smallest Size of Spanwise Surface Corrugation Which Affects Boundary-Layer Transition on an Airfoil*, ARC R&M No. 2120, 1943.

[9] Loftin, L. K., *Effects of Specific Types of Surface Roughness on Boundary-Layer Transition*, NACA ACR L5J29a, February, 1946.

[10] Gregory, N., and Walker, W. S., *The Effect on Transition of Isolated Surface Excrescences in the Boundary Layer*, ARC 13436, 1950.

[11] Cowled, E. H., *The Effects of Surface Irregularities on Transition in the Laminar Boundary Layer*, A.R.L./A. 86, (Australian) April, 1954.

[12] Cowled, E. H., *Experimental Determination of the Critical Heights of Surface Irregularities*, A.R.L. Aero Note 138 (Australian), 1954.

[13] Hama, F. R., Long, J. D., and Hegarty, J. C., *On Transition from Laminar to Turbulent Flow*, University of Maryland Technical Note BN-81, AFOSR-TN-56-381, AD 95817, August, 1956. See also Hama, F. R., *An Efficient Tripping Device*, Journal of the Aeronautical Sciences, Vol. 24, No. 3, pp. 236–237, March, 1957.

[14] von Doenhoff, A. E., and Horton, E. A., *A Low-Speed Experimental Investigation of the Effect of a Sandpaper Type of Roughness on Boundary-Layer Transition*, NACA TN 3858, October, 1956.

[15] Smith, A. M. O., *Transition, Pressure Gradient and Stability Theory*, Proc. IX International Congress of Applied Mechanics, Brussels, 1956.

[16] Pierce, J., Hess, J. L., and Smith, A. M. O., *Velocity Distributions and Shapes for Free-Streamline Bodies Having Wedge-Shaped Noses*, Douglas Aircraft Co., Inc. Report No. E.S. 29123, August, 1958.

[17] Smith, A. M. O., *Rapid Laminar Boundary-Layer Calculations by Piece-Wise Application of Similar Solutions*, Journal of the Aeronautical Sciences, Vol. 23, No. 10, pp. 901–912, October, 1956.

[18] Smith, A. M. O., *Improved Solutions of the Falkner and Skan Boundary Layer Equations*, Institute of the Aeronautical Sciences, Sherman M. Fairchild Fund Paper No. FF-10, March 1954.

[19] Preston, J. H., *The Minimum Reynolds Number for a Turbulent Boundary Layer and the Selection of a Transition Device*, Journal of Fluid Mechanics, Vol. 3, Part 4, pp. 373–384, January, 1958.

[20] Brinich, P. F., *Boundary-Layer Transition at Mach 3.12 With and Without Single Roughness Elements*, NACA TN 3267, December, 1954.

[21] Johnson, D., *Brief Flight Tests on a "Vampire I" Aircraft to Determine the Effects of Isolated Surface Pimples on Transition*, ARC R & M No. 2779, Part II, 1956.

[22] Schlichting, H., *Boundary Layer Theory*, p. 418; McGraw-Hill Book Co., Inc., 1955.

[23] Goddard, F. E., Jr., *Effect of Uniformly Distributed Roughness on Turbulent Skin-Friction Drag at Supersonic Speeds*, California Institute of Technology, Jet Propulsion Laboratory Report No. 20-113, September 3, 1957.

(*Continued on page 256*)

Readers' Forum

BRIEF REPORTS of investigations in the aeronautical sciences and discussions of papers published in the JOURNAL are presented in this special department. Entries must be restricted to a maximum of 1,300 words or the equivalent of one JOURNAL page including formulas and illustrations. Publication is completed as soon as possible after receipt of the material. The Editorial Committee does not hold itself responsible for the opinions expressed by the correspondents.

Contents

Some Exact Solutions to the Magnetohydrodynamic Equations for Incompressible Flow.....F. D. HAINS 246

The Limiting Circulatory Lift of a Wing of Finite Aspect Ratio.....BARNES W. MCCORMICK 247

A Creep Instability of Thin-Walled Tubes Under Internal Pressure.....IAIN FINNIE 248

A Simple Construction for the Determination of the Magnetohydrodynamic Wave Speed in a Compressible Conductor.....NICHOLAS ROTT 249

Concise, Systematic Jacobian Thermodynamics for High-Temperature Real Gases.....RUSSELL J. ARAVE 250

On the Heating Effect in a Resonance Tube.....I. M. HALL AND C. J. BERRY 253

Linear Deformations of Conical Shells...M. D. MC ILROY 253

Laminar Jet Mixing of Electrically Conducting Fluid in a Transverse Magnetic Field.....S. I. PAI 254

Beam Columns on Elastic Supports.....BEN A. NEFFSON 255

Some Exact Solutions to the Magnetohydrodynamic Equations for Incompressible Flow

F. D. Hains

Boeing Scientific Research Laboratories, Seattle, Wash.

October 20, 1958

EXACT SOLUTIONS of the magnetohydrodynamic equations are considered for incompressible, nonviscous flow. The flow field and magnetic field are two-dimensional and functions of x and y only. The steady flow field with magnetic interaction is assumed to be established so that no consideration is given here to the magnetic field when there is no flow or to the flow when the magnetic field is removed. In the subsequent analysis the conductivity σ is constant.

The governing equations are:[1]

$$uu_x + vu_y + p_x/\rho = -J_3H_2/\rho \tag{1}$$

$$uv_x + vv_y + p_y/\rho = J_3H_1/\rho \tag{2}$$

$$u_x + v_y = 0 \tag{3}$$

$$J_3 = \sigma[E_3 + uH_2 - vH_1],\ J_1 = J_2 = 0 \tag{4}$$

$$H_{1x} + H_{2y} = 0 \tag{5}$$

$$4\pi J_3 = H_{2x} - H_{1y} \tag{6}$$

where the subscripts 1, 2, and 3 indicate components in the x, y, z directions, respectively.

Introducing the stream function ψ, p can be eliminated from Eqs. (1) and (2) to yield

$$\psi_y(\psi_{xyy} + \psi_{xzz}) - \psi_x(\psi_{yyy} + \psi_{xzy}) = -H_2J_{3y}/\rho - H_1J_{3x}/\rho \tag{7}$$

A solution is assumed in the following form:

$$\left.\begin{aligned} \psi &= (C_1x + C_2)g(y) \\ H_1 &= (C_1x + C_2)P'(y) \\ H_2 &= F(y) \\ E_3 &= (C_1x + C_2)M(y) \end{aligned}\right\} \tag{8}$$

Contributors Please Note

Readers' Forum items must be confined to the equivalent of one page in the *Journal*. Contributions that exceed this limit will be returned to the authors for condensation and rewrite. To avoid inconvenience and delay, please adhere to the following specifications:

(1) Five, double-spaced, typewritten, manuscript pages ($8\frac{1}{2}$ by 11 in.), including wide margins, formulas, and headings, equal one printed page.

(2) For every illustration, deduct at least one-half or as much as one manuscript page, depending on the size of the illustration.

where C_1 and C_2 are constants. Using Eqs. (3), (4), and (8), Eq. (7) becomes

$$(\rho C_1/\sigma)\,[gg''' - g'g''] = (g'F - C_1P'g)F' + 2P'FC_1g' + C_1P'M + F^2g'' - 4\pi\sigma C_1gF(M + g'F + C_1gP') + FM' \quad (9)$$

Eliminating J_3 from Eqs. (4) and (6)

$$F = (-P''/4\pi\sigma - C_1gP' - M)/g' \quad (10)$$

and combining this with Eq. (5)

$$P''' + [4\pi\sigma C_1g - (g''/g')]P'' - (4\pi\sigma gg''/g')\,C_1P' + 4\pi\sigma M' - (4\pi\sigma g''/g')M = 0 \quad (11)$$

If one of the three quantities g, P, or M is specified, the remaining two are found from Eqs. (9) and (10). This set of equations will also give the trivial solutions $J_3 = \sigma E_3$ which means that the streamlines coincide with the magnetic field lines.

The stagnation-point flow is $g = Ay + B$ where A and B are constants. Eq. (9) is simplified to

$$[AF - C_1P'(Ay + B)]F' + 2P'FC_1A + C_1P'M - 4\pi\sigma C_1F(Ay + B)\,[M + AF + C_1(Ay + B)P'] + FM' \quad (12)$$

Integrating Eq. (11),

$$M = (-P''/4\pi\sigma) - C_1(AY + B)P' + C_1AP + C_3 \quad (13)$$

so that Eq. (10) becomes

$$F = -C_1P + C_3/A \quad (14)$$

Substituting Eqs. (13) and (14) into Eq. (12) results in a third-order ordinary differential equation in P which can be solved numerically.

A simple solution to this equation is obtained by taking

$$\left.\begin{aligned} M &= M_0 = \text{const.} \\ F &= F_0 = \text{const.} \\ C_1 &= 0 \end{aligned}\right\} \quad (15)$$

which automatically satisfy Eqs. (12) and (14). Eq. (13) yields

$$P'' = -4\pi\sigma(M_0 - C_3)\,(y + C_4) \quad (16)$$

so that the solution is

$$\left.\begin{aligned} u &= C_2A \\ v &= 0 \\ E &= M_0 \\ H_1 &= -4\pi\sigma C_2(M_0 - C_3)\,(y + C_4) \\ H_2 &= F_0 \end{aligned}\right\} \quad (17)$$

This is a uniform flow with parabolic magnetic-field lines. The pressure distribution can be obtained from the momentum equations and the temperature distribution from the energy equation.

Reference

[1] Resler, E. L., Jr., and Sears, W. R., *The Prospects for Magneto-Aerodynamics*, Journal of the Aeronautical Sciences, Vol. 25, No. 4, pp. 235–245, 258, April, 1958.

The Limiting Circulatory Lift of a Wing of Finite Aspect Ratio

Barnes W. McCormick

Head, Aeronautical Engineering Department, School of Engineering, University of Wichita, Wichita, Kan.

November 3, 1958

EXPERIMENTAL EVIDENCE INDICATES that the circulatory lift of a jet-flapped wing of finite aspect approaches a maximum as the momentum coefficient of the jet is increased. Reference 1 suggests that this phenomena is the result of strong tip vortices. In that same reference, an experimental curve is given which shows that the maximum circulatory lift of a finite jet-flapped wing varies nearly linearly with the aspect ratio. The analytical study presented here confirms these experimental results. It will be shown that the maximum lift of a finite wing due to circulation, produced by any means whatever (suction BLC, blowing BLC jet-flaps, ordinary flaps) increases linearly with increasing aspect ratio. This behavior is attributed to the severe vertical displacement of the trailing vortex sheet at the high lift coefficients. This vertically displaced vortex sheet not only decreases the angle of attack of each wing element, as calculated in the usual lifting surface theories, but also subtracts from the incoming free-stream velocity, which effect is usually ignored in finite wing calculations. For ease of calculation only the case of the elliptic wing is treated which is sufficient for demonstration purposes.

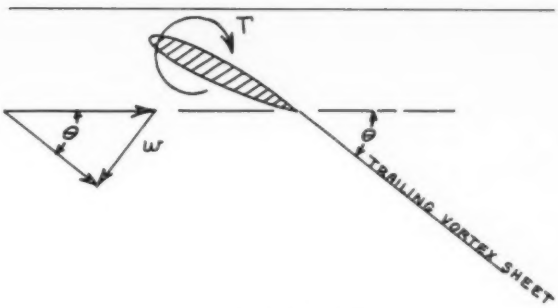

FIG. 1. Wing section.

Theory

The lift coefficient of a wing with a jet-flap can be expressed as the sum of two terms.

$$C_L = C_{L_\Gamma} + C_\mu \sin(\alpha + \delta)$$

$C_{L\Gamma}$ is the dimensionless lift due to the circulation about the airfoil, produced by the angle of attack and the increment due to the jet. The remaining term is that dimensionless lift due to the momentum reaction of the jet in the vertical direction.

The bound circulation, Γ, which may be abnormally high because of the jet-flap effect, must satisfy Helmholz's theorem of vortex continuity resulting in a strong trailing vortex sheet. As stated previously, it is usually assumed that this vortex sheet lies in the plane of the free-stream velocity, and its effect on the wing sections is calculated only as a decrease in the angle of attack of the wing sections.

Consider now a section of the trailing vortex sheet and wing shown in Fig. 1. The vortex sheet is displaced downward due to its own induced velocity. This angle of displacement increases as one moves downstream of the wing. Defining the downwash to be normal to the vortex sheet, the vortex sheet will be displaced from the horizontal at the wing by an angle, θ, given by:

$$\theta = \sin^{-1}(w/V) \quad (1)$$

By the law of Kutta-Joukowski, the resultant force in a given direction is equal to the product of the density, the resultant velocity normal to the direction, and the circulation Γ, or in vector notation

$$\bar{F} = \rho\bar{V} \times \bar{\Gamma} \quad (2)$$

By definition, lift is normal to the free-stream velocity; thus, from Fig. 1

$$\begin{aligned} L &= \rho(V - w\sin\theta)\Gamma \\ &= \rho[V - (w^2/V)]\Gamma \end{aligned} \quad (3)$$

In the general case, the calculation of w and θ would be lengthy; however, consider the elliptic distribution of Γ given by:

$$\Gamma = \Gamma_0\sqrt{1 - (y/b)^2} \quad (4)$$

For this case, the relationship between w, and the wing section lift coefficients are well known.

$$w = \text{constant} = \Gamma_0/2b \quad (5)$$

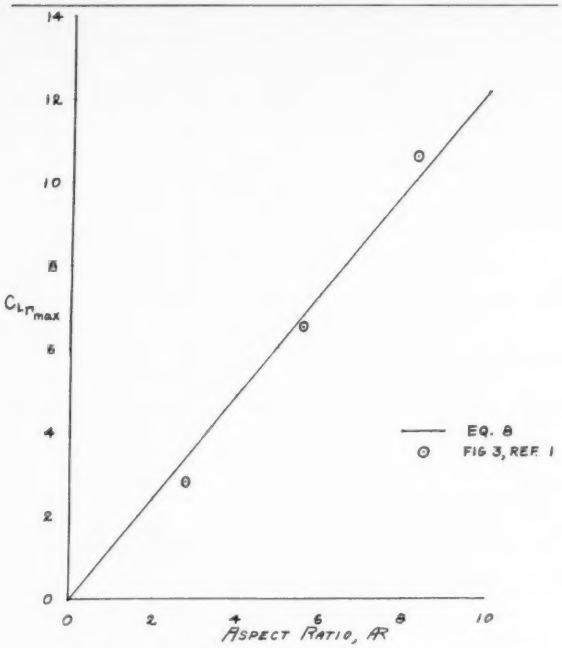

FIG. 2. Comparison of theory and experiment.

Consider, therefore, the mid-span section.

$$L_0 = \rho V \Gamma_0 [1 - (w/V)^2]$$

By definition:

$$C_{l_0} = C_L = L_0/(1/2)\rho V^2 C_0 = 2(\Gamma_0/c_0 V)\ [1 - (1/4)\ (\Gamma_0/bv)^2]$$

Or, since the aspect ratio is given by: $AR = 4b/\pi c_0$.

$$C_L = (\pi AR/2)(\Gamma_0/bV)\ [1 - (1/4)\ (\Gamma_0/bV)^2] \qquad (6)$$

From this equation, it can be seen that C_L reaches a maximum at some value of Γ_0/bV. To find the value of C_L, Eq. (6) is differentiated with respect to Γ_0/bV and equated to zero.

Therefore: $$(\Gamma_0/bV)c_{L_{max}} = 2/\sqrt{3} \qquad (7)$$

Thus: $$C_{L_{max}} = 2\pi/3\sqrt{3}\ AR$$

$$\cong 1.21\ AR \qquad (8)$$

From Fig. 2 it can be seen that Eq. (8) is in substantial agreement with tests performed by the NACA on a series of rectangular wings, as reported in reference 1.

REFERENCES

[1] Lowry, J. G., and Vogler, R. D., *Wind-Tunnel Investigation At Low Speeds to Determine the Effect of Aspect Ratio and End Plates on a Rectangular Wing With Jet Flaps Deflected 85°*, NACA TN, December, 1956.

[2] Lowry, J. G., Riebe, J. M., and Campbell, J. P., *The Jet-Augmented Flap*, presented at Aerodynamics—II Session, IAS 25th Annual Meeting, January 28, 1957. (Available as IAS Preprint No. 715).

A Creep Instability of Thin-Walled Tubes Under Internal Pressure

Iain Finnie
Shell Development Company, Emeryville, Calif.
November 10, 1958

WHEN A THIN-WALLED TUBE of circular cross section, under constant internal pressure, deforms due to creep there is a continuous increase of radius and decrease of wall thickness. The stresses in the tube thus grow with time, which leads to an increasing rate of deformation. The purpose of the present note is to point out that this effect leads to a maximum tube life which can be predicted from tensile creep data.

The average tangential stress in the tube wall may be written as

$$\sigma_T = PR/h = (PR_0/h_0)e^{\epsilon_T - \epsilon_R}$$

where P is the internal pressure, R and h the inside radius and wall thickness of the tube (original values R_0, h_0), and ϵ_T and ϵ_R are the true (natural) tangential and radial strains. Alternatively, we may write the previous expression as

$$\sigma_T = \sigma_{T_0} e^{\epsilon_T - \epsilon_R} \qquad (1)$$

where σ_{T_0} is the initial average tangential stress.

It is found by the experiment[1] that in creep, as in other forms of plastic deformation, the volume of the deformed material does not change. For the tube under internal pressure there is no rotation of the principal strain axes during deformation, and the condition of volume constancy may be written as

$$\epsilon_A + \epsilon_R + \epsilon_T = 0$$

In this equation, ϵ_A is the axial strain, and we have assumed that elastic strains are small enough, relative to creep strains, for elastic volume changes to be neglected.

In an internal pressure test* under creep conditions, it is found that the axial strain is extremely small relative to the other principal strains.[2] Utilizing this fact, we have $\epsilon_T = -\epsilon_R$, and hence Eq. (1) becomes

$$\sigma_T = \sigma_{T_0} e^{2\epsilon_T} \qquad (2)$$

To relate stress and strain, we must now make some assumption about the creep behavior of the tubing. Many materials, when loaded by constant stress, show a creep rate which is initially quite high but soon decreases to a steady value. This steady-state creep rate stays almost constant until rupture occurs.† When considering fairly large strains, as in the present case, it is thus often a good approximation to treat the creep rate as a function only of stress. The empirical relation which usually gives a satisfactory fit to constant-stress creep data is

$$\dot{\epsilon} = B\sigma^n$$

where σ and $\dot{\epsilon}$ are the stress and steady-state creep rate, and B and n are constants which may vary with temperature.

For a tube under internal pressure, it may be shown that the tangential creep rate is given by

$$\dot{\epsilon}_T = B(3/4)^{(n+1)/2}\ \sigma_T{}^n$$

Substituting into Eq. (2) we obtain

$$\dot{\epsilon}_T = \dot{\epsilon}_{T_0} e^{2n\epsilon_T}$$

where $\dot{\epsilon}_{T_0}$ is the initial tangential creep rate. Integration leads to

$$e^{-2n\epsilon_T} = 1 - 2n\dot{\epsilon}_{T_0} t \qquad (3)$$

and it is clear that finite tube deformations are only obtained if $t < 1/2n\dot{\epsilon}_{T_0}$. Thus, an upper limit to the life of the tube may be obtained from creep data alone. Ductile materials, in short-time rupture tests, show a rather large elongation to failure. Under these conditions, we would expect that $t = 1/2n\dot{\epsilon}_{T_0}$ would be a good approximation to the tube life. For specimens which fail at longer times, the elongations to fracture are generally smaller, and we would expect the upper limit ($t = 1/2n\dot{\epsilon}_{T_0}$) to considerably overestimate the rupture life.

To complete the picture, we will now examine the conditions for rupture under increasing stress. We assume that constant-stress tensile rupture data may be fitted by the expression

$$t = A\sigma^{-q}$$

* Strictly speaking, we should specify that we are considering the case in which the axial load due to internal pressure is carried by the tube wall. This is almost always the situation in practice.

† The accelerating creep rate (tertiary creep) observed toward the end of constant-load tensile rupture tests is largely due to the increased stress produced by decreasing specimen diameter. However, it appears that limited tertiary creep also occurs in constant-stress tests.[3]

where t is the rupture life and A and q are constants which may depend on temperature. If t_0 is the rupture life which would correspond to the initial stress and t' is the rupture life which corresponds to the varying stress, we write

$$\int_0^{t'} (dt/t) = \int_0^{t'} (dt/A\sigma^{-q}) = 1$$

This assumes, following Robinson,[4] that in each increment of time a percentage of the rupture life is used up which depends only on the stress during that increment. When the accumulated total of the rupture life fractions equals unity, rupture is assumed to occur. The preceding equation may also be written as

$$\int_0^{t'} (\sigma/\sigma_0)^q \, dt = t_0 \tag{4}$$

This equation applies only to varying uniaxial stress, and we should now consider the problem of predicting the life of a tube under internal pressure from tensile rupture data. The best experimental evidence[5] available at the present shows that for ductile metals the maximum tensile stress in a multiaxial stress system is the criterion of failure. Since the maximum tensile stress in a tube under internal pressure is the tangential stress, we may use the preceding equation with $\sigma = \sigma_T$ and $\sigma_0 = \sigma_{T_0}$. Making this substitution Eqs. (2)–(4) lead to

$$\int_0^{t'} (1 - 2n\dot{\epsilon}_{T_0}t)^{-q/n} \, dt = t_0$$

and hence

$$1 - 2(n - q)\dot{\epsilon}_{T_0}t_0 = (1 - 2n\dot{\epsilon}_{T_0}t')^{(n-q)/q} \text{ if } n \neq q \tag{5}$$

$$\ln (1 - 2n\dot{\epsilon}_{T_0}t') = -2n\dot{\epsilon}_{T_0}t_0 \text{ if } n = q$$

These equations relate the rupture lives at constant stress (t_0) and constant pressure (t') if the various constants (n, p, and B) are known. In cases where the stresses are low, the time to rupture long, and the deformation to failure consequently small, the rupture life predicted by Eq. 5 may be considerably less than given by $t' = 1/2n\dot{\epsilon}_{T_0}$.

Unfortunately, there are few data against which we may compare the predicted maximum life of tubing under internal pressure. A single, rather limited comparison can be made from the test data of Fig. 1. This shows the tangential strain at the outside of a 2S aluminum tube which was loaded by internal pressure at 250°C. (482°F.). The test conditions are such that we might expect the rupture life to be governed by the instability condition. Diameter changes were measured during the test with a special high-temperature feeler gage.[6] We can read from the figure that the rupture life $t' = 72.3$ hours and can estimate the initial (minimum) tangential strain rate as $\dot{\epsilon}_{T_0} = 8.0 \times 10^{-4}$ hours^{-1}. Using the approximation $t' = 1/2n\dot{\epsilon}_{T_0}$, we find $n = 8.6$. This is quite close to values of n which may be estimated from data[7] in the literature for 2S aluminum at 500°F. and comparable stresses and strain rates.

Eq. 3 may be written as

$$\epsilon_T = -(1/2n) \ln (1 - 2n\dot{\epsilon}_{T_0}t) \tag{6}$$

Putting $1/2n\dot{\epsilon}_{T_0} = 72.3$ hours and $n = 8.6$ in Eq. 6 leads to the broken curve shown in Fig. 1. Strictly speaking, the fact that this curve lies close to the measured values only proves that we can reconstruct the curve from its initial slope, $\dot{\epsilon}_{T_0}$, and final abscissa, t'. However, further justification is given by the agreement of the predicted n with data in the literature.

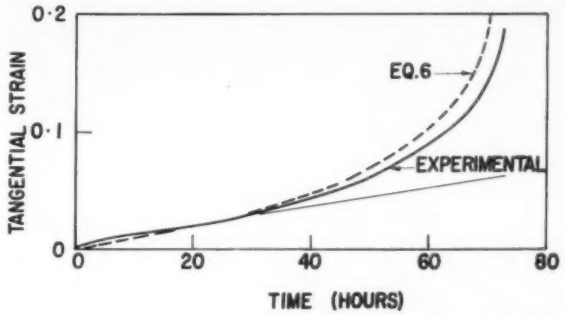

FIG. 1. Solid curve shows tangential strain at outside diameter of a 2S aluminum tube, 1.600 in. outside diameter and 0.100 in. wall thickness, under 290 psi internal pressure at 250°C. Broken curve shows strains calculated from Eq. (6). Thin solid line shows initial (minimum) creep rate.

REFERENCES

[1] Johnson, A. E., *Creep Under Complex Stress Systems at Elevated Temperatures*, Proc. Institution of Mech. Engrs., Vol. 164, pp. 432–447, London, 1951.

[2] Norton, F. H., *Creep in Tubular Pressure Vessels*, Trans. ASME, Vol. 61, pp. 239–245, 1939.

[3] Sully, A. H., *Metallic Creep and Creep Resistant Alloys*, Chap. 4; Butterworth Scientific Publications, London, 1949.

[4] Robinson, E. L., *Effect of Temperature Variation on the Long Time Rupture Strength of Steels*, Trans. ASME, Vol. 74, pp. 777–781, 1952.

[5] Johnson, A. E., Henderson, J., and Mathur, V. D., *Combined Stress Creep Fracture of Commercially Pure Copper at 250°C.*, The Engr., Vol. 196, pp. 261–265, 299–301, 1956.

[6] Finnie, I., *Tube Diameter and Thickness Gauge for High Temperatures*, Review of Scientific Instruments, Vol. 29, p. 1054, 1958.

[7] Servi, I. S., and Grant, N. J., *Creep and Stress Rupture Behavior of Aluminum as a Function of Purity*, J. Metals, Vol. 3, pp. 909–916, 1951.

A Simple Construction for the Determination of the Magnetohydrodynamic Wave Speed in a Compressible Conductor

Nicholas Rott

Professor of Aeronautical Engineering, Graduate School of Aeronautical Engineering, Cornell University, Ithaca, N.Y.

November 19, 1958

THE PROBLEM OF THE MAGNETOHYDRODYNAMIC plasma waves was solved by Herlofson[1] and van de Hulst,[2] and an excellent review of the subject was given by Friedrichs,[3] whose report, unfortunately, belongs to the more or less unavailable "subliterature." The purpose of the present note is to point out a simple *geometric* construction, which gives not only the wave speeds as a function of the wave direction, but also the direction of the resultant particle motion ("polarization") for the different modes. The usefulness of this construction, which, naturally, does not contain new information, is that it permits a quick survey of all possible plasma wave modes—a desirable result in view of the complications of the problem.

Let a be the speed of sound in the perfect gas, in the absence of magnetic fields:

$$a^2 = \gamma(p/\rho) \tag{1}$$

and let b be the Alfvén velocity in an incompressible conductor (of the same density ρ) in the presence of a uniform magnetic field H (using $MKSQ$ units):

$$b^2 = \mu H^2/\rho \tag{2}$$

Consider a plane wave in the compressible conductor whose normal forms an angle ϑ with the direction of the magnetic field. The field components are $H_x = H\cos\vartheta$ and $H_y = H\sin\vartheta$ parallel and perpendicular to the wave normal; the corresponding components of the particle velocity behind the wave, in the plane formed by H and the wave normal, will be called Δu and Δv. [The motion in the third direction (z) will be considered later.] The symbol Δ will be used for the change of any quantity across the wave, and c is the wave speed which is to be determined.

Continuity requires that

$$\rho\Delta u = c\Delta\rho \tag{3}$$

To simplify the present analysis, a result obtained by previous

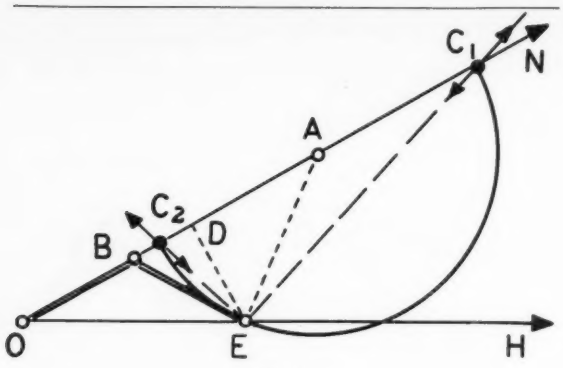

FIG. 1.

investigations will be quoted without proof: weak magneto-hydrodynamic waves are isentropic. This result, which can be used, as in gasdynamics, in lieu of the energy equation, states that

$$\Delta p = a^2 \Delta \rho = \rho(a^2/c)\,\Delta u \tag{4}$$

The momentum equations are influenced by the presence of a body force, caused by the interaction of the magnetic field with a current sheet flowing "in" the wave (in z-direction, perpendicular to the plane of H and the wave normal). The strength of the current sheet, in turn, is measured (according to Ampère's law) by ΔH_y, so that the two momentum equations take the form

$$\Delta p - \rho c \Delta u + \mu H_y \Delta H_y = 0 \tag{5}$$

$$\rho c \Delta v - \mu H_x \Delta H_y = 0 \tag{6}$$

Finally, the induction law (for infinite conductivity*) will be formulated, namely, that the magnetic flux across a particle-fixed closed line remains unchanged. Balancing the changes across a loop formed by lines parallel to the x- and z-directions, one finds

$$c \Delta H_y = H_y \Delta u + H_x \Delta v \tag{7}$$

Elimination of Δp and ΔH_y in Eqs. (5) and (6) by Eqs. (4) and (7) gives

$$\begin{aligned}(a^2 - c^2 + b_y^2)\Delta u + b_x b_y \Delta v &= 0\\ -b_x b_y \Delta u + (c^2 - b_x^2)\Delta v &= 0\end{aligned}$$

where $b_x = b \cos \vartheta$ and $b_y = b \sin \vartheta$. Finally,

$$\Delta v/\Delta u = b_x b_y/(c^2 - b_x^2) = (c^2 - a^2 - b_y^2)/b_x b_y \tag{8}$$

and c fulfills the equation

$$c^4 - c^2(a^2 + b^2) + a^2 b^2 \cos^2 \vartheta = 0 \tag{9}$$

The two solutions for c^2 are

$$c^2_{1,2} = (1/2)(a^2 + b^2) \pm (1/2)\sqrt{a^4 + b^4 - 2a^2 b^2 \cos 2\vartheta} \tag{10}$$

The angle ψ between the particle motion and the wave normal follows from Eq. (8). It is advantageous to construct $\tan^2\psi$ as a product of the two expressions given in Eq. (8):

$$\tan^2 \psi = (\Delta v/\Delta u)^2 = (c^2 - a^2 - b_y^2)/(c^2 - b_x^2)$$

and to consider the angle 2ψ:

$$\cos 2\psi = (1 - \tan^2\psi)/(1 + \tan^2\psi) = (a^2 + b_y^2 - b_x^2)/(2c^2 - a^2 - b^2)$$

which can be written by the use of Eq. (10) in the form

$$\cos 2\psi_{1,2} = \pm(a^2 - b^2 \cos 2\vartheta)/(c_1^2 - c_2^2) \tag{11}$$

The well-known results expressed in Eqs. (10) and (11) lead to the following geometrical construction: let the direction of the magnetic field be along OH, and let ON lie in the direction of the wave normal, so that the angle $HON = \vartheta$ (see Fig. 1). Consider B on ON and E on OH such that $OB = BE = b^2/2$; this makes the angle $NBE = 2\vartheta$. Let $BA = a^2/2$ so that

$$OA = (1/2)(a^2 + b^2) = (1/2)(c_1^2 + c_2^2)$$

according to Eq. (10); also,

$$AE = (1/2)\sqrt{a^4 + b^4 - 2a^2 b^2 \cos 2\vartheta} = (1/2)(c_1^2 - c_2^2)$$

The circle around A with the radius AE cuts ON at the points C_1 and C_2 so that

$$OC_1 = c_1^2, \quad OC_2 = c_2^2$$

Moreover, EC_1 and EC_2 are the directions of particle motion, or the angle $OC_1E = \psi_1$, $OC_2E = \psi_2$.

Proof: OAE can be shown to be 2ψ, by making ED perpendicular to ON, so that

$$BD = BE \cos 2\vartheta = (1/2)b^2 \cos 2\vartheta$$

and

$$AD = AB - BD = (1/2)(a^2 - b^2 \cos 2\vartheta)$$

and finally, $AD/AE = \cos 2\psi_1$, according to Eq. (11).

The two directions of particle motion in the two modes are perpendicular to each other, as is already known.

The construction (which by symmetry only has to be used in the range $0 \leq \vartheta \leq \pi/2$) has the drawback that the "velocity squares" are plotted, but it offers the advantage that it also gives the direction of the particle motion for the modes. It can be shown that if the roles of a^2 and b^2 are reversed, the construction remains valid if the roles of H and N are also reversed.

Finally, a short remark can be made regarding a third possible mode, in which the velocity of the particles is directed in the z-direction, perpendicular to the two directions obtained so far. It can be shown that this mode remains uncoupled with the compressibility effects of the gas, so that its propagation speed equals the Alfvén velocity calculated with the field component parallel to the wave normal, viz., $c_3 = b \cos \vartheta$. It is found that c_3 is always intermediate between c_1 and c_2, except for $\vartheta = 0$ when c_3 coincides with c_2.

* This assumption can be dropped if the changes between two uniform states before and after a weak shock (or wavelet) are considered.

REFERENCES

[1] Herlofson, N., *Magneto-Hydrodynamic Waves in a Compressible Fluid Conductor*, Nature, Vol. 165, p. 1020, 1950.

[2] van de Hulst, H. C., *Interstellar Polarization and Magneto-Hydrodynamic Waves in Problems of Cosmical Aerodynamics*, Proc. Astr. Symposium, Paris, 1949, by Central Air Documents Office, Dayton, Ohio, 1951.

[3] Friedrichs, K. O., *Nonlinear Wave Motion in Magneto-Hydrodynamics*, N.Y.U. Report, 1954.

Concise, Systematic Jacobian Thermodynamics for High-Temperature Real Gases

Russell J. Arave
Thermodynamics Research Engineer, Convair-San Diego, A Division of General Dynamics Corporation, San Diego, Calif.

November 18, 1958

SYMBOLS

A/RT	=	dimensionless Helmholtz function
F/RT	=	dimensionless Gibbs function
$G = E/RT$	=	dimensionless internal energy
$I = H/RT$	=	dimensionless enthalpy
J	=	Jacobian operator
P	=	pressure
R	=	the gas constant
S/R	=	dimensionless entropy
T	=	absolute temperature
$Z = P/\rho RT$	=	compressibility factor
a	=	$J(\ln \rho, \ln T)$
b	=	$J(Z, \ln \rho) = J(G, \ln T)$
c	=	$J(Z, G) = (b^2 - mn)/a$
m	=	$J(\ln T, Z)$
n	=	$J(\ln \rho, G)$
b/a	=	$(\partial G/\partial \ln \rho)_T = G_\rho = -(\partial Z/\partial \ln T)_\rho = -Z_T$
c/a	=	$G_\rho^2 + G_T Z_\rho$
m/a	=	$-(\partial Z/\partial \ln \rho)_T = -Z_\rho$
n/a	=	$(\partial G/\partial \ln T)_\rho = G_T$

x and y = general variables
ln = natural logarithm symbol
ρ = density

MODERN DAY high-velocity flight phenomena are leading scientists into a large number of high-temperature problems. One such problem is introduced by dissociation and ionization of gases. By either decreasing the density or increasing the temperature of a gas, one can force a nearly ideal gas to change into a so-called "real" gas which takes into account the effects of dissociation, etc. Shaw,[2] by functional analysis (or Jacobians), has developed a unique orderly method for obtaining any thermodynamic partial derivative for a simple system — e.g., an ideal gas — in terms of reference partial derivatives. Presented here is a table of common thermodynamic quantities that are generalized in order to account for real-gas effects.

A thermodynamic partial derivative can be represented by a combination of any six (or less) chosen thermodynamical partial derivatives plus certain state variables.[3] These six partials can be reduced to three by the three following steps: proper choice of independent variables (ρ, T); Maxwell's relation ($G_\rho = -Z_T$), and interrelation of the derivatives ($ac - b^2 + mn = 0$). The terms in parentheses that follow each of these three steps are for the particular case which is to be presented here. That is, all of the thermodynamic quantities are taken to be functions of density and temperature. The dimensionless internal energy and the compressibility factor are used as the working dependent variables, thus establishing the three reference partial derivatives G_ρ, G_T, and Z_ρ. Although this choice of parameters is arbitrary, very accurate numerical values for internal energy and compressibility can be obtained by using spectroscopic data. Also, temperature and density have been found by experience to be convenient variables with which to work.

The fundamental equation that relates a Jacobian table to a partial derivative is

$$(\partial x/\partial y)_z = J(x, z)/J(y, z) \qquad (1)$$

The Jacobian formulas of importance for filling in the tables in terms of reference quantities are

$$J(\ln P, x) = (1/Z)J(Z, x) + J(\ln T, x) + J(\ln \rho, x) \qquad (2)$$

$$J(S/R, x) = J(G, x) + G\,J(\ln T, x) - Z\,J(\ln \rho, x) \qquad (3)$$

$$J(I, x) = J(G, x) + J(Z, x) \qquad (4)$$

$$J(A/RT, x) = Z\,J(\ln \rho, x) - G\,J(\ln T, x) \qquad (5)$$

$$J(F/RT, x) = J(A/RT, x) + J(Z, x) \qquad (6)$$

where x is any thermodynamic variable.

In order to obtain the value of $J(x, y)$ from the tables, let the first variable (x) apply to the desired quantity in the left-hand column and let the second variable (y) represent the desired quantity in the row across the top of the tables. Using Table 1 let us find the value of $(\partial P/\partial \rho)_T$ by means of reference quantities whose values are known. Making use of Eq. (1), we find that

$$(\partial P/\partial \rho)_T = (P/\rho)\,(\partial \ln P/\partial \ln \rho)_T =$$
$$(P/\rho)\,J(\ln P, \ln T)/J(\ln \rho, \ln T)$$
$$= (P/\rho)\,[a - (m/Z)]/a = (P/\rho)\,[1 - (m/Za)]$$

Or, by Table 2, we would find in a like manner that

$$(\partial P/\partial \rho)_T = (P/\rho)\,[1 + (Z_\rho/Z)]$$

Table 1 is the more general table in that the choice of independent variables has not been made, whereas Table 2 makes ρ and T the independent variables — each value in Table 1 is divided by $a = J(\ln \rho, \ln T)$. Thus other tables similar to Table 2 can be made by dividing Table 1 through by other such quantities. Table 2 enables one to find the numerical value of any partial derivative (composed of the quantities heading the tables) in terms of just G_ρ, Z_ρ, and G_T, along with G and Z which are all known and are all functions of ρ and T.

The tables are a useful, convenient short-cut procedure for the handling of almost any thermodynamic partial derivative situation. Other related manipulations and second-order partial derivatives[1] can be handled in much the same manner as pre-

TABLE 1

$J(x, y)$ $\quad J(x, y) = -J(y, x) \quad J(x, x) = 0 \quad$ Example: $J[(A/RT), G] = Gb + Zn$

x ↓ y →	$\ln P$	$\ln \rho$	$\ln T$	S/R	G	Z	I	A/RT	F/RT
$\ln P$	0	$\frac{b}{Z} - a$	$a - \frac{m}{Z}$	$Ga + Za + n$ $-2b + \frac{c - Gm}{Z}$	$\frac{c}{Z} - b + n$	$m - b$	$\frac{c}{Z} - 2b +$ $n + m$	$b - Ga - Za$ $+ \frac{Gm}{Z}$	$m - Ga$ $-Za + \frac{Gm}{Z}$
$\ln \rho$	$-\frac{b}{Z} + a$	0	a	$Ga + n$	n	$-b$	$n - b$	$-Ga$	$-b - Ga$
$\ln T$	$-a + \frac{m}{Z}$	$-a$	0	$Za - b$	$-b$	m	$m - b$	$-Za$	$m - Za$
S/R	$-Ga - Za - n$ $+2b - \frac{c}{Z} + \frac{Gm}{Z}$	$-Ga - n$	$-Za + b$	0	$-Gb - Zn$	$Gm + Zb - c$	$Gm - Gb$ $-Zn + Zb - c$	$-Gb - Zn$	$Gm - Gb$ $-Zn + Zb - c$
G	$-\frac{c}{Z} + b - n$	$-n$	b	$Gb + Zn$	0	$-c$	$-c$	$-Gb - Zn$	$-Gb - Zm - c$
Z	$-m + b$	b	$-m$	$-Gm - Zb$ $+c$	c	0	c	$Gm + Zb$	$Gm + Zb$
I	$-\frac{c}{Z} + 2b$ $-n - m$	$-n + b$	$-m + b$	$-Gm + Gb$ $+Zn - Zb + c$	c	$-c$	0	$Gm + Zb$ $-Gb - Zn$	$Gm + Zb$ $-Gb - Zn - c$
A/RT	$-b + Ga + Za$ $- \frac{Gm}{Z}$	Ga	Za	$Gb + Zn$	$Gb + Zn$	$-Gm - Zb$	$-Gm - Zb$ $+ Gb + Zn$	0	$-Gm - Zb$
F/RT	$-m + Ga$ $+Za - \frac{Gm}{Z}$	$b + Ga$	$-m + Za$	$-Gm + Gb$ $+Zn - Zb + c$	$Gb + Zn + c$	$-Gm - Zb$	$-Gm - Zb$ $+ Gb + Zn + c$	$Gm + Zb$	0

TABLE 2

$J(x, y)$

$x \downarrow$ $y \rightarrow$	$\ln P$	$\ln \rho$	$\ln T$	S/R	G	Z	I	A/KT	F/RT
$\ln P$	0	$\frac{G_\rho}{Z} - 1$	$\frac{Z_\rho}{Z} + 1$	$-2G_\rho + G + Z + G_T + \left[\frac{(G_\rho)^2 + GZ_\rho + G_T Z_\rho}{Z}\right]$	$-G\rho + G_T + \left[\frac{(G\rho)^2 + G_T Z\rho}{Z}\right]$	$-G_\rho - Z_\rho$	$-2G_\rho + G_T - Z_\rho + \left[\frac{(G_\rho)^2 + G_T Z_\rho}{Z}\right]$	$-G - Z + G_\rho - \frac{GZ_\rho}{Z}$	$-\left[G + Z + Z_\rho + \frac{GZ_\rho}{Z}\right]$
$\ln \rho$	$-\frac{G_\rho}{Z} + 1$	0	1	$G + G_T$	G_T	$-G_\rho$	$-G_\rho + G_T$	$-G$	$-G - G_\rho$
$\ln T$	$-\frac{Z_\rho}{Z} - 1$	-1	0	$Z - G_\rho$	$-G_\rho$	$-Z_\rho$	$-G_\rho - Z_\rho$	$-Z$	$-Z - Z_\rho$
S/R	$2G_\rho - G - Z - G_T - \left[\frac{(G_\rho)^2 + GZ_\rho + G_T Z_\rho}{Z}\right]$	$-G - G_T$	$-Z + G_\rho$	0	$-ZG_T - GG_\rho$	$-\frac{(G_\rho)^2 - GZ_\rho}{-G_T Z_\rho + ZG_\rho}$	$-\frac{(G_\rho)^2 - GZ_\rho - G_T Z_\rho}{+ZG_\rho - ZG_T - GG_\rho}$	$-ZG_T - GG_\rho$	$-\frac{(G_\rho)^2 - GZ_\rho - G_T Z_\rho}{+ZG_\rho - ZG_T - GG_\rho}$
G	$-\left[\frac{G_\rho - G_T}{\frac{(G_\rho)^2 + GZ_\rho + G_T Z_\rho}{Z}}\right]$	$-G_T$	G_ρ	$ZG_T + GG_\rho$	0	$-\frac{(G_\rho)^2 - Z_\rho G_T}{}$	$-\frac{(G_\rho)^2 - Z_\rho G_T}{}$	$-GG_\rho - ZG_T$	$-\frac{(G_\rho)^2 - GG_\rho}{-ZG_T - Z_\rho G_T}$
Z	$G_\rho + Z_\rho$	G_ρ	Z_ρ	$\frac{(G_\rho)^2 + GZ_\rho}{+G_T Z_\rho - ZG_\rho}$	$(G_\rho)^2 + Z_\rho G_T$	0	$(G_\rho)^2 + Z_\rho G_T$	$-GZ_\rho + ZG_\rho$	$-GZ_\rho - ZG_\rho$
I	$2G_\rho - G_T + Z_\rho - \left[\frac{(G_\rho)^2 - G_T Z_\rho}{Z}\right]$	$G_\rho - G_T$	$G_\rho + Z_\rho$	$\frac{(G_\rho)^2 + GZ_\rho + G_T Z_\rho}{-ZG_\rho + ZG_T + GG_\rho}$	$(G_\rho)^2 + Z_\rho G_T$	$-\frac{(G_\rho)^2 - Z_\rho G_T}{}$	0	$-\frac{GG_\rho - GZ_\rho}{-ZG_T + ZG_\rho}$	$-\frac{(G_\rho)^2 - GZ_\rho - G_T Z_\rho}{-GG_\rho - ZG_T + ZG_\rho}$
A/RT	$G + Z - G_\rho + \frac{GZ_\rho}{Z}$	G	Z	$ZG_T + GG_\rho$	$GG_\rho + ZG_T$	$GZ_\rho - ZG_\rho$	$\frac{GG_\rho + GZ_\rho}{+ZG_T - ZG_\rho}$	0	$-ZG_\rho + GZ_\rho$
F/RT	$G + Z + Z_\rho + \frac{GZ_\rho}{Z}$	$G + G_\rho$	$Z + Z_\rho$	$\frac{(G_\rho)^2 + GZ_\rho + G_T Z_\rho}{-ZG_\rho + ZG_T + GG_\rho}$	$\frac{(G_\rho)^2 + GG_\rho}{+ZG_T + Z_\rho G_T}$	$GZ_\rho - ZG_\rho$	$\frac{(G_\rho)^2 + GZ_\rho + G_T Z_\rho}{+GG_\rho + ZG_T - ZG_\rho}$	$ZG_\rho - GZ_\rho$	0

sented here. For further details on Jacobians, one should consult Shaw.[2]

REFERENCES

[1] Arave, Russell, J., *The Thermodynamic Properties of High Temperature Gases Via the Jacobian Method*, Convair-San Diego Thermodynamics Report TG-122A, August 1, 1958.

[2] Shaw, A. N., *The Derivation of Thermodynamical Relations for a Simple System*, Trans. Royal Society (London), A234, pp. 299–328, May 31, 1935.

[3] Einbinder, Harvey, *The Application of Jacobians to Statistical Thermodynamics*, J. Chem. Phys., Vol. 21, No. 12, pp. 2134–2142, December, 1953.

On the Heating Effect in a Resonance Tube

I. M. Hall and C. J. Berry*

Aerodynamics Division, National Physical Laboratory, Teddington, England

November 17, 1958

IN A RECENT NOTE[1] Sibulkin and Vrebalovich have drawn attention to Sprenger's work on heating in resonance tubes.[2] It is mentioned that the dissipative mechanism inside the tube might be shock waves, and recent work at the National Physical Laboratory has shown that this is the case.

A 2-in. long, 3/16-in. square resonance tube, closed at one end, was excited by a supersonic jet issuing from an orifice of the same cross section as the tube. The pressure ratio across the orifice was about 4. When the mouth of the resonance tube was in one of the compression regions of the jet, the air column in the tube resonated, producing an intense note with a wavelength of approximately four times the length of the tube. The most intense sound occurred when the mouth was in the first compression region, and in this case the temperature at the closed end of the tube was about 140°C., the total temperature of the jet being about 20°C.

Short-duration (about 1 microsec.) shadow photographs were taken using a Cranz-Schardin system which takes eight photographs at intervals of the order of 50 microsec. Four photographs from such a series are shown in Fig. 1. The shock wave is clearly seen in its passage down the tube but is more difficult to distinguish on its return [(c) and (d) in Fig. 1]. A correlation between the flow inside and outside the tube is clear from these photographs. When the shock wave is moving into the tube, the external pattern is similar to the case of a jet impinging on a flat surface with spillage sideways as a wall-jet. In the second pair of photographs, where the internal shock wave is moving out of the tube, the jet appears to penetrate into the tube with little or no spillage.

The precise mechanism of the heating effect is not yet completely understood although it is clearly related to the nonisentropic flow inside the tube. Further investigations are in progress which, it is hoped, will enable a complete explanation of the process to be obtained.

* The authors acknowledge the assistance of R. J. North who designed the Cranz-Shardin system.

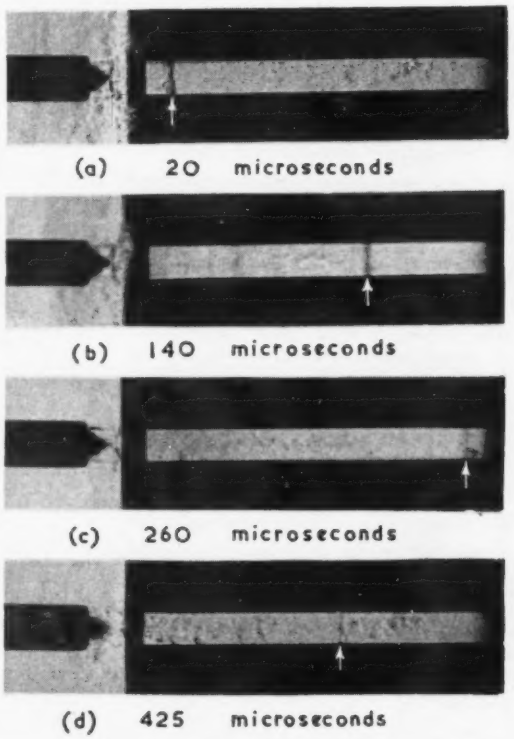

FIG. 1. Shadow photographs of the resonance tube showing four stages in the cycle. The times shown are measured from an arbitrary zero. In (a) and (b) the shock wave, indicated by a white arrow, is moving toward the bottom of the tube while in (c) and (d) it is moving away from the bottom.

REFERENCES

[1] Sibulkin, M., and Vrebalovich, T., *Some Experiments with a Resonance Tube in a Supersonic Wind Tunnel*, Journal of the Aeronautical Sciences, Readers' Forum, Vol. 25, No. 7, pp. 465–466, July, 1958.

[2] Sprenger, H., *Thermal Effects in Resonance Tubes*, Mitteilungen aus dem Institut für Aerodynamik, No. 21, pp. 18–34, 1954.

Linear Deformations of Conical Shells

M. D. Mc Ilroy

Bell Telephone Laboratories, Inc., Murray Hill, N.J.

November 10, 1958

THIS NOTE DESCRIBES a complete set of solutions to the linearized problem of elastic deformations of thin shallow conical shells.* The relevant differential equations are[1]

$$\left.\begin{aligned} C^{-1}\nabla^4 F + r^{-1}\tan\alpha\,\partial^2 w/\partial r^2 &= 0 \\ D\nabla^4 w - r^{-1}\tan\alpha\,\partial^2 F/\partial r^2 &= 0 \end{aligned}\right\} \tag{1}$$

where F is a stress function, w is transverse displacement, α is elevation of cone generators above a base plane normal to the shell axis, and C and D are material constants.

The system in Eq. (1) is transformed into a set of independent fourth-order ordinary differential equations of generalized hypergeometric type,[2]

$$\left.\begin{aligned} \{(\delta - n)(\delta + n)(\delta - 2 - n)(\delta - 2 + n) - z\delta(\delta - 1)\}\, W'_n &= 0 \\ \delta = z\,d/dz, \quad n &= 0, 1, 2 \ldots \end{aligned}\right\} \tag{2}$$

by writing $$w - i(CD)^{-1/2}F = W'_n(z)\cos n\theta \tag{3}$$

and performing straightforward algebraic transformations. The independent variable z is

$$z = i\,r/a, \quad a = \cot\alpha\sqrt{D/C} \tag{4}$$

Two independent "cone function" solutions of Eq. (2), found by the Frobenius method, and denoted $Co_1(z, n)$ and $Co_2(z, n)$, are elementary functions. Two other solutions, found through Euler transform integral representations, and denoted $Co_3(z, n)$ and $Co_4(z, n)$, are transcendental functions expressible in terms of Bessel functions. In terms of the cone functions, solutions to Eq. (1) may be expressed by

* For details of this work see a doctoral thesis accepted by the Massachusetts Institute of Technology, September, 1958, entitled *On the solution of the differential equations of conical shells*, and supervised by E. Reissner.

$$\left.\begin{aligned} w &= \sum_{j=1}^{4} [A_j \text{ Re } Co_j(ir/a, n) + \\ &\qquad B_j \text{ Im } Co_j(ir/a, n)] \cos n\theta \\ F/\sqrt{CD} &= \sum_{j=1}^{4} [-A_j \text{ Im } Co_j(ir/a, n) + \\ &\qquad B_j \text{ Re } Co_j(ir/a, n)] \cos n\theta \end{aligned}\right\} \quad (5)$$

where the A_j and B_j are arbitrary real constants.

As solutions to problems concerning conical shells of sufficiently large extent that $r/a \gg 1$, the functions Co_3 and Co_4 embody boundary-layer (exponential edge effect) deformations. The functions Co_1 and Co_2, however, have different interpretations accordingly as $n = 0$, $n = 1$, or $n \geq 2$. Associated with the constants of Eq. (5) are the following types of solution:

$n = 0$	A_1 rigid motion	A_2 interior state
	B_1 nugatory	B_2 dislocation
$n = 1$	A_1 nugatory	A_2 dislocation
	B_1 rigid motion	B_2 interior state
$n \geq 2$	A_1, A_2, B_1, B_2 interior states	

Here an interior state, as distinguished from a boundary-layer state, is any deformation of membrane and/or inextensional bending type. A nugatory solution is one for which all stresses and displacements vanish. On the assumption of rotational completeness of the shell, dislocations (in the sense of Volterra) as well as nugatory solutions must be rejected. In their stead may be appended an arbitrary torsional deformation, axial rotation, lateral translation, and the singular solution

$$\left.\begin{aligned} w &= A_2 \text{ Re } Co_2(ir/a, 1) \cos\theta \\ F/\sqrt{CD} &= -A_2 \text{ Im } Co_2(ir/a, 1) \cos\theta + A_2(r/a)\theta \sin\theta \end{aligned}\right\} \quad (6)$$

As $r \to \infty$ all meaningful solutions defined above approach in an appropriate sense approximate solutions given for the conical shell by Love,[3] while as $r \to 0$, the solutions approach those for a flat plate.

The solution to any properly set boundary-value problem involving shallow ($\tan\alpha \ll 1$) conical shells can be expressed in terms of solutions outlined above. Also solutions to Seide's approximate differential equations for the deep conical shell,[4] which are identical to the system in Eq. (1), are comprised here; except that the n of the shallow-shell theory must be replaced by $n/\cos\alpha$, Eq. (2) follows from Seide's equations. The cone functions are adequate to any case for which $n/\cos\alpha$ is an integer, but a satisfactory extension of the cone functions to nonintegral order is required to handle Seide's equations in general.

Formulas for the cone functions are:

$$\left.\begin{aligned} &Co_1(z, 0) = 1,\ Co_1(z, 1) = (1/2)\, z, \\ &Co_1(z, n) = \sum_{0}^{n-2} \frac{\Gamma(2n-2-k)\Gamma(2n-k) z^{-n+2+k}}{\Gamma(n-k)\Gamma(n-1-k)\Gamma(3+k)k!}, \\ &\qquad\qquad n = 2, 3 \ldots \end{aligned}\right\} \quad (7)$$

$$Co_2(z, 0) = -\log z + z + \Psi(2) + \Psi(1), \quad (8)$$

$$Co_2(z, 1) = 3z^{-1} - 2,$$

$$Co_2(z, n) = \frac{\Gamma(2n)\Gamma(2n+2)}{\Gamma(n+1)\Gamma(n+2)} z^{-n} - \frac{\Gamma(2n-1)\Gamma(2n+1)}{\Gamma(n+1)\Gamma(n)} z^{-n+1} -$$
$$\log z\, Co_1(z, n) - \sum_{0}^{n-2} \frac{\Gamma(2n-2-k)\Gamma(2n-k) z^{-n+2+k}}{\Gamma(n-k)\Gamma(n-1-k)\Gamma(3+k)k!} \times$$
$$[\Psi(n-k) + \Psi(n-1-k) - \Psi(2n-2-k) - \Psi(2n-k) - \Psi(3+k) - \Psi(1+k)] + z/(n^2-1),$$
$$n = 2, 3 \ldots$$

$$\left.\begin{aligned} &Co_3(z, 0) = \int_0^z I_2(2z^{1/2})\, dz - 1, \\ &Co_3(z, n) = z^{n+2} d^n/dz^n \{z^{n-2} d^{n-1}/dz^{n-1} [z^{-n} I_2(2z^{1/2})]\}, \\ &\qquad\qquad n = 1, 2 \ldots \end{aligned}\right\} \quad (9)$$

$$Co_4(z, 0) = -2 \int_\infty^z K_2(2z^{1/2}) dz, \quad (10)$$

$$Co_4(z, n) = -2z^{n+2} (d^n/dz^n) \{z^{n-2} (d^{n-1}/dz^{n-1}) [z^{-n} K_2(2z^{1/2})]\}$$

References

[1] Johnson, M. W., and Reissner, E., *On inextensional deformations of shallow elastic shells*, J. Math. & Phys., Vol. 34, pp. 335–346, 1956.

[2] Erdelyi, A., et al., *Higher Transcendental Functions 1*, pp. 182–185; McGraw-Hill Book Co., New York, 1953.

[3] Love, A. E. H., *A Treatise on the Mathematical Theory of Elasticity*, pp. 590–613; Dover, N. Y., 1944.

[4] Seide, P., *Donnell type theory for asymmetrical bending and buckling of thin conical shells*, J. Appl. Mech., Vol. 24, pp. 547–556, 1957.

Laminar Jet Mixing of Electrically Conducting Fluid in a Transverse Magnetic Field*

S. I. Pai

Research Professor, Institute for Fluid Dynamics and Applied Mathematics, University of Maryland, College Park, Md.

November 24, 1958

In this note we discuss the effect on laminar jet mixing of an electrically conducting, incompressible, and viscous fluid under an applied transverse magnetic field. We assume a jet of this fluid issuing from a small two-dimensional slit and mixing with the surrounding medium of the same fluid. There is an externally applied transverse magnetic field $H_0(x) = H_1 x^{-n}$ where x is the distance along the axis of the jet and n is an arbitrary constant. There is no external pressure gradient in the present problem. We shall consider only the case of small electrical conductivity σ or small magnetic Reynolds Number so that the induced magnetic field may be neglected. Under this condition and the usual boundary-layer approximations, the fundamental equations of our problem are[1]

$$u(\partial u/\partial x) + v(\partial u/\partial y) = -(Q/9)x^{-2n} u + \nu(\partial^2 u/\partial y^2) \quad (1)$$

$$(\partial u/\partial x) + (\partial v/\partial y) = 0 \quad (2)$$

where the external magnetic field is taken as

$$H_0(x) = H_1 x^{-n} \quad (3)$$

and

$$Q = 9(\sigma/\rho)\, \mu_e^2 H_1^2 \quad (4)$$

H_1 is a constant. $H_0(x)$ is in the y-direction which is perpendicular to the jet axis. ρ is the density of the fluid and μ_e is the magnetic permeability. The MKS system is used.

The boundary conditions of our problem are

$$\begin{aligned} &y = 0: \quad v = 0,\ (\partial u/\partial y) = 0 \\ &y = \infty: \quad u = 0 \end{aligned} \quad (5)$$

We introduce the stream function ψ such that

$$u = \partial\psi/\partial y, \quad v = -(\partial\psi/\partial x) \quad (6)$$

Eq. (2) is automatically satisfied. We replace the $x - y$ coordinates by the following variables

$$\zeta = x, \quad \eta = (1/3\nu^{1/2})\, (y/x^{2/3}) \quad (7)$$

In order to solve Eq. (1), we write the stream function ψ in the following form:

$$\psi = \nu^{1/2} \zeta^{1/3} f(\zeta, \eta) = \nu^{1/2} \zeta^{1/3} [f_0(\eta) + Q\zeta^m f_1(\eta) + (Q\zeta^m)^2 f_2(\eta) + \ldots] \quad (8)$$

* This work was supported by the Air Force Office of Scientific Research under Contract AF 49(638) 401.

where $m = (4/3) - 2n$.

Substituting Eqs. (6) to (8) into Eq. (1) and collecting terms of the same power of $Q\zeta^m$, we have

$$f_0''' + (f_0 f_0') = 0 \tag{9}$$

$$f_1''' - f_0 f_1'' - (3m - 2) f_0' f_1' = f_0', \text{ etc.} \tag{10}$$

With the boundary conditions

$$\eta = 0; f_0 = f_1 = \ldots = 0; f_0' = f_1' = \ldots = 0 \tag{11}$$
$$\eta = \infty; f_0' = f_1' = \ldots = 0$$

where prime refers to differentiation with respect to η.

Eq. (9) is the well-known equation of laminar jet mixing of ordinary fluid dynamics.[2] The equation for f_1, f_2, etc., are all linear differential equations, with variable coefficients, and they may be easily solved by numerical integration.

For first approximation, if we take $f = f_0 + Q\zeta^m f_1$, the increment of the axial velocity component u over the corresponding value in the ordinary fluid dynamics increases with Q.

Similar Solution

If $n = 2/3$, $m = 0$. Such a solution may be called a similar solution because the shapes of velocity distribution u at various x-stations are similar. The solution (8) to (11) for this problem holds true for small value of Q because we use the method of series expansion.

Some general conclusions for this similar solution may be drawn from the following considerations. In the similar solution $f(\zeta, \eta) = f(\eta)$ which is satisfied by the equation†

$$f''' + (ff')' = Qf' \tag{12}$$

if we expand the function $f(\eta)$ in power series of the parameter Q, we have the same results as given in Eqs. (8)–(11).

Now we introduce the following transformation

$$f = \sqrt{Q}\, F\left(\sqrt{Q}\,\eta\right) = \sqrt{Q} F(z) \tag{13}$$

Eq. (12) becomes

$$F''' + (FF')' = F' \tag{14}$$

where primes refer to differentiation with respect to z. Now it is interesting to notice that F is independent of Q explicitly—i.e., the same function $F(z)$ holds for any value of Q within the approximations of our analysis.

The x-component of velocity in the jet is

$$u = (1/3x^{1/3})\,(df/d\eta) = (Q/3x^{1/3})\,(dF/dz) \tag{15}$$

Here u increases with Q which checks with our result by the method of series expansion.

The spread of the jet mixing region is proportional to

$$b = 3\sqrt{\nu/Q}\, x^{2/3} \tag{16}$$

Hence the spread of the jet mixing region decreases as $(1/\sqrt{Q})$ decreases.

The important parameter Q may be written as

$$Q = (9U/L) R_H R_\sigma \tag{17}$$

where $R_\sigma = \mu_e \sigma UL$ = magnetic Reynolds Number (18)

$R_H = \mu_e H_1^2/\rho U^2$ = modified magnetic pressure number (19)

If H_0 is independent of x, R_H reduces to the conventional magnetic pressure number. Here U and L are the characteristic velocity and length of the problem respectively. The parameter Q increases with the product of R_σ and R_H.

References

Rossow, V. J., *On the Flow of Electrically Conducting Fluids Over a Flat Plate in the Presence of a Transverse Magnetic Fluid*, NACA TN 3971, May, 1957.

[2] Pai, S. I., *Fluid Dynamics of Jets*, p. 77; D. Van Nostrand Co., Inc., Princeton, N.J., 1954.

† Prof. J. M. Burgers pointed out to the author that there is no analytic solution of Eq. (12) throughout the whole domain to satisfy the boundary condition (5). This point will be further discussed elsewhere.

Beam Columns on Elastic Supports

Ben A. Neffson
Design Specialist, North American Aviation, Inc., Los Angeles, Calif.
November 28, 1958

In the analysis of a beam column, one is sometimes confronted with the problem of effective end restraint. Although the rotational rigidity of the supports can often be determined with comparative ease and accuracy, the matter is usually resolved by using an arbitrary "fixity factor" to reduce the effective column length, with no attempt made to also decrease the maximum moment as a logical consequence. In either case, considerable labor is required to compute the true moments, and the procedure is not suitable for routine analysis.

The following discussion shows that it is possible to represent the effects of end restraint and lateral load as functions of a single nondimensional parameter. Thus, regardless of whether arbitrary fixity factors or actual rotational rigidities are used, it becomes feasible to represent many cases of practical interest by a series of plots which reduce the computational work considerably. The theory upon which this note is based can be found in a number of texts—e.g., Chapter 1 of reference 1.

We consider the beam column shown in Fig. 1 with an arbitrary lateral load, W, and end moments M_A and M_B due to the elastic nature of the supports. Since the final rotation of the end tangents is a linear combination of the separate effects, we may write

$$\left.\begin{aligned} \theta_A &= k_1 M_A + k_2 M_B + f_A(W) \\ \theta_B &= k_2 M_A + k_1 M_B + f_B(W) \end{aligned}\right\} \tag{1}$$

where the k's and f's may be thought of as generalized stiffness coefficients.

If, noting reference 1, we now refer to M_A and M_B as the moments produced by the rotations against the elastic restraints at A and B, we have

$$\theta_A = -(M_A/\alpha) \quad \theta_B = -(M_B/\beta)$$

where α and β are coefficients describing the degree of fixity at A and B—i.e., α = moment required to produce unit rotation at A, etc. If we let

$$\gamma = f_B(W)/f_A(W)$$

Eqs. (1) may be rewritten as

$$\left.\begin{aligned} [k_1 + (1/\alpha)] M_A + k_2 M_B &= -f_A(W) \\ k_2 M_A + [k_1 + (1/\beta)] M_B &= -\gamma f_A(W) \end{aligned}\right\} \tag{2}$$

If we further define

$$D = \begin{vmatrix} k_1 + (1/\alpha) & k_2 \\ k_2 & k_1 + (1/\beta) \end{vmatrix} \tag{3}$$

Then:

$$\left.\begin{aligned} M_A &= f_A(W)\left[\frac{\gamma k_2 - [k_1 + (1/\beta)]}{D}\right] \\ M_B &= f_A(W)\left[\frac{k_2 - \gamma[k_1 + (1/\alpha)]}{D}\right] \end{aligned}\right\} \tag{4}$$

It is evident, therefore, that, except for the nondimensional factor, γ, the bracketed expressions in Eqs. (4) are independent of the lateral load W. If the load is symmetrical with respect to the beam center line, $\gamma = 1.0$. Otherwise, the dependency is of the simple form shown above and readily evaluated.

It is easily shown that

$$k_1 = (\lambda \cot \lambda l/P) - (1/Pl)$$
$$k_2 = (1/Pl) - (\lambda/P \sin \lambda l)$$

where $\lambda = \sqrt{P/EI}$

Substituting the above values of k_1 and k_2 into Eqs. (4), we arrive, after some algebraic manipulation, at the following expressions for M_A and M_B:

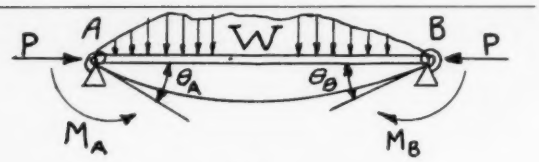

FIG. 1.

$$M_A = f_A(W)\left\{\frac{(\alpha\beta/Pl)\,[f_1(\lambda l)] + (\alpha\beta/Pl)\gamma[f_2(\lambda l)] + \alpha}{[(\alpha+\beta)/Pl]\,[f_1(\lambda l)] + (2\alpha\beta/P^2l^2)\,[f_3(\lambda l)] + 1}\right\} \tag{5a}$$

$$M_B = f_A(W)\left\{\frac{(\alpha\beta/Pl)\gamma[f_1(\lambda l)] + (\alpha\beta/Pl)\,[f_2(\lambda l)] + \gamma\beta}{[(\alpha+\beta)/Pl]\,[f_1(\lambda l)] + (2\alpha\beta/P^2l^2)\,[f_3(\lambda l)] + 1}\right\} \tag{5b}$$

where

$$f_1(\lambda l) = \lambda l \cot \lambda l - 1$$

$$f_2(\lambda l) = (\lambda l - \sin \lambda l)/\sin \lambda l$$

$$f_3(\lambda l) = \lambda l[\tan (\lambda l/2) + (\lambda l/2)]$$

Except for a possible additive or multiplicative constant, it is obvious that $f(W)$ may also be expressed as a function of λl.

Hence a solution for the end moments now becomes feasible by representing the various functional relations in a series of plots where, for example, one plot of $f_n(\lambda l)$, where $n = 1, 2, 3$, suffices for any column loading. The principle of superposition then permits a limited number of plots of $f(W)$ and $\gamma(\lambda l)$ to account for almost any conceivable lateral load. It will be noted that for the linear combination represented by Eqs. (1), $f(W)$ becomes infinite as λl approaches π. Therefore, while the theoretical maximum value of λl is 2π, the plots of the above functions can be terminated at $\lambda l = \pi$.

The restraint coefficients α and β may be chosen so as to correspond to some reduced column length, l', such that $c = (l/l')^2$, where c is the so-called fixity factor and l the actual column length. The relation between c and α and β may be established from the condition that at the critical load the determinant given by Eq. (3) must vanish. A family of curves may then be drawn giving P_{cr}/P_e as functions of the nondimensional parameters $\alpha l/EI$ and $\beta l/EI$. Here P_{cr} is the critical column load for the effective length l' and P_e the Euler load for a pin-ended column of length l. Since the definition $c = P_{cr}/P_e$ also holds, the correspondence between c and α and β is thus established. In closing, it should also be noted that the above family of curves may be used for determining the critical column load for any arbitrary degree of end restraint represented by α and β. For stresses above the proportional limit, however, the determination only holds for effective column lengths, with the critical load then being found from any suitable column curve of the material.

REFERENCE

[1] Timoshenko, S., *Theory of Elastic Stability*, McGraw-Hill Book Co., Inc., New York, 1936.

The Smallest Height of Roughness Capable of Affecting Boundary-Layer Transition

(*Continued from page 245*)

[24] Wijker, H., *Experiments on Disturbed Regions in the Laminar Boundary Layer Behind Isolated Surface Excrescences for Two- and Three-Dimensional Flow*, Nationaal Luchtvaartlaboratorium Report A. 1207, (Dutch) 1951.

[25] Haines, A. B., Holder, D. W., and Pearcey, H. H., *Scale Effects of High Subsonic and Transonic Speeds, and Methods for Fixing Boundary-Layer Transition in Model Experiments*, British R&M No. 3012, 1957.

[26] Liepmann, H. W., and Goddard, F. E., Jr., *Note on the Mach Number Effect Upon the Skin Friction of Rough Surfaces*, Journal of the Aeronautical Sciences, Readers' Forum, Vol. 24, No. 10, p. 784, October, 1957.

[27] van Driest, E. R., and Boison, J. Christopher, *Experiments on Boundary-Layer Transition at Supersonic Speeds*, Journal of the Aeronautical Sciences, Vol. 24, No. 12, pp. 885–899, December, 1957.

[28] Braslow, A. L., *Effect of Distributed Granular-Type Roughness on Boundary-Layer Transition at Supersonic Speeds with and without Surface Cooling*, NACA RML58A17, March 1958.

[29] Chapman, Dean R., and Rubesin, Morris W., *Temperature and Velocity Profiles in the Compressible Laminar Boundary Layer with Arbitrary Distribution of Surface Temperature*, Journal of the Aeronautical Sciences, Vol. 16, No. 9, pp. 547–565, September, 1949.

[30] Luther, Marvin, *Fixing Boundary-Layer Transition on Supersonic Wind-Tunnel Models*, Journal of Aeronautical Sciences, Vol. 24, No. 8, pp. 579–586, August, 1957.

[31] Laufer, John, and McClellan, Robert, *Measurement of Heat Transfer from Fine Wires in Supersonic Flows*, Journal of Fluid Mechanics, Vol. 1, Part 3, pp. 276–289, September, 1956.

[32] Chapman, Dean R., Kuehn, Donald M., and Larson, Howard K., *Investigation of Separated Flows in Supersonic and Subsonic Streams with Emphasis on the Effect of Transition*, NACA TN 3869, March, 1957.

[33] Greber, Isaac, Hakkinen, R. J., and Trilling, Leon, *Some Problems of Laminar Boundary Layer Shock Wave Interactions*, Heat Transfer and Fluid Mechanics Institute, Preprints of Papers, pp. 138–158, 1957.

[34] Jack, John R., Wisniewski, Richard J., and Diaconis, N. S., *Effects of Extreme Surface Cooling on Boundary-Layer Transition*, NACA TN 4094, October, 1957.

[35] Diaconis, N. S., Wisniewski, Richard J., and Jack, John R., *Heat Transfer and Boundary-Layer Transition on Two Blunt Bodies at Mach Number 3.12*, NACA TN 4099, October, 1957.

[36] Liepmann, H. W., and Roshko, A., *Elements of Gasdynamics*, GALCIT Aeronautical Series, John Wiley and Sons, Inc., New York, 1957.

[37] Bogdonoff, S. M., Vas, I. E., and Hammitt, A. G., *An Experimental Investigation of the Flow Over Simple Two-Dimensional and Axial Symmetric Bodies at Hypersonic Speeds*, Jet Propulsion, Vol. 28, No. 2, pp. 97–104, February, 1958.

[38] Lees, Lester, *Recent Developments in Hypersonic Flow*, Jet Propulsion, Vol. 27, No. 11, pp. 1162–1178, November, 1957.

[39] Sibulkin, Mervin, *Estimation of Turbulent Heat Transfer at the Sonic Point of a Blunt-Nosed Body*, Jet Propulsion, Vol. 28, No. 8, Part 1, pp. 548–554, August, 1958.

REQUIREMENTS *for* CONTRIBUTIONS

to the publications of the

INSTITUTE *of the* AERONAUTICAL SCIENCES

The Institute of the Aeronautical Sciences invites both members and nonmembers from any country to submit papers for publication in the JOURNAL OF THE AERO/SPACE SCIENCES and AERO/SPACE ENGINEERING. The Institute, following the practice of other societies, does not pay for contributions.

The following directions for the preparation of papers, if followed by authors, will save correspondence, avoid the return of papers for changes, minimize the work of preparation for the printer, and save the expense due to the charges made for "author's corrections."

MANUSCRIPTS: The original typewritten copy of the paper is desired. **To expedite review, an additional copy of both the manuscript and figures should be submitted.** The manuscript must be double or triple spaced on one side of white paper sheets, consecutively numbered. There should be wide margins to allow for the marking of directions to the printer. Correcting, changing, or adding to papers after they are in type is costly. It is, therefore, imperative that papers submitted be in final form. Typographical errors may be corrected on proofs, but if authors wish to add material, they may do so at their own expense. In mailing, drawings may be rolled, but manuscripts should be sent flat. Send by first-class mail (register if you wish for your own protection) to the Editorial Office, Institute of the Aeronautical Sciences, 2 East 64th Street, New York 21, N.Y. All manuscripts will be examined by the Editorial Committee and by the Editor. Authors will be advised as promptly as possible whether the paper is acceptable for publication.

TITLES: The title of the paper should be brief. The name and initials of the author should be written as he prefers. The use of the full name of an author is advocated because of the frequent duplication of initials and surnames which sometimes makes it difficult to establish the identity of the author. This is particularly important for large annual indexing and abstracting services. All titles and degrees or honors are omitted. The name of the organization with which the author is associated should be placed after his name on a separate line. The date on which the paper is received will be inserted by the Editor. The author's title or position should be indicated in a footnote.

SUMMARIES OR ABSTRACTS: An abstract to be printed at the beginning should accompany each article. It should be adequate as an *index* and as a *summary*. It should contain a statement of major conclusions reached, since summaries in many cases constitute the only source of information used in compiling scientific reference indexes. Abstracts printed in other journals, especially foreign, in most cases consist of summaries from printed papers. The summary should explain as adequately as possible the major conclusions to a nonspecialist in the subject and should contain from 100 to 300 words, depending on the length of the paper.

SUBHEADINGS: Subheadings should be inserted by the author at frequent intervals. The work of editorial preparation will be simplified by the author's provision of many subheadings.

MATTER USUALLY DELETED: Photographs or illustrations of little technical interest and not showing advances in general practice. Too detailed tabular matter (general results of such tables may be included in the text). Lengthy descriptions of materials or processes or of preliminary experiments or theories that preceded final results; salient features only are of interest.

REFERENCES: References should be numbered consecutively and grouped together at the end of the manuscript, with only the corresponding number being mentioned in the text. The arrangement should be as follows. For books: [1] Durand, W. F., *Aerodynamic Theory*, 1st Ed., Vol. 1, p. 23; Julius Springer, Berlin, 1934. For magazines: [1]England, C. R., Crawford, A. B., and Mumford, W. W., *Some Results of a Study of Ultra-Short-Wave Transmission Phenomenon*, Proc. IRE, Vol. 20, No. 12, pp. 481–482, March, 1933. Please give author, title, edition, volume, number, page, publisher, and place and date of publication as indicated. Omission of one required fact causes much extra editorial work and possible inaccuracies.

ILLUSTRATIONS: Illustrations should accompany manuscripts, and each should always be referred to in the text by number. Drawings or graphs should not be larger than 12 × 16 inches, and must be made with jet black India ink on white paper or tracing cloth, the latter being preferred. *Do not use typewriter for lettering.* The smallest lettering on 8 × 10 inch figures should be no less than $^1/_4$ inch high. Cross-section paper (white with black lines) may be used, but it should not have more than 4 lines per inch. If finer ruled paper is used, the major division lines should be drawn in with black ink, omitting the finer divisions. In the case of finely ruled paper, only blue-lined paper can be accepted. *Tracing paper and blueprints* are not acceptable. Lettering and all markings must be large enough to be readable after reduction to single-column width ($3^1/_{16}$ in.). Mail rolled or flat; never fold. Drawings that cannot be reproduced (including pencil drawings) will be returned to the author for redrawing, thus delaying publication of the paper. Photographs should be distinct and show clear black and white contrasts. They must be on glossy white paper. Avoid round and oval photographs.

CAPTIONS AND LEGENDS: Legends or captions must accompany each drawing or photograph submitted. If written on the drawing or photograph, they should be placed below and well outside the part to be reproduced. Each table should have a caption such as Table 1, Table 2, Table 3, etc. Captions should be complete in themselves so as to make the data intelligible to the reader without reference to the text. A duplicate list of captions for figures should be included as the last page of the manuscript. Use "Fig. 1" (not Figure 1). "Figs. 3 and 4," etc., in both the text and the numbering of illustrations. In the text, "Eq. (1)" or "Eqs. (1) and (2)" is used, not "Equation (1)." In captions, legends, and in table headings, write all words in full; do not abbreviate, except for "Fig." and "Eq."

MATHEMATICAL WORK: Formulas may be typewritten or carefully written in pen and ink, the writing to be large enough so that it can be marked for the printer. Considerable space for marking should be allowed above and below all equations. All complicated equations should be repeated on separate sheets with plenty of space left for marking. The solidus should be used for simple fractions appearing within the text. Make all expressions clear to the typesetter. Greek letters used in formulas should be clearly designated by name in the margin of the manuscript. The difference between capital and lower-case letters should be clearly distinguished and care taken to avoid confusion between zero (0) and the letter (o), between the numeral (one) and the letter (ell) and the prime (′), between alpha and a, kappa and k, u and mu, v and nu, n and eta. All subscripts and exponents should be clearly distinguished. Avoid complicated exponents and subscripts. Dots and bars over letters or mathematical expressions should also be avoided. When it is necessary to repeat a complicated expression, it should be represented by some convenient symbol.

SYMBOLS AND ABBREVIATIONS: The symbols recommended in the American Standard Association "Letter Symbols for Aeronautical Sciences," ASA Y10.7—1954, should be used wherever practicable. All symbols should be clearly written and carefully checked. Standard abbreviations should be used, and it should be noted that most abbreviations are lower case, such as m.p.h., b.m.e.p., i.h.p., b.hp., hp., etc.

Corporate Members

OF THE

Institute of the Aeronautical Sciences

AC SPARK PLUG DIVISION, GENERAL MOTORS CORPORATION
ACADEMY OF AERONAUTICS
ADAMS RITE MANUFACTURING COMPANY
AEROJET-GENERAL CORPORATION
AEROLAB DEVELOPMENT COMPANY
AERONCA MANUFACTURING CORPORATION
AERONUTRONIC SYSTEMS, INC.
AEROQUIP CORPORATION
AGAWAM AIRCRAFT PRODUCTS, INC.
ALLIED RESEARCH ASSOCIATES, INC.
ALLIS-CHALMERS MANUFACTURING COMPANY
ALLISON DIVISION, GENERAL MOTORS CORPORATION
ALUMINUM COMPANY OF AMERICA
AMERICAN AIRLINES, INC.
AMERICAN BOSCH ARMA CORPORATION
AMERICAN NON-GRAN BRONZE COMPANY
AMERICAN STEEL & WIRE DIVISION, UNITED STATES STEEL CORPORATION
AMOCO CHEMICALS CORPORATION
AMPHENOL-BORG ELECTRONICS CORPORATION
ANDERSON, GREENWOOD & CO.
ARDE ASSOCIATES
ASSOCIATED AVIATION UNDERWRITERS
AVCO RESEARCH LABORATORY
AVIEN, INC.
AVRO AIRCRAFT LIMITED
BAKER STEEL & TUBE COMPANY
BEECH AIRCRAFT CORPORATION
BELL AIRCRAFT CORPORATION
BENDIX AVIATION CORPORATION
BOEING AIRPLANE COMPANY
BOOZ, ALLEN & HAMILTON
THE BRISTOL AEROPLANE COMPANY (U.S.A.) INC.
BULOVA RESEARCH AND DEVELOPMENT LABORATORIES, INC.
CANADAIR, LTD.
THE CESSNA AIRCRAFT COMPANY
CHANCE VOUGHT AIRCRAFT, INCORPORATED
THE CHASE MANHATTAN BANK
CHICAGO AERIAL INDUSTRIES, INC.
THE CLEVELAND PNEUMATIC INDUSTRIES, INC.
CONSOLIDATED CONTROLS CORPORATION
CONTINENTAL MOTORS CORPORATION
CORNELL AERONAUTICAL LABORATORY, INC.
CURTISS-WRIGHT CORPORATION
THE DECKER CORPORATION
DEL MAR ENGINEERING LABORATORIES
DELCO-REMY DIVISION, GENERAL MOTORS CORPORATION
DOAK AIRCRAFT COMPANY, INC.
DOUGLAS AIRCRAFT COMPANY, INC.
DZUS FASTENER COMPANY, INC.
EASTERN AIR LINES, INC.
EDO CORPORATION
ELASTIC STOP NUT CORPORATION OF AMERICA
ELECTROL INCORPORATED
ENGINEERING SUPERVISION COMPANY
ESSO STANDARD OIL COMPANY
FAIRCHILD CAMERA AND INSTRUMENT CORPORATION
FAIRCHILD ENGINE AND AIRPLANE CORPORATION
THE FIRESTONE TIRE & RUBBER COMPANY
THE GARRETT CORPORATION
GENERAL DYNAMICS CORPORATION
GENERAL ELECTRIC COMPANY
GENERAL PRECISION EQUIPMENT CORPORATION
G. M. GIANNINI & CO., INC.
GIANNINI PLASMADYNE CORPORATION
THE B. F. GOODRICH COMPANY
GOODYEAR AIRCRAFT CORPORATION
GRUMMAN AIRCRAFT ENGINEERING CORPORATION
HYDRO-AIRE, INC.
INSURANCE COMPANY OF NORTH AMERICA COMPANIES
INTERNATIONAL BUSINESS MACHINES CORPORATION
THE INTERNATIONAL NICKEL COMPANY, INC.
ITT LABORATORIES, DIVISION OF INTERNATIONAL TELEPHONE AND TELEGRAPH CORPORATION
JANITROL AIRCRAFT DIVISION, SURFACE COMBUSTION CORPORATION
JOHNS-MANVILLE SALES CORPORATION
EARLE M. JORGENSEN CO.
KELSEY-HAYES COMPANY
WALTER KIDDE & COMPANY, INC.
KOLLSMAN INSTRUMENT CORPORATION
LAVELLE AIRCRAFT CORPORATION
LEAR, INCORPORATED
C. W. LEMMERMAN, INC.
LIBRASCOPE, INCORPORATED
THE LIQUIDOMETER CORPORATION
LOCKHEED AIRCRAFT CORPORATION
LOEWY-HYDROPRESS DIVISION OF BALDWIN-LIMA-HAMILTON CORPORATION
LONGINES-WITTNAUER WATCH COMPANY, INC.
MARQUARDT AIRCRAFT COMPANY
THE MARTIN COMPANY
MARTIN STEEL PRODUCTS CORPORATION
McDONNELL AIRCRAFT CORPORATION
MELETRON CORPORATION
MID-CONTINENT MANUFACTURING, INC.
MINNEAPOLIS-HONEYWELL REGULATOR COMPANY
NATIONAL CREDIT OFFICE, INC.
NORTH AMERICAN AVIATION, INC.
NORTHROP CORPORATION
NUCLEAR DEVELOPMENT CORPORATION OF AMERICA
PAN AMERICAN WORLD AIRWAYS, INC.
THE RALPH M. PARSONS COMPANY
PESCO PRODUCTS DIVISION, BORG-WARNER CORPORATION
PHILLIPS PETROLEUM COMPANY
PIASECKI AIRCRAFT CORPORATION
RADIO CORPORATION OF AMERICA DEFENSE ELECTRONIC PRODUCTS
REPUBLIC AVIATION CORPORATION
ROHR AIRCRAFT CORPORATION
PAUL ROSENBERG ASSOCIATES
RYAN AERONAUTICAL COMPANY
SANDBERG-SERRELL CORPORATION
SHAFER BEARING DIVISION, CHAIN BELT COMPANY
SHELL OIL COMPANY
SIMMONDS AEROCESSORIES, INC.
SOCONY MOBIL OIL COMPANY, INC.
SOLAR AIRCRAFT COMPANY
SOUTHWEST PRODUCTS CO.
R. DIXON SPEAS ASSOCIATES
SPERRY GYROSCOPE COMPANY DIVISION OF SPERRY RAND CORPORATION
STANDARD OIL COMPANY OF CALIFORNIA
STANDARD OIL COMPANY (INDIANA)
STANDARD-THOMSON CORPORATION CLIFFORD MANUFACTURING DIVISION
STANLEY AVIATION CORPORATION
THIOKOL CHEMICAL CORPORATION
THOMPSON RAMO WOOLDRIDGE INC.
TRANS WORLD AIRLINES, INC.
TURBO PRODUCTS, INC.
UNION CARBIDE CORPORATION
UNITED AIR LINES, INC.
UNITED AIRCRAFT CORPORATION
UNITED STATES AVIATION UNDERWRITERS, INC.
VARD, INC.
VERTOL AIRCRAFT CORPORATION
VITRO CORPORATION OF AMERICA
WESTERN GEAR CORPORATION
WESTINGHOUSE ELECTRIC CORPORATION
WESTON INSTRUMENTS DIVISION OF DAYSTROM, INC.
WYMAN-GORDON COMPANY
YOUNG RADIATOR COMPANY